Multiplexed, multimodal profiling of the intracellular activity, interactions, and druggability of protein variants using LABEL-seq

Jessica J. Simon[1], Douglas M. Fowler[2,3,5], and Dustin J. Maly[1,4,5]

[1]Department of Chemistry, University of Washington, Seattle, WA, United States

[2]Department of Genome Sciences, University of Washington, Seattle, WA, United States

[3]Department of Bioengineering, University of Washington, Seattle, WA, United States

[4]Department of Biochemistry, University of Washington, Seattle, WA, United States

[5]Co-corresponding authors: dfowler@uw.edu, djmaly@uw.edu

Abstract

Multiplexed assays of variant effect are powerful tools for assessing the impact of protein sequence variation, but are limited to measuring a single protein property and often rely on indirect readouts of intracellular protein function. Here, we developed LAbeling with Barcodes and Enrichment for biochemicaL analysis by sequencing (LABEL-seq), a platform for the multimodal profiling of thousands of protein variants in cultured human cells. Multimodal measurement of ~20,000 variant effects for ~1,600 BRaf variants using LABEL-seq revealed that variation at positions that are frequently mutated in cancer had minimal effects on folding and intracellular abundance but could dramatically alter activity, protein-protein interactions, and druggability. Integrative analysis of our multimodal measurements identified networks of positions with similar roles in regulating BRaf's signaling properties and enabled predictive modeling of variant effects on complex processes such as cell proliferation and small molecule-promoted degradation. LABEL-seq provides a scalable approach for the direct measurement of multiple biochemical effects of protein variants in their native cellular context, yielding insight into protein function, disease mechanisms, and druggability.

27 **Introduction**

28 A protein's sequence defines its properties, including biophysical characteristics, intracellular
29 function, pathogenicity, druggability and drug resistance. Measurement of protein variant effects has
30 provided valuable insight into mechanisms of protein allostery[1, 2] and regulation[3], drug resistance and
31 sensitivity[4, 5], molecular evolution[6, 7], and the effects of germline and somatic mutations[8-10]. Probing how
32 protein sequence variation affects protein properties has also guided design and engineering efforts[11] as
33 well as enabled the development and benchmarking of computational models of protein stability and
34 structure. Multiplexed assays of variant effect (MAVEs) are powerful tools for characterizing the
35 consequences of protein sequence variation because they leverage high-throughput DNA sequencing to
36 enable the measurement of thousands of protein variants in a single experiment. However, while first-
37 generation MAVEs have enabled measurement of the properties and functions of millions of variants of
38 100s of proteins[12], they are generally confined to measuring a single protein property or function, are
39 crafted for a specific protein or related family members, are difficult to scale, and may divorce the protein
40 from its cellular context. Many MAVEs also measure aspects of protein function indirectly; for example,
41 using cell proliferation as a proxy for enzymatic activity. Thus, a general, scalable platform for measuring
42 the effects of protein sequence variation using direct biochemical readouts of protein properties in a
43 human intracellular environment is urgently needed.

44 The multi-domain kinase BRaf is emblematic of the need for such a platform. BRaf plays a central
45 role in oncogenic signaling and >250 somatic mutations have been identified so far in The Cancer Genome
46 Atlas (TCGA), ClinVar, and COSMIC databases[13-15]. While numerous elegant biochemical and cellular
47 studies have been performed, they have focused on a limited subset of variants and do not provide a
48 comprehensive view of the effects of BRaf sequence variation[16, 17]. Thus, our understanding of the
49 mechanistic basis of BRaf regulation and signaling, the role that BRaf wild type (WT) and specific variants
50 play in disease-relevant signaling, and the druggability of clinically-observed variants remains limited. In
51 unstimulated cells, BRaf WT exists mainly within an autoinhibited complex. Upon activation, BRaf
52 undergoes a series of large conformational changes and reprogramed protein-protein interactions that
53 tune its ability to modulate downstream signaling. Consequently, BRaf sequence variation can affect
54 multiple coupled intra- and intermolecular interactions. Therefore, to fully understand BRaf's function,
55 multiple biochemical properties must be measured in the native human cell signaling environment where
56 all regulatory components and interaction partners are present. Applying existing MAVEs to measure all
57 of these properties would require considerable effort and the creation of a new assay for each biochemical
58 property.

Thus, we developed LAbeling with Barcodes and Enrichment for biochemicaL analysis by sequencing (LABEL-seq), which enables multiplexed, multimodal biochemical profiling of thousands of protein variants in cultured human cells. LABEL-seq can be used to comprehensively profile intracellular abundance, activity, protein-protein interactions and other properties of a protein variant library. Applying LABEL-seq to ~1,600 BRaf variants revealed that substitutions at positions where somatic mutations are frequently observed minimally affected folding and intracellular abundance. However, mutations at many of these same positions had dramatic effects on activity, interactions with multiple signaling partners, and druggability. Integrative analysis of our multimodal variant effect data revealed groups of positions that play similar mechanistic roles in modulating BRaf's regulation and function and illustrated how LABEL-seq-derived biochemical measurements can enable predictive modeling of the gain-of-function properties that BRaf variants acquire to promote growth factor-independent proliferation. Finally, LABEL-seq revealed that, surprisingly, 22.9% of BRaf variants were sensitized and 13.5% were resistant to small molecule-promoted degradation. These biochemical variant effects were integrated to construct a model that predicted sensitivity and resistance to small-molecule protein degradation, shedding light on the factors influencing druggability. In total, applying LABEL-seq to ~1,600 BRaf variants generated ~20,000 variant effect measurements of abundance, activity, protein-protein interactions, and druggability. Thus, LABEL-seq is a platform technology for measuring protein variant effects applicable to multiple biochemical properties and functions, facilitating a deeper understanding of the complex cellular behavior of proteins.

Results

LABEL-seq, a modular platform for multiplexed profiling of protein variants

To facilitate direct biochemical analyses of protein variant properties in a human cellular environment, we developed LABEL-seq, a modular platform that utilizes the intracellular self-assembly of proteins with nucleic acid barcodes to form complexes that remain stably associated following cell lysis and biochemical enrichment (Fig. 1a). LABEL-seq enables multiplexed profiling of the biochemical properties of protein variants in an intracellular environment by quantifying barcodes using high-throughput DNA sequencing following biochemical enrichment. Multiple biochemical properties of the same protein variant can be measured by tailoring which protein component self-assembles with a nucleic acid barcode and by modifying the enrichment strategy.

As the barcoding component of LABEL-seq, we developed nucleic acids that are (1) transcriptionally generated, (2) stable to cellular and biochemical enrichment conditions, (3) tolerant of the addition of a 15-20 nucleotide barcode and, most importantly, (4) contain the MS2 RNA stem loop, which stably self-assembles with the viral MS2 coat protein (MCP)[18]. Because RNA can be transcriptionally generated, we selected single-stranded RNA as the genetically-encoded barcoding component. Due to the general instability of RNA, we pursued a ribozyme-assisted circRNA architecture that has been shown to be highly stable in an intracellular environment[19, 20]. We used RNAfold to guide the placement of a 19 nucleotide MS2 hairpin and a 16 nucleotide barcode within two different circRNA architectures ("MS2-circRNAs", Fig. 1b and Extended Data Fig. 1a,b) and identified seven MS2-circRNA designs where barcode insertion and replacement of a stem loop with the MS2 hairpin were predicted to minimally alter the folding of the terminal ribozymes required for circularization. We found that most of these designs expressed at comparably high levels to the parent circRNAs and were minimally affected by barcode identity (Fig. 1c and Extended Data Fig. 1c). MS2-circRNAs 1 and 2, which represent the two different circRNA architectures, were selected for further investigation.

We fused four different variants of MCP (Extended Data Fig. 1d) to the N-terminus of the tyrosine kinase Lck and tested each for their ability to enrich co-expressed MS2-circRNA. We found that all four MCP-Lck fusions efficiently enriched co-expressed MS2-circRNA 2 when captured with the immobilized kinase inhibitor dasatinib, but that undetectable levels of each MCP-Lck fusion and MS2-circRNA 2 were captured in the presence of a free dasatinib competitor (Extended Data Fig. 1e). We selected a tandem MCP dimer (tdMCP) that contains a deletion that prevents higher-order oligomerization[21-23] and an affinity-enhancing mutation (V29I)[21, 23] for further characterization and observed that this tdMCP variant efficiently co-enriched MS2-circRNAs 1 and 2 (Fig. 1d).

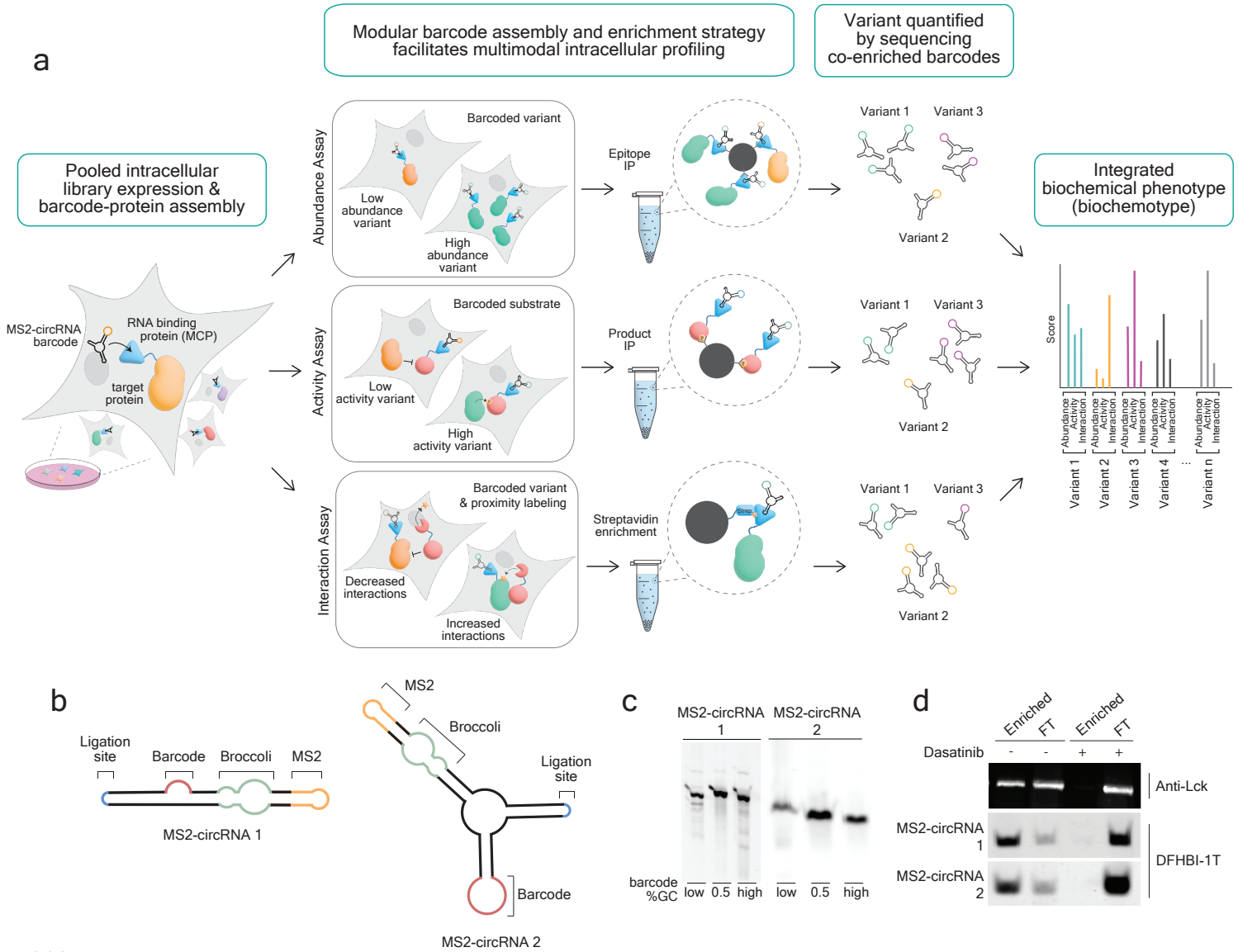

Fig. 1 | Overview of LABEL-seq and development of the RNA and protein components. a, Schematic depicting the LABEL-seq workflow. Immunoprecipitation (IP). **b,** Two MS2-circRNA architectures containing MS2 RNA hairpins and degenerate 16 nucleotide barcodes. **c,** In-gel fluorescence of total RNA extracted from cells expressing MS2-circRNAs 1 or 2 and stained with DFHBI-1T. **d**, Enrichment of tdMCP-Lck protein fusions complexed with MS2-circRNAs 1 or 2 with the immobilized ATP-competitive inhibitor dasatinib. FT = flow through of enrichment. + = presence of free dasatinib competitor.

Self-assembled tdMCP:MS2-circRNA complexes maintain fidelity between protein variant-barcode associations

We engineered a HEK293 landing pad line[24], circRNA-Protein Landing Pad (RPLP), that facilitates efficient integration of a single protein variant and a single MS2-circRNA barcode sequence per cell in a pooled format (Extended Data Fig. 2a). The RPLP line contains a Bxb1 recombination site at a single genomic locus that is flanked by Tet-inducible and U6 promoters (Extended Data Fig. 2b), which allows a transgenic cassette containing a protein variant and MS2-circRNA barcode sequence pair to be expressed only after recombination. We next recombined the RPLP with plasmids containing a MS2-circRNA 1b library (~20,000 unique barcode sequences) and a Flag-tagged tdMCP-BRaf fusion. Immunoprecipitation of tdMCP-BRaf from cell lysate revealed barcode sequence counts were robustly correlated between two replicate enrichments (Pearson's R^2 = 0.93, Fig. 2a). Pulldowns from as few as 25 cells per barcode provided high correlation between barcode sequence quantifications (Pearson's R^2 = 0.80; Extended Data Fig. 2c) as did immunoprecipitations of a different protein kinase target, tdMCP-BTK, co-expressed with a library of MS2-circRNA barcode sequences (Pearson's R^2 = 0.98, Extended Data Fig 2d).

Each barcode sequence must remain stably associated with its cognate protein following lysis and during enrichment because dissociation and reassociation of protein:MS2-circRNA complexes would diminish dynamic range. Therefore, we measured the extent of MS2-circRNA barcode sequence misassociation following cell lysis and a prolonged enrichment (Fig. 2b). Into the RPLP, we separately integrated a MS2-circRNA 1b (Extended Data Fig. 1b) library containing ~20,000 barcode sequences encoding a Flag-tagged tdMCP-BRaf fusion and an MS2-circRNA 1b library containing ~20,000 orthogonal barcode sequences encoding a Myc-tagged tdMCP-BRaf fusion. After recombination, we combined the two orthogonally barcoded libraries, performed parallel Myc and Flag immunoprecipitations, and sequenced the barcodes from each enrichment. Only ~1% of barcode sequences enriched in the Flag immunoprecipitation were associated with the Myc library, despite equal input frequencies (Fig. 2c,d). Notably, the fraction of barcode sequences associated with the Myc library did not vary at different immunoprecipitation timepoints, suggesting that minimal barcode exchange occurred during enrichment. Furthermore, we observed that when an excess of an MS2-circRNA that does not contain a barcode and cannot be reverse transcribed ("dummy" MS2-circRNA, Extended Data Fig. 2e) was added to the lysis buffer, only ~0.3% of the quantified barcode sequences encoded Myc after a 105 min enrichment (Fig. 2c,d). Comparably low levels of off-target Flag-tdMCP-BRaf barcode sequences were enriched following immunoprecipitation of Myc-tdMCP-BRaf (Fig. 2d and Extended Data Fig. 2f,g). Together, libraries of MS2-circRNAs efficiently express and assemble with co-expressed tdMCP-protein fusions and protein variant-

155 barcode sequence associations are maintained during prolonged enrichments, thereby enabling the
156 analysis of variant libraries at scale.

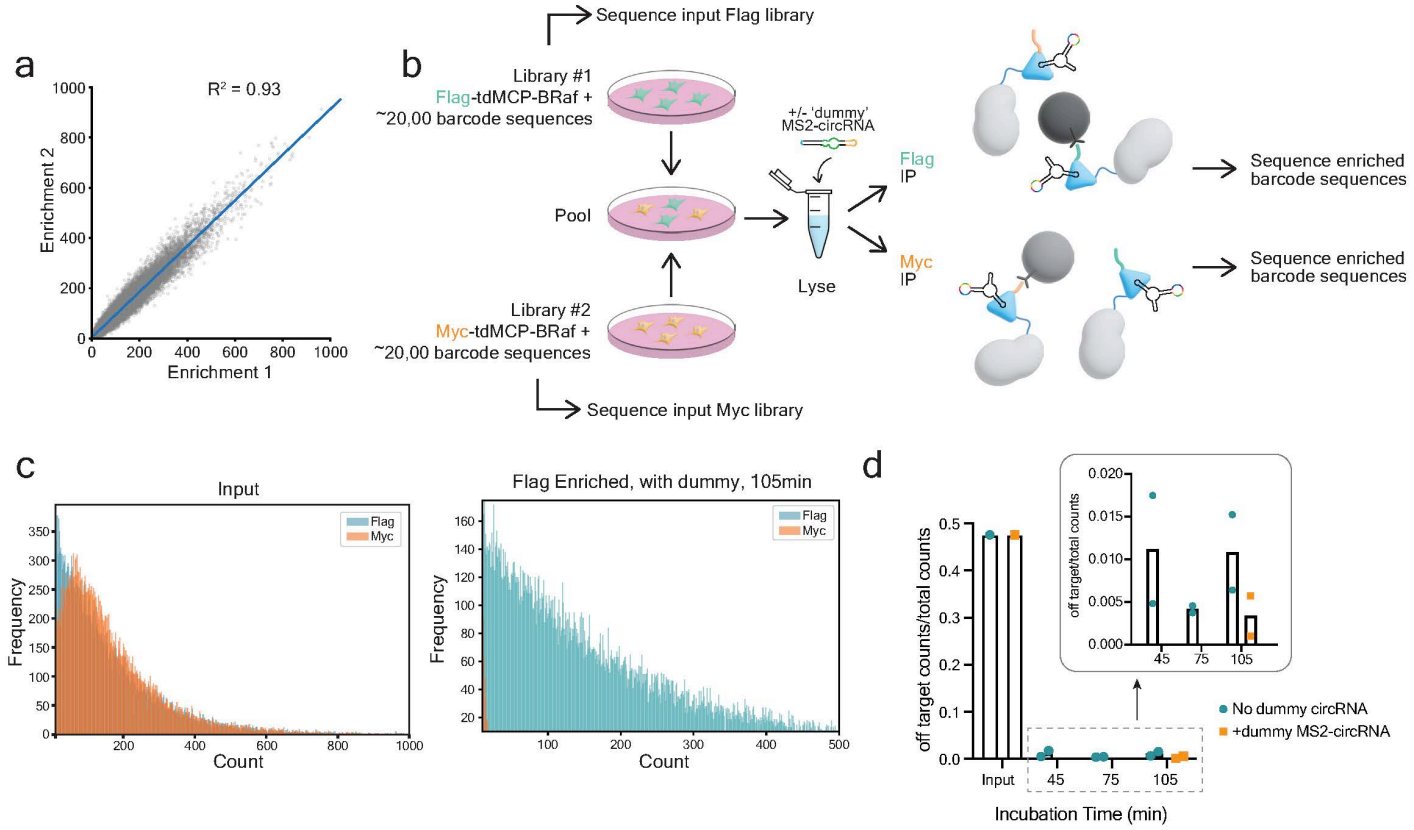

158 **Fig. 2 | Protein:MS2-circRNA complexes are stable during biochemical enrichment. a,** Sequenced
159 barcode counts derived from two independent Flag immunoprecipitations (IP) of Flag-tdMCP-BRaf co-
160 expressed with a library of MS2-circRNA 1b barcode sequences (Pearson's R^2 = 0.93). **b,** Experimental
161 workflow of the barcode sequence misassociation experiment. Dummy MS2-circRNA does not contain a
162 barcode or the priming site required for reverse transcription. **c,** Results from the experiment shown in **b**.
163 Relative frequencies of barcode sequence counts matched to Flag-tdMCP-BRaf and Myc-tdMCP-BRaf
164 libraries in unenriched lysate (left) and after 105 min Flag immunoprecipitation performed with lysate
165 that was generated with dummy MS2-circRNA in the lysis buffer (right). **d,** Quantification of the data
166 shown in **c**. The y-axis is the fraction of barcode sequence counts encoding the Myc-tagged library (n=2
167 expression, lysis, enrichment, and sequencing replicates).
168
169

170 **Profiling of protein variant abundance with LABEL-seq**

171 We selected the multi-domain kinase BRaf to demonstrate the multimodal profiling capabilities
172 of LABEL-seq due to the complexity of its regulation, BRaf's ability to interact with multiple signaling
173 partners, and the prevalence of disease-associated mutations[25]. We first confirmed that an N-terminal
174 tdMCP fusion[26, 27] of BRaf behaves like untagged BRaf. We observed that previously characterized BRaf
175 variants promoted expected levels of pMek (Fig. 3a), co-expression of CRaf enhanced tdMCP-BRaf's
176 activation of downstream signaling (Extended Data Fig. 3a), and that tdMCP-BRaf possessed similar levels
177 of phosphorylation at a regulatory site as untagged BRaf. (Extended Data Fig. 3b). In order to understand
178 how sites that have been observed to be mutated in cancer affect the signaling properties of BRaf, we
179 generated a library of single amino acid variants at all positions in BRaf that contain two or more missense
180 mutations in TCGA and COSMIC databases (Supplementary Table 1). Two positions (R509 and I666) that
181 contain biochemically well-characterized variants were also varied, for a total of 80 positions that are
182 distributed throughout the entire protein (Fig. 3b and Extended Data Fig. 3c). Long read sequencing of the
183 resulting ~1,600 member tdMCP-BRaf variant library indicated each variant was represented by ~30
184 unique MS2-circRNA 1b barcode sequences (Extended Data Fig. 3d), which was recombined into the RPLP.

185 Quantitative measurements of protein variant abundance are important because all proteins
186 must express at high enough levels to perform their cellular function[10, 28, 29] and many complex biochemical
187 properties, such as activity and protein-protein interactions, cannot be fully understood in the absence of
188 protein stability information[30]. To enable the measurement of a range of protein abundances, we
189 developed a LABEL-seq abundance assay that involves co-expressing Flag-tdMCP-tagged protein variants
190 with a Myc-tdMCP standard, which serves as an intracellular competitor for MS2-circRNAs (Fig. 3c), and
191 calculating the ratio of barcode sequence counts obtained from parallel Flag and Myc
192 immunoprecipitations. This ratiometric quantification provides a direct readout of abundance that is not
193 dependent on the relative intracellular expression levels of MS2-circRNAs and protein variants. Prior to
194 abundance profiling of our tdMCP-BRaf variant library, we confirmed that the sequencing-derived
195 abundance scores of cells co-expressing the Myc-tdMCP standard with tdMCP-BRaf WT or G466V, and
196 treated with a variant-selective BRaf PrOteolysis TArgeting Chimera (PROTAC)[31], reflected levels
197 determined by western blot analysis (Fig. 3d and Extended Data Fig. 3e).

198 We next used the LABEL-seq abundance assay to profile the ~1600 BRaf variants in our library
199 (Fig. 3e and Supplementary Table 2). We found that abundance scores were highly correlated (Pearson's
200 R^2=0.75, Extended Data Fig. 3f) between biological replicates, and that the synonymous WT and nonsense
201 score distributions were well separated (Fig. 3f). As expected, we observed that proline and charged

202 amino acid substitutions most negatively impact BRaf abundance (Extended Data Fig. 3g)[29]. Notably, the
203 LABEL-seq-calculated abundance scores of individual BRaf variants representing a range of expression
204 levels were highly correlated with the levels of variants that were not fused to tdMCP assessed by western
205 blot quantification (Pearson's R^2=0.95, Fig. 3g). Thus, LABEL-seq can accurately and precisely measure
206 protein variant abundance at scale.

207 Our abundance profiling shows that the 80 profiled positions of BRaf were highly tolerant of
208 substitution, with 86.8% of missense variants demonstrating WT-like abundance (Fig. 3f and Extended
209 Data Fig. 3g). The permissiveness of these 80 positions to undergo substitution without affecting
210 abundance is notable based upon previous observations where up to 50% of substitutions are not
211 tolerated in some proteins[28], but is consistent with their location on BRaf. Profiled regions of BRaf include
212 the linker connecting the cysteine-rich domain (CRD) to the kinase domain, the kinase domain's
213 phosphate-binding loop (P-loop), activation loop, and C-terminal tail, which are all flexible and structurally
214 dynamic (Extended Data Fig. 3h,i). In comparing the structures of autoinhibited and activated BRaf, many
215 of the positions profiled also undergo large conformational transitions between regulatory states[32, 33](Fig.
216 3h). Calculation of position-averaged abundance scores showed that select positions are relatively
217 intolerant to substitution (Fig. 3h). These positions are situated in regions that are comparably less
218 conformationally dynamic than other profiled positions, with four of the five lowest average abundance
219 scores being constituents of β-strands despite only 12.5% of all profiled positions being classified as β-
220 stranded (Extended Data Fig. 3i). The two positions that were least tolerant to substitution, I582 and I592,
221 are located on adjacent β-strands, make hydrophobic contacts, and are structurally invariant in the
222 autoinhibited and active forms of BRaf (Fig. 3h and Extended Data Fig. 3j). Our results are consistent with
223 systematic analyses showing that disease-relevant mutations commonly alter the biochemical properties
224 of a protein without dramatically affecting its folding and stability,[34,35] and suggest that most sites of
225 somatic cancer mutations in BRaf can readily accumulate gain-of-function activities because substitutions
226 at these positions have a minimal effect on abundance.
227
228
229
230

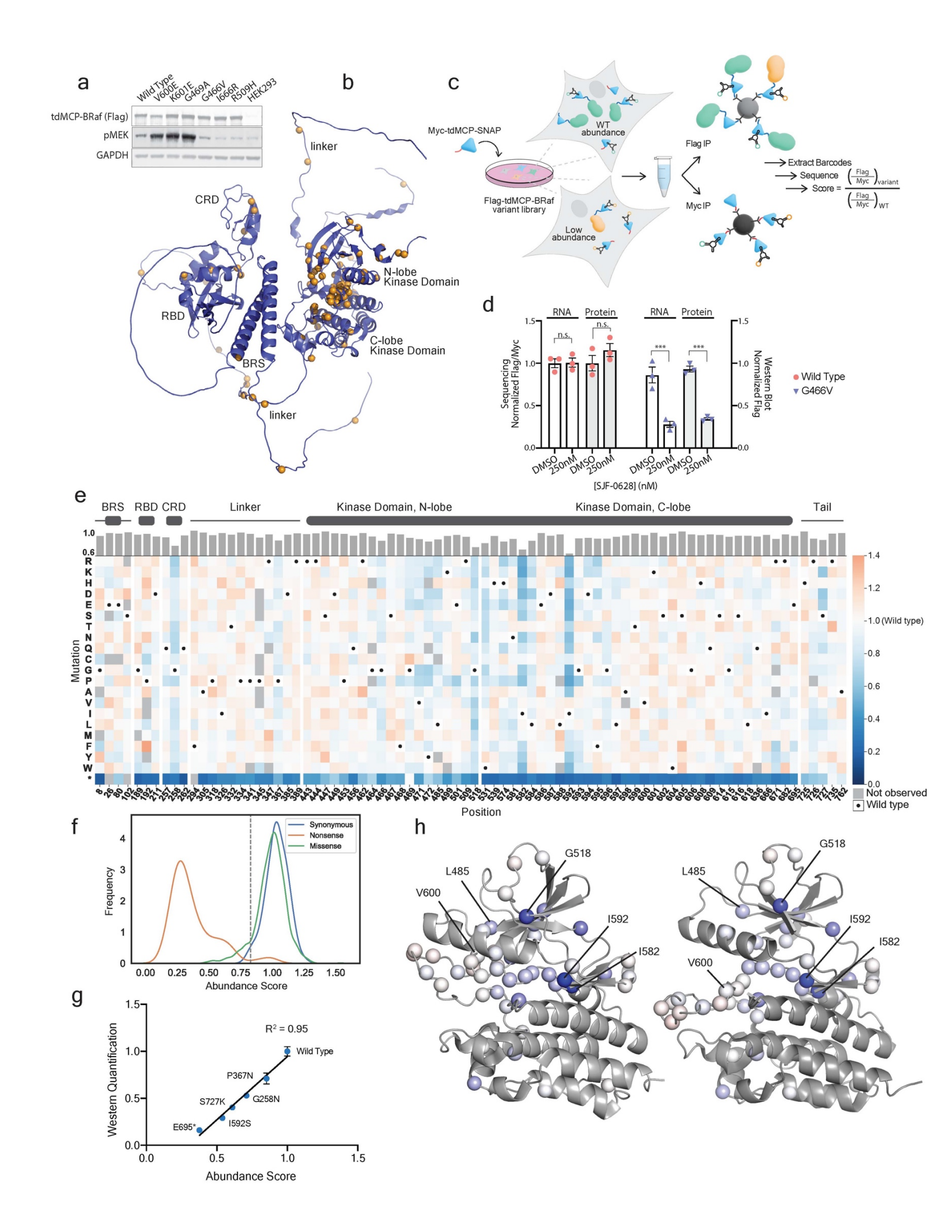
a
Wild Type
V600E
K601E
G469A
G466V
I666R
R509H
HEK293
tdMCP-BRaf (Flag)
pMEK
GAPDH
b
linker
CRD
RBD
BRS
N-lobe
Kinase Domain
C-lobe
Kinase Domain
linker
c
Myc-tdMCP-SNAP
Flag-tdMCP-BRaf
variant library
WT
abundance
Low
abundance
Flag IP
Myc IP
Extract Barcodes
Sequence
Score =
d
RNA
Protein
RNA
Protein
n.s.
n.s.
***
***
Sequencing
Normalized Flag/Myc
Western Blot
Normalized Flag
Wild Type
G466V
DMSO
250nM
DMSO
250nM
DMSO
250nM
DMSO
250nM
[SJF-0628] (nM)
e
BRS
RBD
CRD
Linker
Kinase Domain, N-lobe
Kinase Domain, C-lobe
Tail
Mutation
Position
Not observed
Wild type
1.0 (Wild type)
f
Synonymous
Nonsense
Missense
Frequency
Abundance Score
g
R² = 0.95
Wild Type
P367N
G258N
S727K
I592S
E695*
Western Quantification
Abundance Score
h
G518
L485
V600
I592
I582

232 **Fig. 3 | Multiplexed abundance measurements reveal BRaf's tolerance for substitution at positions**
233 **where somatic mutations are frequently observed. a,** Western blot analysis of HEK293 RPLP cells stably
234 expressing tdMCP-BRaf variants. **b,** AlphaFold2 model (AF-15056-F1) of full-length human BRaf. Varied
235 positions in the untagged and tdMCP-BRaf variant libraries are shown as orange spheres. **c,** Schematic
236 depicting the LABEL-seq abundance assay in which a tdMCP standard (Myc-tdMCP-SNAP) is co-expressed
237 with a tdMCP-variant library. Abundance scores are WT-normalized ratios of variant barcode sequence
238 counts derived from parallel Flag and Myc immunoprecipitations (IP). **d,** Comparison of abundance
239 measurements obtained by western blotting (right, y-axis = ratio of Flag signal to Myc signal normalized
240 to Flag-tdMCP-BRaf WT-expressing cells treated with DMSO) or by quantifying co-enriched MS2-circRNA
241 barcode sequences with high-throughput sequencing. (left, y-axis = the ratio of barcode sequence counts
242 derived from parallel Flag and Myc enrichments normalized to Flag-tdMCP-BRaf WT-expressing cells
243 treated with DMSO). HEK293T cells co-expressing MS2-circRNAs, the Myc-tdMCP-SNAP standard, and
244 Flag-tdMCP-BRaf WT (pink circles) or G446V (blue triangles) were treated with DMSO or the variant-
245 selective degrader SJF0628 for 24 h prior to lysis. The average of 4 barcode sequence ratios per condition
246 is shown per replicate (marked by symbol). Error bars = standard error of the mean (SEM) of replicate
247 scores. Westerns are shown in Extended Data 3f. **e,** Sequence-abundance map for BRaf variants in the
248 tdMCP-BRaf library. The abundance scores shown are the average of two replicates, each involving an
249 independent Myc-tdMCP-SNAP standard transduction, cell lysis, parallel Flag and Myc
250 immunoprecipitations, and quantification by high-throughput sequencing. Black dots in the map indicate
251 the WT amino acid and gray tiles indicate missing data. Position-averaged abundance scores are shown in
252 the bar graph above the heatmap. **f,** LABEL-seq abundance score distributions for all synonymous WT and
253 nonsynonymous BRaf variants. The gray dashed line indicates the abundance score value (>2 standard
254 deviations of the synonymous distribution lower than WT) we defined as decreased abundance. **g,**
255 Individually assessed variant abundances measured by western blotting (n=3) compared to abundance
256 scores determined with the LABEL-seq abundance assay for a panel of BRaf variants (Pearson's R^2 = 0.95).
257 Error bars = SEM. **h,** Position-averaged abundance scores for each position in the tdMCP-BRaf variant
258 library (represented as spheres) projected onto the structures of (left) autoinhibited (PDB ID: 6NYB) and
259 (right) active BRaf (PDB ID: 4MNE). The shade of blue indicates position-averaged abundance score: white
260 = 1, darkest blue = 0.72.
261

262 **Profiling of intracellular BRaf variant activity with LABEL-seq**

263 We next developed a LABEL-seq assay that provides quantitative measurements of intracellular
264 enzymatic activity by co-expressing untagged protein variants and their encoding MS2-circRNAs with
265 tdMCP-fused substrates and selectively enriching products (Fig. 4a). Because Raf activates Mek and the
266 activation loop of Erk is only phosphorylated by Mek (Fig. 4b), we used Flag-tdMCP-Erk2 as the substrate
267 (pErk reporter) and anti-pErk enrichment as a readout of Raf variant activity. We first confirmed that the
268 pErk reporter was efficiently enriched from lysate (Extended Data Fig. 4a) and that enriched barcode
269 sequence frequencies were higher from cells expressing hyperactive BRaf V600E compared to BRaf WT
270 (Fig. 4c). Next, we used the LABEL-seq activity assay to profile an untagged BRaf variant library (Extended
271 Data Fig. 3d) in RPLP cells co-overexpressing CRaf because WT and many BRaf variants signal as
272 heterodimers (Fig. 4d,e)[34]. Activity scores were calculated using the ratio of WT-normalized barcode
273 sequence counts derived from parallel pErk and Flag immunoprecipitations (Fig. 4d and Supplementary
274 Table 2). Activity scores from two biological replicates were well correlated (Pearson's R^2 = 0.80, Fig. 4f
275 and Extended Data Fig. 4b,c) and BRaf variants previously shown to promote elevated pErk[34-36] had
276 significantly higher activity scores than WT (Extended Data Fig. 4c). Activity scores of individual BRaf
277 variants that represent a range of activity levels were also highly correlated with pErk levels quantified by
278 western blotting (Pearson's R^2 = 0.95, Fig. 4g).

279 We classified variants as activating or inactivating (Extended Data Fig. 4d,e), and found that 32.8%
280 and 2.3% were activating and inactivating, respectively (Extended Data Fig. 4e,f). The small percentage of
281 inactivating variants and the observation that positions involved in the formation of active Raf dimers
282 possessed the lowest average activity scores (Extended Data Fig. 4g) is consistent with BRaf WT existing
283 primarily as an autoinhibited monomer in unstimulated HEK293 cells. Observed activating variants are
284 broadly distributed across BRaf, with a number of positions containing multiple activating mutations.

285 Because BRaf WT mainly exists in an inactive monomeric state stabilized by a network of
286 interactions in unstimulated cells, we reasoned that positions participating in autoinhibitory interactions
287 should possess multiple activating mutations. We identified 17 potentially autoinhibitory positions where
288 >75% of substitutions were classified as activating (Supplementary Table 3). Two of these positions–G258
289 and P367–are in BRaf's N-terminal CRD and RBD domains, respectively, and substitutions at these
290 positions likely disrupt autoinhibitory protein-protein interactions (Extended Data Fig. 4h,i). Nine
291 potentially autoinhibitory positions form a spatial cluster in the kinase domain of autoinhibited but not
292 active BRaf (Fig. 4h). In the autoinhibited conformation, the side chains of four of these positions in the
293 activation loop (L597, T599, V600 and K601) form interactions with three positions in the P-loop (S467,

294 F468, and G469) and L485. The side chain of W604 does not form obvious contacts with these positions
295 but appears to be part of this autoinhibitory network based on its proximity and high percentage of
296 activating mutations. Our data are consistent with previous speculation based on structural studies that
297 eight of these nine positions participate in stabilizing an "autoinhibitory turn"[36-38], and suggest that this
298 region of BRaf's kinase domain contains a finely tuned autoinhibitory interaction network that can readily
299 be disrupted through mutation to achieve increased BRaf activity.

300 To examine the effects of heterodimerization on BRaf variant activity, we repeated the LABEL-seq
301 activity assay in the absence of overexpressed CRaf, which provided broadly similar patterns of activating
302 and inactivating mutations (Extended Data Fig. 5a-d), and calculated the difference in activity score with
303 and without CRaf ("CRaf-promoted activity", Figure. 4i). We observed that seven of the ten positions with
304 the highest average CRaf-promoted activity scores are highly conserved across the human kinome[39] and
305 are largely clustered in and around the ATP-binding pocket (Fig. 4j and Extended Data Fig. 5e). Among
306 these highly conserved positions, mutations at G466, N581, D594, and G596 have been previously
307 demonstrated to impair BRaf's kinase activity[34, 36] while retaining the ability to increase cellular pErk levels
308 through heterodimerization and transactivation of CRaf[34]. Two other positions with the highest average
309 CRaf-promoted activity, G615 and S616, are not conserved but are positioned on the BRaf:Mek interface
310 (Fig. 4j), suggesting that substitutions at these positions disrupt BRaf's interaction with its substrate but
311 not its ability to activate CRaf in trans. Together, our data show that disruption of catalytic machinery
312 within the ATP-binding site or prevention of Mek binding is a general mechanism for increasing BRaf's
313 reliance on CRaf for promoting downstream signaling.
314
315

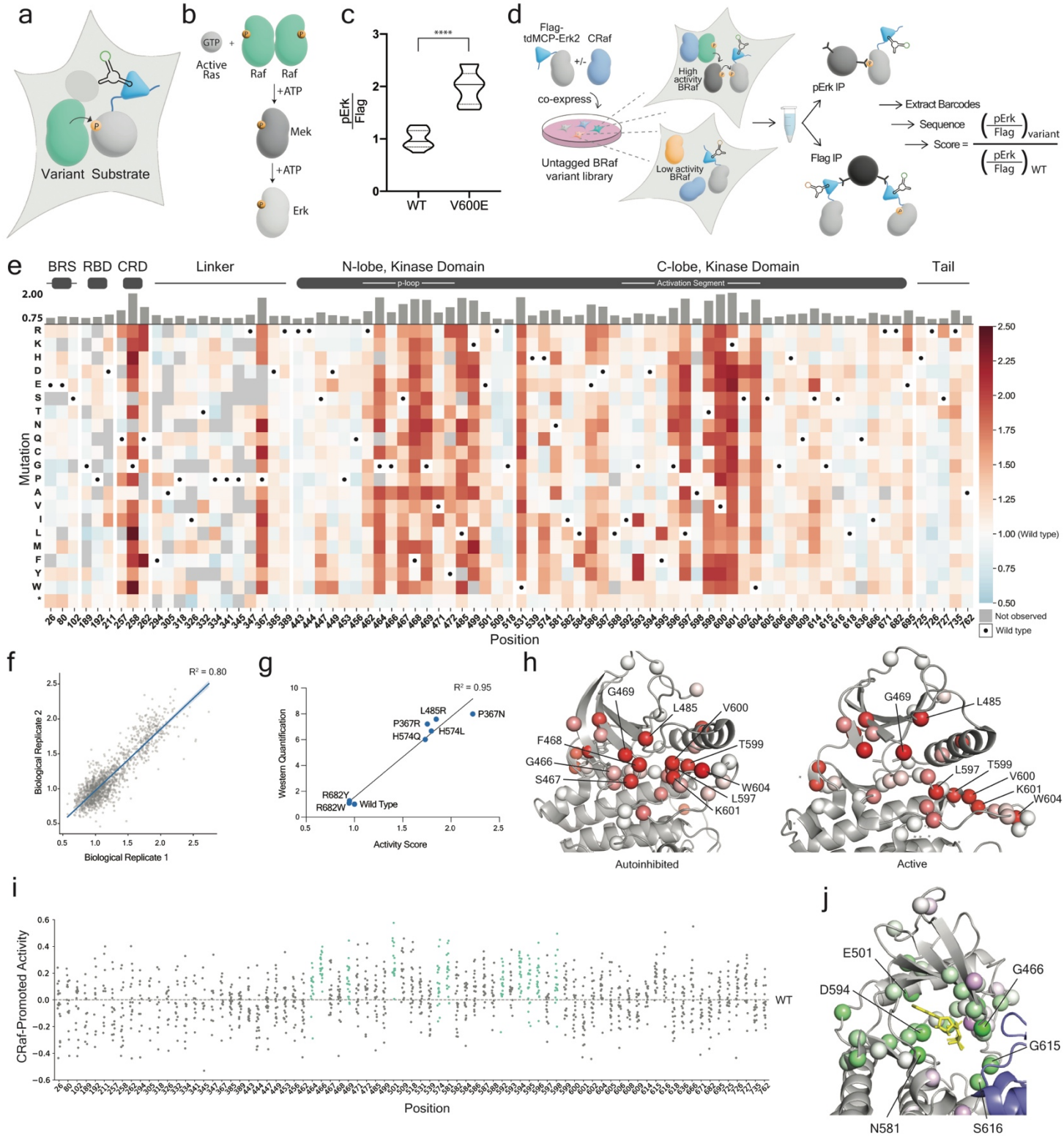
a
Variant
Substrate
b
GTP
Active Ras
Raf
Raf
+ATP
Mek
+ATP
Erk
c
pErk / Flag
WT
V600E
d
Flag-tdMCP-Erk2
CRaf
+/-
co-express
Untagged BRaf variant library
High activity BRaf
Low activity BRaf
pErk IP
Flag IP
Extract Barcodes
Sequence
Score =
e
BRS
RBD
CRD
Linker
N-lobe, Kinase Domain
C-lobe, Kinase Domain
Tail
p-loop
Activation Segment
Mutation
Position
Not observed
Wild type
1.00 (Wild type)
f
Biological Replicate 1
Biological Replicate 2
g
Western Quantification
Activity Score
P367N
L485R
P367R
H574L
H574Q
R682Y
R682W
Wild Type
h
G469
L485
V600
T599
F468
G466
S467
W604
L597
K601
Autoinhibited
Active
i
CRaf-Promoted Activity
WT
Position
j
E501
G466
D594
G615
N581
S616

317 **Fig. 4 | A pErk reporter enables profiling of intracellular BRaf variant activity. a,** General schematic of
318 the LABEL-seq activity assay. **b,** The canonical Raf-Mek-Erk signaling pathway. **c,** Activities (represented as
319 the ratio of pErk and Flag barcode sequence counts) of BRaf WT and V600E in HEK293T cells co-expressing
320 Flag-tdMCP-Erk2 (pErk reporter) and MS2-circRNAs. Cells were lysed, parallel Flag and pErk
321 immunoprecipitations were performed, and the ratio of pErk/Flag counts for each co-enriched MS2-
322 circRNA barcode sequence was calculated. Center line = mean; dotted lines = inner quartiles. n=10-11
323 barcodes per variant. ****P<0.001. **d,** Schematic of the LABEL-seq assay for the multiplexed measurement
324 of untagged BRaf variant activity with the pErk reporter. **e,** Sequence-activity map for variants in the
325 untagged BRaf library co-expressed with CRaf. The activity scores shown are the average of two replicates,
326 each involving independent cell culturing, lysis, parallel pErk and Flag immunoprecipitations, and
327 quantification with high-throughput sequencing. Black dots in the map indicate the WT amino acid and
328 gray tiles indicate missing data. Position-averaged activity scores are shown in the bar graph above the
329 heatmap. The average activity score at each position is shown in the bar graph above the heatmap. **f,**
330 Scatterplot showing activity score correlations between the two independent replicates shown in **e**
331 (Pearson's R^2 = 0.80). **g,** Individually assessed pErk levels measured by western blotting (n=3) compared
332 to activity scores determined with the LABEL-seq activity assay for a panel of BRaf variants (Pearson's R^2
333 = 0.95). Error = SEM. **h,** The number of activating variants at each position in the untagged BRaf variant
334 library (represented as spheres) projected onto the (left) inactive (PDB ID: 6NYB) and (right) active
335 conformations (PDB ID: 4MNE) of BRaf's kinase domain. The number of activating variants at a position is
336 represented by the shade of red: white = 0 activating variants, brightest red = 19 activating variants. G466,
337 S467, and F468 are not resolved in the active conformation of BRaf's kinase domain. **i,** CRaf-promoted,
338 BRaf variant activity at each position in the untagged BRaf variant library. CRaf-promoted activity scores
339 were calculated by determining the difference between BRaf variant activity scores, which were each
340 normalized to BRaf WT in the absence or presence of co-expressed CRaf. Positions highly conserved
341 amongst protein kinases are shown in green. Gray dashed line indicates the WT score (0). Positive and
342 negative values indicate more or less activity promoted by CRaf, respectively. **j,** Position-averaged CRaf-
343 promoted activity scores projected onto the structure of the autoinhibited BRaf:Mek complex (PDB ID:
344 6NYB) bound to ATP-γ-S. Purple spheres are scores less than 0 (decreased activity with CRaf) and green
345 spheres are scores greater than 0 (increased activity with CRaf).
346
347
348

349 **Proximity labeling-based profiling of intracellular protein-protein interactions with LABEL-seq**

350 Raf activity is modulated by a number of intracellular protein-protein interactions. In the absence
351 of active Ras, BRaf WT is stabilized as an autoinhibited monomer in a complex with its substrate, Mek,
352 and two 14-3-3 proteins. Upon Ras activation, BRaf undergoes large conformational changes and forms
353 active homodimers or heterodimers with CRaf. To gain a comprehensive understanding of how sequence
354 variation affects BRaf's intracellular interactions, we developed a LABEL-seq interaction assay using
355 TurboID proximity labeling and streptavidin enrichment (Fig. 5a and Extended Data 6a-e). We first
356 validated that TurobID could reliably report on BRaf interactions by co-expressing a TurboID-Mek1 fusion
357 with tdMCP-BRaf WT or I666R, a BRaf:Mek-disrupting variant, and treating cells with biotin. We observed
358 that tdMCP-BRaf I666R showed expected reduced biotinylation levels relative to WT (Fig. 5b) and that
359 streptavidin enrichment followed by barcode sequence quantification recapitulated these differences
360 (Fig. 5c). Both tdMCP-BRaf variants showed markedly higher signals than an unrelated cytosolic kinase
361 (tdMCP-BTK), which was used as an estimate of non-specific labeling (Fig. 5c). We further found that the
362 LABEL-seq interaction assay provided expected increases in tdMCP-BRaf WT labeling by TurboID-CRaf or
363 TurboID-BRaf in cells treated with a dimer-promoting inhibitor (Fig. 5d-f and Extended Data Fig. 6f).

364 We first used our LABEL-seq interaction assay to profile BRaf:CRaf heterodimerization by co-
365 expressing TurboID-CRaf with the tdMCP-BRaf variant library, labeling cells with biotin, and calculating
366 CRaf interaction scores (Fig. 5g,h and Supplementary Table 1). We observed that interaction scores were
367 well correlated between biological replicates (Pearson's R^2 = 0.96, Extended Data 7b) and between 5 min
368 and 45 min labeling times (Pearson's R^2 = 0.86, Extended Data Fig. 7a). We further found that the
369 interaction score of BRaf WT was markedly higher than the non-specific labeling control, tdMCP-BTK, and
370 that BRaf variants previously shown to exhibit elevated heterodimerization with CRaf[34] had interaction
371 scores significantly above BRaf WT (Extended Data Fig. 7c). We next classified variants as forming
372 increased or decreased CRaf interactions (Extended Data Fig. 7d,e). Consistent with BRaf WT mainly
373 existing as an autoinhibited monomer in unstimulated HEK293 cells, only 5.1% of BRaf variants were
374 classified as decreased interaction (Extended Data 7e). There are a number of positions distributed
375 throughout BRaf where a majority of variants were classified as increased CRaf interaction (Fig. 5i),
376 suggesting that substitutions at these positions disrupt specific interactions that stabilize monomeric
377 BRaf. Notably, nonsense mutations that truncate BRaf C-terminal to the RBD and CRD provided some of
378 the highest interaction scores, confirming that BRaf's CRD can act in trans with CRaf's kinase domain[40].
379 Given that BRaf WT signals as a dimer, we were curious whether most mutations that promote CRaf
380 heterodimerization are also activating. Although we did not find a strong correlation between activity and

381 CRaf interaction scores (Extended Data Fig. 7f), 82% (406) of the 493 missense variants classified as
382 activating were also classified as increased CRaf interaction. Together, our CRaf interaction data support
383 the model that BRaf WT exists primarily as an autoinhibited monomer, which somatic mutations or
384 upstream signaling events are capable of releasing to allow CRaf heterodimerization.

385 We next profiled the interactions of BRaf with its substrate by co-expressing TurboID-Mek1 with
386 the tdMCP-BRaf variant library, labeling cells with biotin (Fig. 5j and Supplementary Table 1), and
387 calculating Mek1 interaction scores (Pearson's R^2 = 0.80, Extended Data Fig. 7g-i). Interaction scores for
388 BRaf I666R and the non-specific labeling control were both significantly lower than BRaf WT (Extended
389 Data Fig. 7j), and Mek1 interaction scores were consistent with levels of Mek1 co-IP'd with individual BRaf
390 variants (Extended Data Fig. 7k). Unlike CRaf, a larger percentage of mutations decreased (28.4%) rather
391 than increased (6.0%) BRaf's interaction with Mek1 (Extended Data Fig. 7h), consistent with autoinhibited
392 BRaf WT existing in a stable complex with Mek. As expected, the lowest interaction scores were for
393 nonsense variants that truncated BRaf prior to the disordered C-terminal tail of the kinase domain (Fig. 5j
394 and Extended Data Fig. 7i) and the five sites directly lining the BRaf:Mek interface. Notably, 84% of
395 missense variants not on the BRaf:Mek interface that were classified as decreased Mek interaction were
396 also classified as increased CRaf interaction, suggesting that weakening the interaction with Mek allows
397 heterodimerization with CRaf.

398 To obtain a structural understanding of which positions contribute to BRaf's interactions with CRaf
399 and Mek1, we projected position-averaged interaction scores onto the structure of autoinhibited BRaf
400 bound to an ATP analogue (Fig. 5k,l). Consistent with ATP interactions stabilizing monomeric BRaf[37], we
401 observed that most positions that line the ATP-binding pocket possessed high position-averaged CRaf
402 interaction scores. Intriguingly, positions with low average Mek1 interaction scores also line the ATP-
403 binding pocket, suggesting that disruption of BRaf's interactions with ATP weakens a stable BRaf:Mek
404 autoinhibitory complex (Fig. 5l and Extended Data Fig. 7l,m). Together, our data highlight a unique feature
405 of BRaf regulation where ATP, Mek, and monomeric BRaf form a stable autoinhibitory complex that can
406 readily be disrupted through mutation to allow BRaf:CRaf heterodimerization.
407

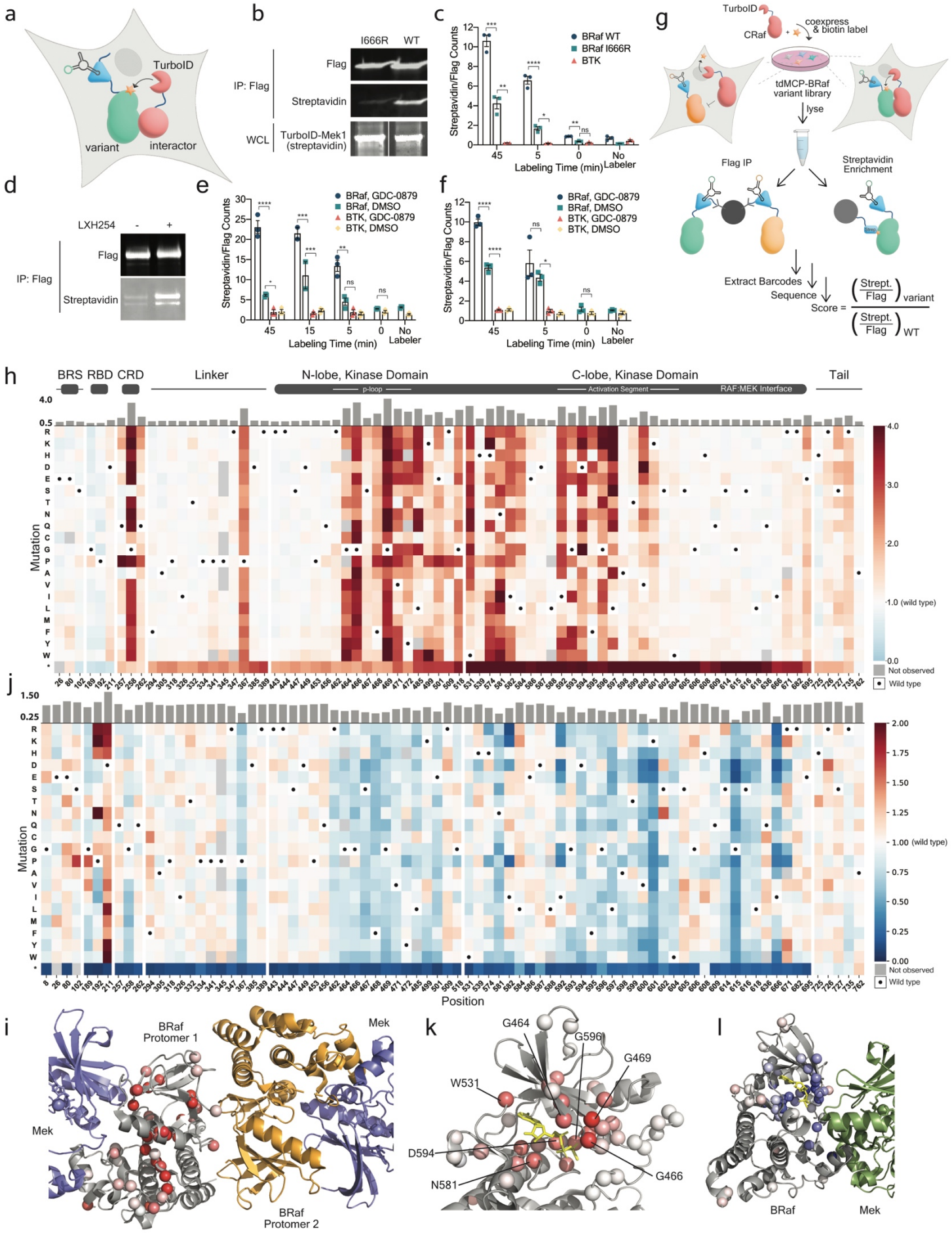
a
TurboID
variant
interactor
b
I666R
WT
IP: Flag
Flag
Streptavidin
WCL
TurboID-Mek1 (streptavidin)
c
BRaf WT
BRaf I666R
BTK
Streptavidin/Flag Counts
Labeling Time (min)
45
5
0
No Labeler
d
LXH254
-
+
IP: Flag
Flag
Streptavidin
e
BRaf, GDC-0879
BRaf, DMSO
BTK, GDC-0879
BTK, DMSO
Streptavidin/Flag Counts
Labeling Time (min)
45
15
5
0
No Labeler
f
BRaf, GDC-0879
BRaf, DMSO
BTK, GDC-0879
BTK, DMSO
Streptavidin/Flag Counts
Labeling Time (min)
45
5
0
No Labeler
g
TurboID
CRaf
coexpress & biotin label
tdMCP-BRaf variant library
lyse
Flag IP
Streptavidin Enrichment
Extract Barcodes
Sequence
Score = (Strept./Flag)variant / (Strept./Flag)WT
h
BRS
RBD
CRD
Linker
N-lobe, Kinase Domain
C-lobe, Kinase Domain
Tail
p-loop
Activation Segment
RAF:MEK Interface
Mutation
1.0 (wild type)
Not observed
Wild type
j
Mutation
Position
1.0 (wild type)
Not observed
Wild type
i
BRaf Protomer 1
Mek
Mek
BRaf Protomer 2
k
G464
G596
G469
W531
D594
N581
G466
l
BRaf
Mek

409 **Fig. 5 | LABEL-seq measurements of the intracellular interactions of BRaf variants with CRaf and Mek1.**
410 **a,** General schematic of the proximity labeling-based LABEL-seq interaction assay. **b,** Biotinylation levels
411 of Flag-tdMCP-BRaf I666R (left) and WT (right) in HEK293 cells co-expressing TurboID-Mek1 and labeled
412 with biotin for 90 min. **c**, Biotinylation levels (represented as the ratio of streptavidin and Flag barcode
413 sequence counts) of Flag-tdMCP-BRaf WT (blue circles), I666R (teal squares) and background control Flag-
414 tdMCP-BTK (pink triangles) in HEK293T cells co-expressing TurboID-Mek1 and MS2-circRNAs, and treated
415 with biotin for 0, 5, or 45 min. Following biotin treatment, cells were lysed, pooled, parallel streptavidin
416 and Flag enrichments were performed, co-enriched barcodes were quantified by high-throughput
417 sequencing, and the ratio of streptavidin and Flag counts for each co-enriched MS2-circRNA barcode
418 sequence was calculated (n=3 barcodes/treatment, mean +/- SEM, *P<0.0332, **P<0.0021, ***P<0.0002,
419 ****P<0.0001). **d**, Biotinylation levels of Flag-tdMCP-BRaf WT in HEK293T cells co-expressing TurboID-
420 CRaf, treated with DMSO (left) or type 2 inhibitor LXH-254 (right) for 4 h, and then labeled with biotin for
421 90 min. **e,** Biotinylation levels (represented as the ratio of streptavidin and Flag barcode sequence counts)
422 of Flag-tdMCP-BRaf WT and Flag-tdMCP-BTK in HEK293T cells co-expressing TurboID-CRaf and MS2-
423 circRNAs, which were treated DMSO or GDC-0879 for 2 h followed by labeling with biotin for 0, 5, 15, or
424 45 min. Following biotin addition, cells were lysed, parallel streptavidin and Flag enrichments were
425 performed, and the ratio of streptavidin and Flag counts for each co-enriched MS2-circRNA barcode
426 sequence was calculated using high-throughput sequencing. **f,** Biotinylation levels (represented as the
427 ratio of streptavidin and Flag barcode sequence counts) of Flag-tdMCP-BRaf WT and Flag-tdMCP-BTK in
428 HEK293T cells co-expressing TurboID-BRaf and MS2-circRNAs, which were treated DMSO or GDC-0879 for
429 2 h followed by labeling biotin for 0, 5, or 45 min. Following biotin addition, cells were treated as described
430 in **e**. For **e**,**f** (n=2-3 barcodes/treatment, mean +/- SEM, *P<0.0332, **P<0.0021, ***P<0.0002,
431 ****P<0.0001) **g**, Schematic of the LABEL-seq assay for the multiplexed measurement of intracellular BRaf
432 variant interactions. **h,** Sequence-CRaf interaction map for variants in the tdMCP-BRaf library co-
433 expressed with TurboID-CRaf and labeled with biotin for 5 min. The interaction scores shown are the
434 average of two replicates, each involving an independent cell culturing, biotin labeling, parallel
435 streptavidin and Flag enrichments, and quantification with high-throughput sequencing. Black dots in the
436 map indicate the WT amino acid and gray tiles indicate missing data. Position-averaged CRaf interaction
437 scores are shown in the bar graph above the heatmap. **i,** The number of variants at each position that
438 were classified as increased CRaf interaction in **h** projected onto a structure of BRaf's kinase domain within
439 the active BRaf dimer complex (PDB: 4MNE). White = 0 increased CRaf interaction variants, brightest red
440 = 19 increased CRaf interaction variants. **j,** Sequence-Mek1 interaction map for variants in the tdMCP-

441 BRaf library co-expressed with TurboID-Mek1 and labeled with biotin for 5 min. The Mek1 interaction
442 scores shown are the average of two replicates, each involving an independent transfection, biotin
443 labeling, parallel streptavidin and Flag enrichments, and quantification with high-throughput sequencing.
444 Black dots indicate the WT amino acid and gray tiles indicate missing data. Position-averaged Mek1
445 interaction scores are shown in the bar graph above the heatmap. **k,** Position-averaged CRaf interaction
446 scores for each position in the tdMCP-BRaf variant library (represented as spheres) projected onto a
447 structure of autoinhibited BRaf bound to ATP-γ-S (PDB ID: 6NYB). The shade of red indicates the position-
448 averaged CRaf interaction score: white = 1, brightest red > 3.2. **l,** Position-averaged Mek1 interaction
449 scores projected onto the structure of the autoinhibited BRaf complex (PDB ID: 6NYB). The shade of blue
450 indicates the position-averaged Mek1 interaction score: white = 1, darkest blue < 0.5.
451
452 **Hierarchical clustering identifies groups of BRaf positions with similar biochemotypes**
453 Our profiling data indicate substitutions at certain positions in BRaf result in dramatic changes to
454 multiple biochemical properties, but we were unable to identify positions with similar functions or gain a
455 mechanistic understanding of the positional effects of substitution using pairwise analyses (Extended Data
456 Fig. 8a). Therefore, we performed hierarchical clustering based on the six biochemical properties
457 measured with LABEL-seq to group positions into nine distinct biochemical phenotypes (biochemotypes)
458 (Fig. 6a,b). Clusters 7–9, which encompassed 64% of profiled positions, were characterized by a
459 biochemotype in which most variants exhibited modest effects on the six measured biochemical
460 properties. In contrast, cluster 1 positions are defined by a biochemotype where mutations resulted in
461 some of the largest decreases in Mek interactions and largest increases in activity and CRaf
462 heterodimerization, with minimal CRaf-promoted activity (Fig. 6a,c). One cluster 1 position–P367–is
463 proximal to the autoinhibitory phosphorylation site, S365[41], and sits within a 14-3-3 binding pocket in the
464 autoinhibited BRaf complex (Extended Data Fig. 4i). Substitutions at P367 likely disrupt the autoinhibited
465 BRaf complex and allow formation of active Raf dimers based on the known binding specificity of 14-3-3
466 proteins[42] and the biochemotype of this position. The six other cluster 1 positions are located in two
467 different regions of BRaf's ATP-binding site (Fig. 6c). Four of these positions (F468, L485, L597 and V600)
468 are components of the autoinhibitory turn (Fig. 4h) and are spatially clustered in the autoinhibited but
469 not the active form of BRaf, suggesting that mutations at these positions promote increased activity and
470 CRaf heterodimerization by disrupting autoinhibitory interactions. Despite their disparate locations,
471 positions in cluster 1 appear to share a common functional role in stabilizing the autoinhibited state, which

472 can be readily disrupted by mutations without compromising the ability of BRaf variants to form
473 catalytically active Raf dimers.
474 Cluster 2 positions, proximal to cluster 1 autoinhibitory turn positions (Extended Data Fig. 8b),
475 exhibited the biochemotype of increased activity and decreased Mek interactions upon substitution like
476 cluster 1, but without the accompanying strong increase in CRaf heterodimerization. The ability of
477 mutations in cluster 2 to increase kinase activity and decrease Mek interactions suggest that these
478 positions also play a role in stabilizing autoinhibited BRaf. However, mutations at cluster 2 positions
479 appear to compromise BRaf's strong association with CRaf once autoinhibition is released. Positions in
480 clusters 4 and 5 demonstrated a biochemotype where substitutions strongly promoted CRaf
481 heterodimerization and decreased Mek interactions, but, in contrast to clusters 1 and 2, only modestly
482 increased Raf activity, which was highly CRaf dependent. Cluster 4 and 5 positions are located deep within
483 BRaf's active site (Fig. 6b,d) and form a contiguous spatial network in the active form of BRaf (Fig. 6d).
484 Additionally, nearly all positions in clusters 4 and 5 are highly conserved amongst protein kinases[39, 43] and
485 many make contacts with ATP[37] or are part of the kinase catalytic machinery (Extended Data Fig. 5e). The
486 biochemotype of clusters 4 and 5 suggest that these positions participate in the stabilization of
487 autoinhibited BRaf. However, mutations at these positions likely impair BRaf's kinase activity, rendering
488 cluster 4 and 5 variants dependent on their ability to form strong CRaf heterodimers for Mek activation.
489 Together, our multimodal analysis reveals that a number of positions in BRaf that are frequently mutated
490 in cancer participate in finely tuned autoinhibitory interactions that most mutations are capable of
491 destabilizing. The signaling properties of these BRaf variants with disrupted autoinhibition can be
492 classified into several distinct biochemotypes based on their location.
493
494 **LABEL-seq-guided prediction of a variant-promoted cellular phenotype**
495 We next determined whether LABEL-seq data could be used to predict which biochemical
496 properties of BRaf variants are capable of driving complex phenotypes such as cell proliferation. Here, we
497 trained logistic models using previously collected data that classified 65 BRaf variants as activating,
498 inactivating, or neutral based on their ability to promote the growth factor-independent proliferation of
499 Ba/F3 and MCF10A cells[44]. Models that used only one biochemical property had modest classification
500 accuracy (balanced accuracy: 0.33-0.57l; Fig. 6e). However, a model that used all six biochemical
501 properties measured with LABEL-seq provided the highest accuracy (balanced accuracy = 0.68) and,
502 critically, was the only model capable of correctly identifying BRaf variants of all three classifications
503 (activating, incactivating, or neutral; Fig. 6e). We applied this six-property classifier to the 239 somatic

504 mutations cataloged in TCGA, COSMIC, and ClinVar and for which we obtained LABEL-seq data, and found
505 that 40.6% were predicted to be activating and 14.2% were predicted to be inactivating (Supplemental
506 Table 3). Notably, 92% of somatic variants previously determined to be activating based on increased
507 intracellular pErk levels or growth factor-independent cell proliferation in separate analyses were
508 correctly classified by our model as activating (Supplemental Table 1). Thus, measuring multiple
509 biochemical properties for the same variant, enabled by LABEL-seq, facilitated prediction of a complex
510 cellular phenotype.
511
512 **Measurement and modeling of small molecule-promoted BRaf degradation**
513 We next explored whether LABEL-seq data could be used to provide insight into another poorly
514 understood cellular process: small molecule-promoted protein degradation[45]. Specifically, we
515 investigated the Vemurafenib-based PROTAC SJF0628 (Extended Data Fig. 9a), which promotes selective
516 degradation of several BRaf variants[31]. We first used the LABEL-seq abundance assay to profile the
517 degradation of the tdMCP-BRaf variant library across a range of SJF0628 concentrations (Fig. 6f and
518 Supplementary Table 1) and calculated degradation scores for all ~1,600 variants (Extended Data Fig.
519 9b,c). As expected, BRaf WT was largely resistant to degradation by SJF0628 (Supplementary Table 2) but
520 a number of variants, including previously characterized SJF0628-sensitive variants[31] (Extended Data Fig.
521 9d), showed dose-dependent decreases in abundance. Additionally, LABEL-seq-derived degradation
522 scores were consistent with levels of protein degradation quantified by western blot (Extended Data Fig.
523 9c). We classified variants as sensitized or resistant to degradation at the highest concentration of SJF0628
524 tested and observed that 22.9% of variants were sensitized and 13.5% were resistant (Extended Data Fig.
525 9e and Supplementary Table 1). Among the 239 somatic mutations for which we measured degradation
526 scores and that are listed in TCGA, COSMIC, or ClinVar, we found that 32.3% were sensitized to
527 degradation relative to BRaf WT and 9.2% were resistant. Notably, variants at the same position were
528 generally either all sensitized or all resistant, suggesting that susceptibility to degradation by SJF0628 is
529 largely defined by the position of a mutation rather than its identity.
530 We explored the structural basis for the location dependence of BRaf variant PROTAC sensitivity
531 by projecting position-averaged degradation scores onto the structure of Vemurafenib-bound BRaf
532 (Extended Data Fig. 9f). Several positions within the Vemurafenib-binding pocket generally conferred
533 resistance to degradation when substituted but, surprisingly, some of the most sensitive positions were
534 located on nearby positions without an obvious structural rationale for either property. Although
535 projecting position-averaged degradation scores onto the autoinhibited structure of BRaf bound to an

536 ATP analogue revealed that substitutions at positions that make direct contacts with ATP were largely
537 sensitizing (Fig. 6g), positions with the lowest average degradation scores did not fit within any of the
538 biochemotypes we identified. Furthermore, none of the biochemical properties we measured correlated
539 strongly (R^2 = 0.051-0.36) with variant sensitivity (Extended Data Fig. 9g).

540 We performed logistic modeling to identify which biochemical properties of BRaf variants were
541 most predictive of PROTAC sensitivity. To provide additional properties that relate to ATP-competitive
542 inhibitor binding of BRaf, we used the LABEL-seq interaction assay to measure CRaf heterodimerization
543 levels promoted by the type 1.5 inhibitor Vemurafenib and the type 2 inhibitor LXH254[46] (Extended Data
544 Fig. 10a,b). The resulting eight biochemical properties, along with a subset of our measured degradation
545 classifications were used to train a logistic model to predict whether a BRaf variant was sensitized,
546 resistant, or WT-like in its degradation response at the highest concentration of SJF0628. Models using
547 any one property yielded modest classification accuracy (balanced accuracy = 0.33-0.43), but the model
548 using all eight properties was most accurate (balanced accuracy = 0.67, Fig. 6h). Only the model
549 incorporating all eight properties could accurately distinguish BRaf variants across all three classifications
550 (Fig. 6h). The properties most heavily weighted in predicting variant sensitivity to SJF0628 were the CRaf
551 interaction and Type 2 inhibitor (LXH254)-promoted heterodimerization scores (Fig. 6i), suggesting that
552 dimerization is an important component of degradation. Low basal abundance and Type 2 inhibitor
553 (LXH254)-promoted heterodimerization scores were the most predictive of whether a variant was
554 resistant to SJF0628. Notably, our data also indicate that it is not a particular "active" conformation of a
555 variant that is most predictive of SJF0628 degradation, as previously speculated[31], but each variant's
556 overall capacity to be promoted into Raf dimers. The ability of LABEL-seq to provide multimodal profiling
557 of biochemical properties facilitates the analysis of complex cellular processes that are otherwise difficult
558 to understand using single measurements.
559
560

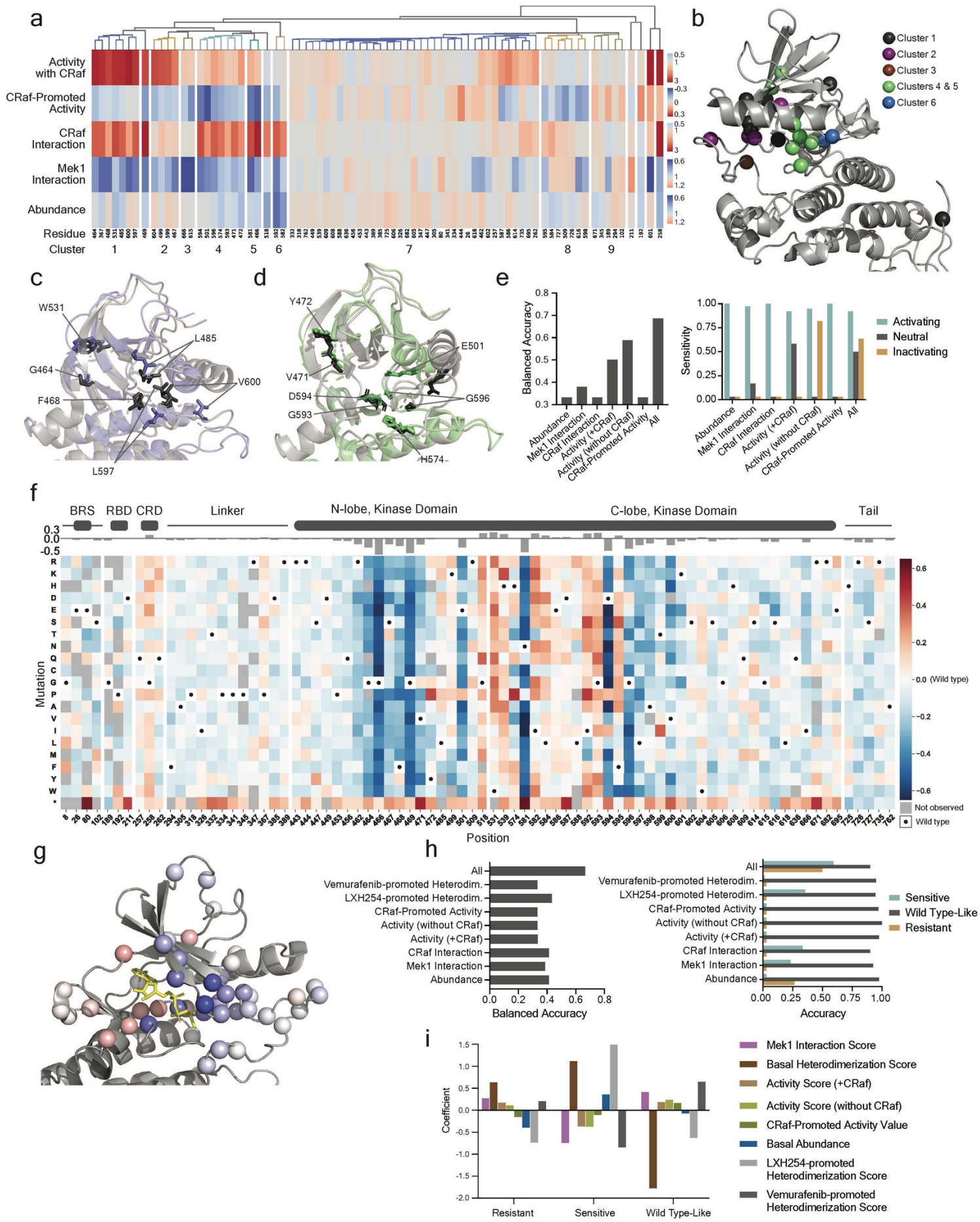
a
Activity with CRaf
CRaf-Promoted Activity
CRaf Interaction
Mek1 Interaction
Abundance
Residue
Cluster
b
Cluster 1
Cluster 2
Cluster 3
Clusters 4 & 5
Cluster 6
c
W531
L485
G464
V600
F468
L597
d
Y472
E501
V471
D594
G596
G593
H574
e
Balanced Accuracy
Abundance
Mek1 Interaction
CRaf Interaction
Activity (+CRaf)
Activity (without CRaf)
CRaf-Promoted Activity
All
Sensitivity
Activating
Neutral
Inactivating
f
BRS
RBD
CRD
Linker
N-lobe, Kinase Domain
C-lobe, Kinase Domain
Tail
Mutation
Position
(Wild type)
Not observed
Wild type
g
h
All
Vemurafenib-promoted Heterodim.
LXH254-promoted Heterodim.
CRaf-Promoted Activity
Activity (without CRaf)
Activity (+CRaf)
CRaf Interaction
Mek1 Interaction
Abundance
Balanced Accuracy
Accuracy
Sensitive
Wild Type-Like
Resistant
i
Coefficient
Resistant
Sensitive
Wild Type-Like
Mek1 Interaction Score
Basal Heterodimerization Score
Activity Score (+CRaf)
Activity Score (without CRaf)
CRaf-Promoted Activity Value
Basal Abundance
LXH254-promoted Heterodimerization Score
Vemurafenib-promoted Heterodimerization Score

562 **Fig. 6 | Integration of multimodal measurements. a,** Heatmap, with the dendrogram shown above,
563 showing hierarchical clustering of positions within BRaf based on six biochemical properties measured
564 with LABEL-seq. Clustering was performed using the average distance metric, which grouped positions
565 based on similarities in response to specific substitutions. Clusters of positions, which were selected based
566 on the dendrogram, are numbered. The heatmap color indicates the average score for each biochemical
567 property at each position. The color scale for each biochemical property is shown on the far right. **b,**
568 Positions within clusters 1-6 mapped onto the kinase domain of the autoinhibited BRaf complex (PDB ID:
569 6NYB). **c,** Alignment of BRaf's ATP-binding pocket in the active (purple, PDB ID: 4MNE) and autoinhibited
570 (gray, PDB ID: 6NYB) conformations, with cluster 1 positions shown as sticks. F468 is not resolved in the
571 active conformation of BRaf. **d,** Alignment of BRaf's ATP-binding pocket in the active (green, PDB ID:
572 4MNE) and autoinhibited (gray, PDB ID: 6NYB) conformations, with cluster 4 positions shown as sticks. **e,**
573 Performance of our logistic model predicting variant-driven proliferation of Ba/F3 and MCF10A cells in the
574 absence of growth factor. (left) Balanced accuracy for models that were fit by using a single property
575 versus all properties. (right) Model accuracy for each classification. **f,** Sequence-degradation map for BRaf
576 variants in the tdMCP-BRaf library treated with 2.5 μM SJF0628. Degradation score = [abundance score
577 for a BRaf variant at 2.5 μM SJF0628 - abundance score for a variant in DMSO]/abundance score for a
578 variant in DMSO. The degradation scores shown are the average of two replicates, each involving an
579 independent cellular treatment with SJF0628, parallel Flag and Myc immunoprecipitations, and
580 quantification by high-throughput sequencing. Black dots in the map indicate the WT amino acid and gray
581 tiles indicate missing data. The position-averaged degradation score is shown in the bar graph above the
582 heatmap. **g,** Position-averaged degradation scores for each position in the tdMCP-BRaf variant library
583 (represented as spheres) projected onto the structure of autoinhibited BRaf bound to ATP-γ-S (PDB ID:
584 6NYB). The color indicates the position-averaged degradation score: white = 0, darkest blue < -0.5,
585 brightest red > 0.18. **h,** Performance of a logistic model predicting SJF0628 sensitivity. (left) Balanced
586 accuracy for models fit using a single property versus all properties. (right) Model accuracy for each
587 classification. **i,** Coefficients for each property in the most accurate model.
588
589 **Discussion**
590 At-scale measurements of protein variant effects have provided valuable insights into numerous
591 biological processes, facilitated advances in protein engineering and design, and deepened our
592 understanding of drug sensitivity and resistance[4, 8, 12]. To expand the scope of protein targets and
593 functional properties that can be profiled at scale, we developed LABEL-seq, a general, scalable platform

594 that enables the multimodal analysis of protein variants in human cells using high-throughput DNA
595 sequencing for quantification.

596 A key strength of LABEL-seq is its modularity, which enables the profiling of multiple properties
597 for a common set of protein variants. Reconfiguration of the RNA and protein components of LABEL-seq
598 and tailoring of the biochemical enrichment step to measure specific protein properties enabled profiling
599 of the abundance, activity, protein-protein interactions, and drug sensitivity of a library of BRaf variants.
600 The high precision and sensitivity of quantification, and the flexibility to incorporate diverse biochemical
601 enrichment strategies into the LABEL-seq workflow suggest that it can be used to profile numerous
602 additional protein properties and functions. Even intracellular assays that have not been previously
603 employed for studying protein variant properties, such as our use of proximity labeling to quantify both
604 high and low affinity intracellular protein-protein interactions, are compatible with LABEL-seq. Finally,
605 since LABEL-seq only necessitates the fusion of an RNA-binding domain to a target protein of interest or
606 its substrate, it has the potential to be applied to a wide range of proteins beyond the three (BRaf, BTK,
607 and Lck) described in this study.

608 We used LABEL-seq for the multimodal profiling of BRaf positions frequently mutated in cancer,
609 complementing and expanding upon previous cellular, biochemical, and structural characterization of
610 individual BRaf variants[34, 47]. Notably, we found that most mutations at cancer-associated positions in BRaf
611 do not compromise BRaf's folding and intracellular abundance. We confirmed previous observations that
612 mutations at many of these same positions can promote increased Raf activity and dimerization[16, 36, 37].
613 Our LABEL-seq profiling data suggest that many positions in BRaf are precisely tuned to maintain an
614 autoinhibited state, which is disrupted by most sequence variations. Consequently, BRaf is finely poised
615 to acquire mutations that lead to enhanced downstream oncogenic signaling, likely due, at least in part,
616 to its ability to form functionally active dimers upon disruption of autoinhibition. As our profiling
617 experiments were conducted in the absence of elevated levels of active Ras, the biochemical properties
618 of some BRaf variants that are relevant to oncogenic signaling may have been missed. Because LABEL-seq
619 assays can be performed under variable cellular conditions, such as growth factor simulation or the co-
620 expression of an active Ras mutant, future profiling experiments that capture these properties are
621 feasible. Furthermore, while our profiling studies were conducted in HEK293 cells, it should be
622 straightforward to achieve single protein variant and single MS2-circRNA barcode sequence integration
623 into other cell lines, which will allow LABEL-seq profiling in other cellular contexts.

624 Our ability to use the LABEL-seq abundance assay to measure SJF0628's degradation of BRaf
625 variants allowed us to conduct the first comprehensive analysis of how sequence variation affects a

626 neosubstrate's degradation by a PROTAC. Remarkably, we observed that substitutions at multiple
627 positions in BRaf provided strong sensitization to degradation, with SJF0628 selectively degrading ~30%
628 of somatic variants cataloged in TCGA, ClinVar, and COSMIC relative to BRaf WT. By modeling the multiple
629 biochemical measurements obtained with LABEL-seq, we were able to obtain insight into which properties
630 sensitize a BRaf variant to degradation by SJF0628. Although no single biochemical property was
631 dominant, the ability of a BRaf variant to be recruited into heterodimers with CRaf was the most predictive
632 of sensitivity to SJF0628-mediated degradation. We also identified several positions in BRaf that contained
633 multiple mutations that conferred resistance to PROTAC-mediated degradation, providing insights into
634 resistance mechanisms that complement those revealed by a previous CRISPR-suppressor scan of the
635 neosubstrates GSPT1 and RBM39[48]. Conducting additional LABEL-seq assays with PROTACs that
636 incorporate different E3 ligase recruiters and/or alternative ATP-competitive inhibitors will enable
637 determination of whether the patterns of sensitization and resistance we observed are common to all
638 BRaf-targeting PROTACs or are specific to SJF0628, which contains a ligand for recruiting the E3 ligase von
639 Hippel-Lindau linked to the type 1.5 inhibitor vemurafenib. Furthermore, incorporating additional
640 biochemical properties into models that more accurately predict BRaf variant degradation susceptibility
641 to different PROTACs should yield additional mechanistic insight into this process.
642 Overall, we envision LABEL-seq will find widespread use for the multimodal profiling of diverse
643 proteins under different cellular conditions. The multi-dimensional profiling data obtained with this
644 platform will be a valuable resource for understanding intracellular protein function and druggability, and,
645 when integrated with MAVEs that assess composite behaviors such as transcriptional outputs and
646 proliferation, should provide invaluable insight into protein properties that drive complex cellular
647 processes.
648
649 **Acknowledgements**
650 We thank David Shechner (UW, Seattle) for guidance on RNA barcode design and Madeline Walsh (UW,
651 Seattle) for critical feedback on the manuscript. This work was supported by the NIH, grant no.
652 R01GM145011 (NIGMS) and R01GM086858 (NIGMS) to D.J.M.
653
654 **Author contribution statement**
655 J.J.S., D.M.F., and D.J.M. conceived of the work and wrote the manuscript. J.J.S. developed the LABEL-seq
656 method, performed all profiling experiments and data analysis.
657

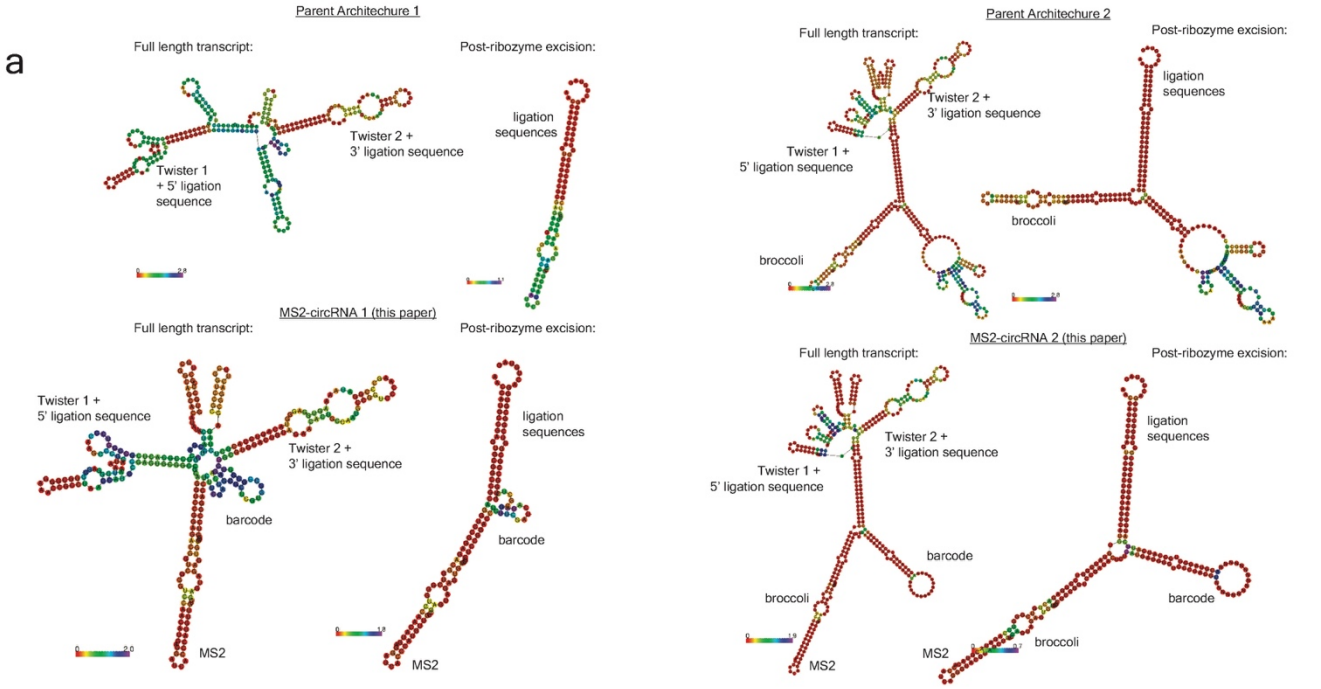
a
Parent Architechure 1
Full length transcript:
Post-ribozyme excision:
Twister 1
+ 5' ligation
sequence
Twister 2 +
3' ligation sequence
ligation
sequences
Parent Architechure 2
Full length transcript:
Post-ribozyme excision:
Twister 2 +
3' ligation sequence
Twister 1 +
5' ligation sequence
ligation
sequences
broccoli
broccoli
MS2-circRNA 1 (this paper)
Full length transcript:
Post-ribozyme excision:
Twister 1 +
5' ligation sequence
Twister 2 +
3' ligation sequence
barcode
ligation
sequences
barcode
MS2
MS2
MS2-circRNA 2 (this paper)
Full length transcript:
Post-ribozyme excision:
Twister 2 +
3' ligation sequence
Twister 1 +
5' ligation sequence
ligation
sequences
barcode
barcode
broccoli
broccoli
MS2
MS2

b
Barcode
MS2-circRNA
2
Increased stem
Barcode
MS2-circRNA
1
MS2
Increased Stem
Barcode
Priming Site
MS2-circRNA
1b
Barcode
MS2-circRNA
3
MS2-circRNA
4
Barcode
MS2-circRNA
5
Increased Stem
Barcode
Increased Stem
MS2-circRNA
6
Barcode
MS2-circRNA
7
Barcode
MS2-circRNA
8
Barcode
MS2-circRNA
9

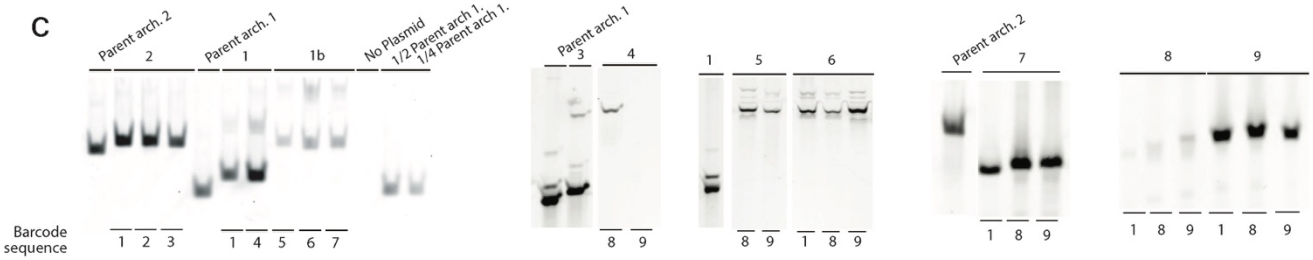
c
Parent arch. 2
2
Parent arch. 1
1
1b
No Plasmid
1/2 Parent arch 1.
1/4 Parent arch 1.
Parent arch. 1
3
4
1
5
6
Parent arch. 2
7
8
9
Barcode
sequence
1 2 3
1 4 5 6 7
8 9
8 9 1 8 9
1 8 9
1 8 9 1 8 9

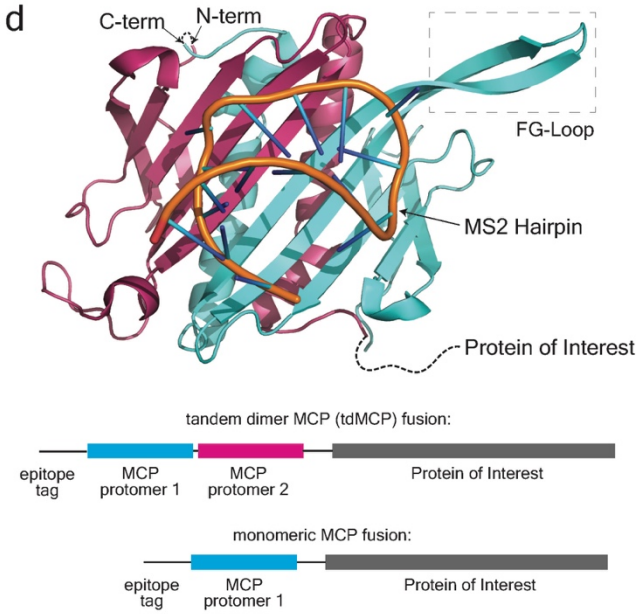
d
C-term
N-term
FG-Loop
MS2 Hairpin
Protein of Interest
tandem dimer MCP (tdMCP) fusion:
epitope
tag
MCP
protomer 1
MCP
protomer 2
Protein of Interest
monomeric MCP fusion:
epitope
tag
MCP
protomer 1
Protein of Interest

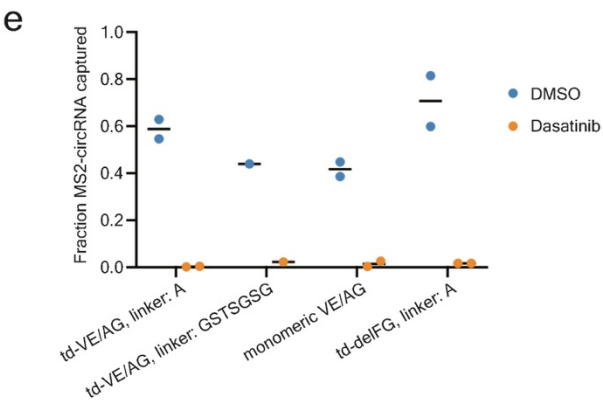
e
Fraction MS2-circRNA captured
1.0
0.8
0.6
0.4
0.2
0.0
DMSO
Dasatinib
td-VE/AG, linker: A
td-VE/AG, linker: GSTSGSG
monomeric VE/AG
td-delFG, linker: A

659 **Extended Data Fig. 1| Design, expression, and characterization of MS2-circRNAs and MCP protein**
660 **fusions. a,** In-silico folding predictions for circRNA architectures pre- and post-ribozyme excision.
661 Predictions were run using RNAfold and the colors indicate positional entropy values. Parent architectures
662 do not contain MS2 and are the designs published by Litke and Jaffrey[19] which correspond to addgene
663 plasmids #124360 (left) and #124362 (right). **b,** MS2-circRNA designs that contain a 16 nucleotide barcode
664 and 19 nucleotide MS2 hairpin. MS2-circRNA 1b contains an added priming site specifically for reverse
665 transcription. **c,** In-gel DFHBI-1T fluorescence of total RNA extracted from cells expressing the MS2-
666 circRNAs shown in b. 2-3 barcode sequences of varying GC content for each MS2-circRNA were tested.
667 Gels 1, 4, and 5 were non-denaturing 6% acrylamide gels and gels 2 and 3 were denaturing 10% acrylamide
668 gels. **d,** Structure (PDB ID: 2BU1) of the MCP dimer bound to an MS2 hairpin (top). Linear representations
669 of monomeric and tandem-dimer (td) MCP protein fusions (bottom). In a tandem dimer, the N-terminus
670 of one MCP protomer is linked to the C-terminus of a second MCP protomer by a short linker. **e,** Variants
671 of MCP-Lck protein fusions were co-expressed with MS2-circRNA 2. Lck was enriched using dasatinib-
672 conjugated agarose beads and the co-enriched MS2-circRNA was visualized by in-gel DFHBI-1T
673 fluorescence. DMSO or a free dasatinib competitor was included during enrichment to probe for specific
674 protein enrichment. td- indicates tandem dimer designs. VE/AG variants contain V75E and A81G
675 mutations, which prevent MCP oligomerization. delFG variants possess a deletion of the FG loop (V67-
676 A81), which also prevents MCP oligomerization. All MCP variants contain the high affinity V29I mutation.
677 The linkers are positioned between MCP protomers. The delFG variant was used in all subsequent
678 experiments and is referred to as 'tdMCP' throughout the manuscript.
679

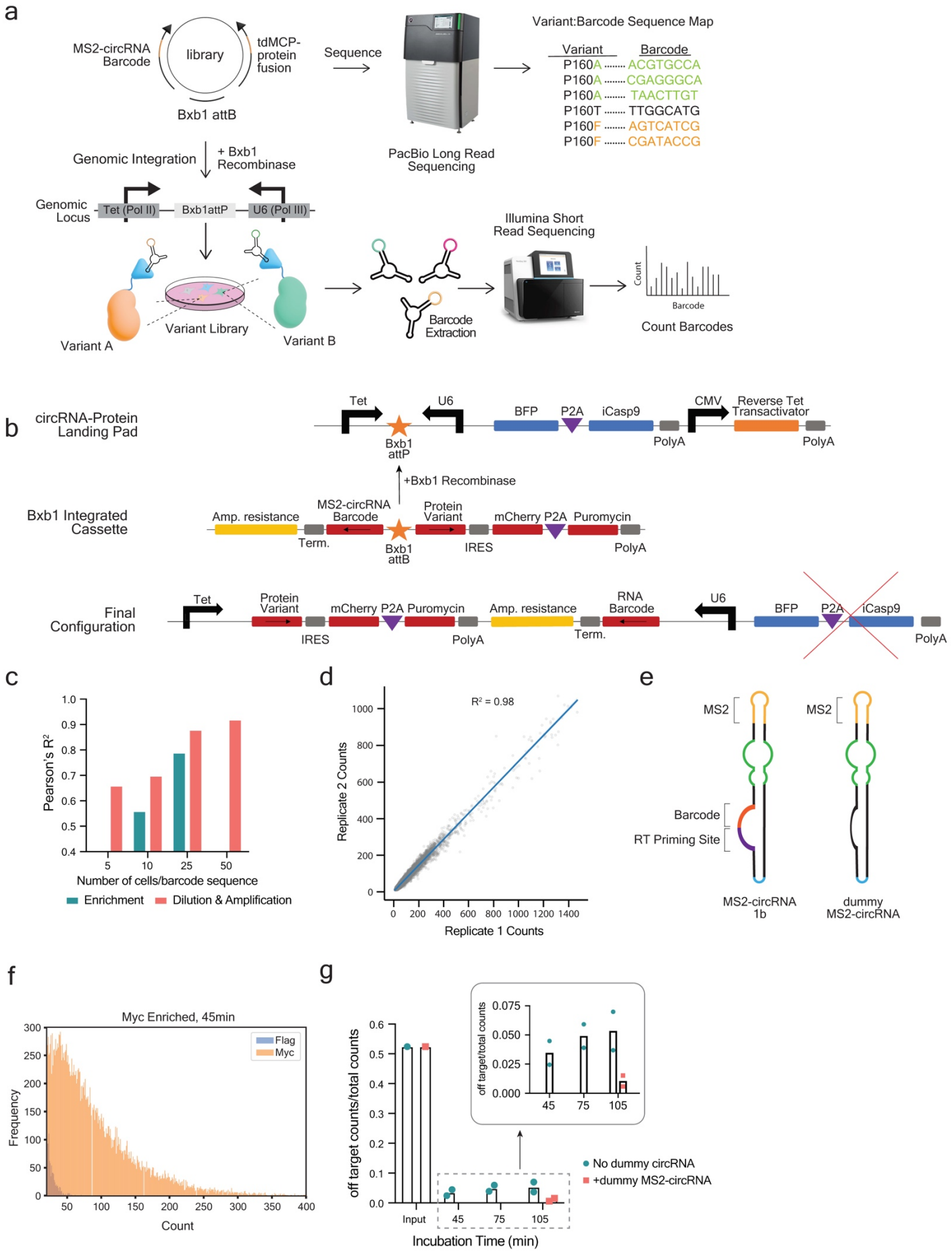
a
MS2-circRNA Barcode
library
tdMCP-protein fusion
Bxb1 attB
Sequence
PacBio Long Read Sequencing
Variant:Barcode Sequence Map
Variant Barcode
P160A ACGTGCCA
P160A CGAGGGCA
P160A TAACTTGT
P160T TTGGCATG
P160F AGTCATCG
P160F CGATACCG
Genomic Integration
+ Bxb1 Recombinase
Genomic Locus
Tet (Pol II)
Bxb1attP
U6 (Pol III)
Variant A
Variant Library
Variant B
Barcode Extraction
Illumina Short Read Sequencing
Count
Barcode
Count Barcodes
b
circRNA-Protein Landing Pad
Tet
U6
BFP
P2A
iCasp9
CMV
Reverse Tet Transactivator
Bxb1 attP
PolyA
PolyA
+Bxb1 Recombinase
Bxb1 Integrated Cassette
Amp. resistance
MS2-circRNA Barcode
Protein Variant
mCherry P2A
Puromycin
Term.
Bxb1 attB
IRES
PolyA
Final Configuration
Tet
Protein Variant
mCherry P2A Puromycin
Amp. resistance
RNA Barcode
U6
BFP
P2A
iCasp9
IRES
PolyA
Term.
PolyA
c
Pearson's R²
1.0
0.9
0.8
0.7
0.6
0.5
0.4
5
10
25
50
Number of cells/barcode sequence
Enrichment
Dilution & Amplification
d
R² = 0.98
Replicate 2 Counts
Replicate 1 Counts
0
200
400
600
800
1000
1200
1400
e
MS2
MS2
Barcode
RT Priming Site
MS2-circRNA 1b
dummy MS2-circRNA
f
Myc Enriched, 45min
Flag
Myc
Frequency
Count
300
250
200
150
100
50
0
50
100
150
200
250
300
350
400
g
off target counts/total counts
0.6
0.5
0.4
0.3
0.2
0.1
0.0
Input
45
75
105
Incubation Time (min)
off target/total counts
0.075
0.050
0.025
0.000
45
75
105
No dummy circRNA
+dummy MS2-circRNA

681 **Extended Data Fig. 2 | Engineering of a multiplexed MS2-circRNA barcoding platform. a,** Subassembly,
682 used to link protein variants to nucleotide barcodes, is achieved by sequencing the cloned plasmid library
683 using long-read high-throughput sequencing. In parallel, the plasmid library is integrated into the RPLP to
684 generate a cell line stably expressing tdMCP:MS2-circRNA complexes for use in biochemical experiments.
685 **b,** Schematic of the RPLP cell line. Recombination of Bxb1 attB-containing plasmids into the RPLP stably
686 integrates protein variants and MS2-circRNA barcodes under genomic transcriptional control. Selection
687 for successful recombinants is run using AP1903 and/or puromycin. **c,** Parallel Flag immunoprecipitations
688 were performed using serial dilutions of lysate generated from RPLP cells stably expressing Flag-tdMCP-
689 BRaf WT and a library of 20,000 MS2-circRNA 1b barcode sequences. Pearson's R^2 correlation coefficients
690 of barcode sequence counts are reported for replicate enrichments or RT-PCR amplifications. **d,**
691 Sequenced barcode counts derived from two independent expressions and Flag immunoprecipitations of
692 Flag-tdMCP-BTK co-expressed with a library of MS2-circRNA 2 barcode sequences. Pearson's $R^2 = 0.98$. **e,**
693 Schematics of MS2-circRNA 1b, the architecture used to encode variants in the tdMCP- and untagged BRaf
694 variant libraries, and dummy MS2-circRNA, which is included in the lysis buffer to minimize barcode
695 sequence missassociation. **f,** Relative frequencies of barcode sequence counts matched to Myc-tdMCP-
696 BRaf and Flag-tdMCP-BRaf libraries after 45 min Myc immunoprecipitation. **g,** Quantification of the data
697 shown in **f**. The y-axis is the fraction of barcode sequence counts encoding the Flag-tagged library (n=2
698 expression, lysis, enrichment, and sequencing replicates).

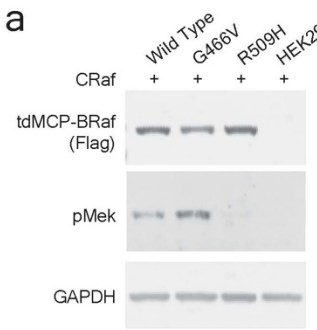

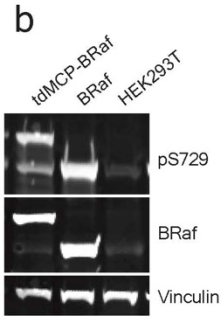

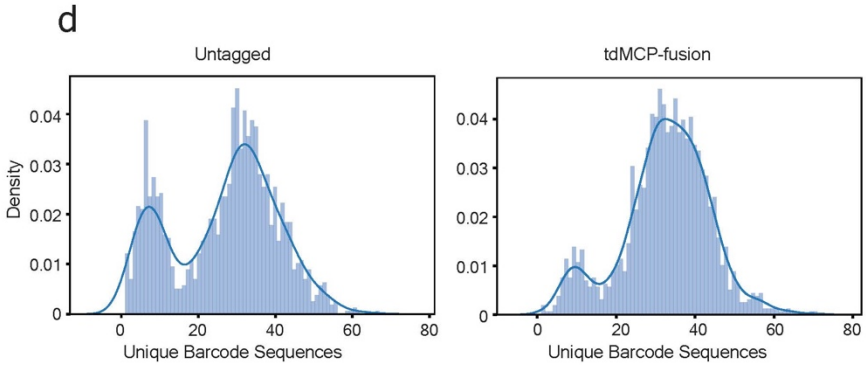

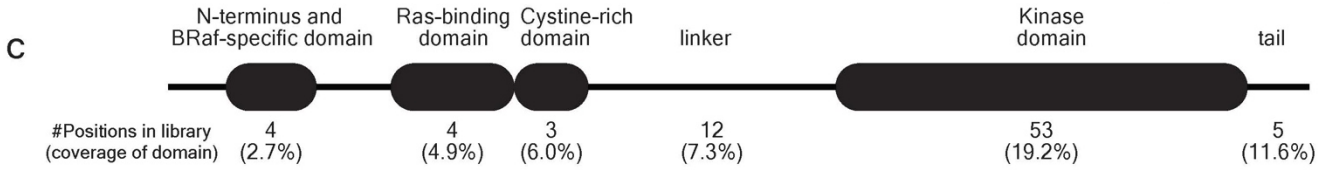

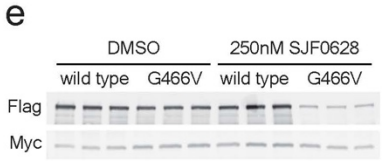

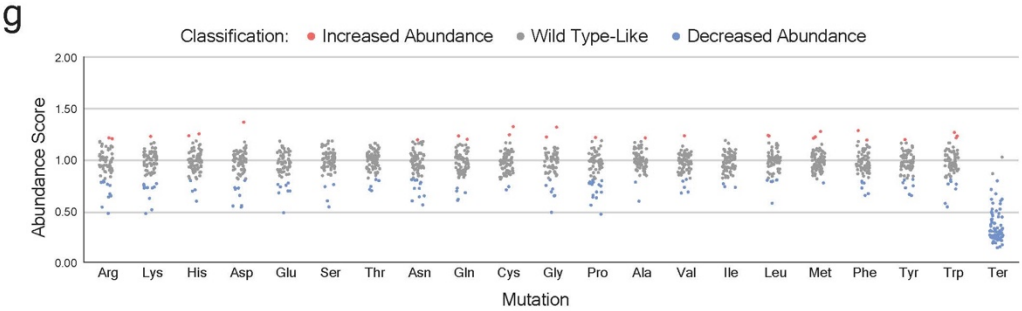

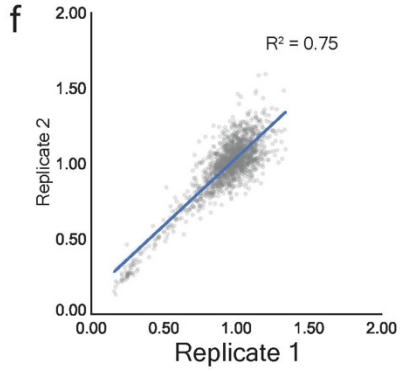

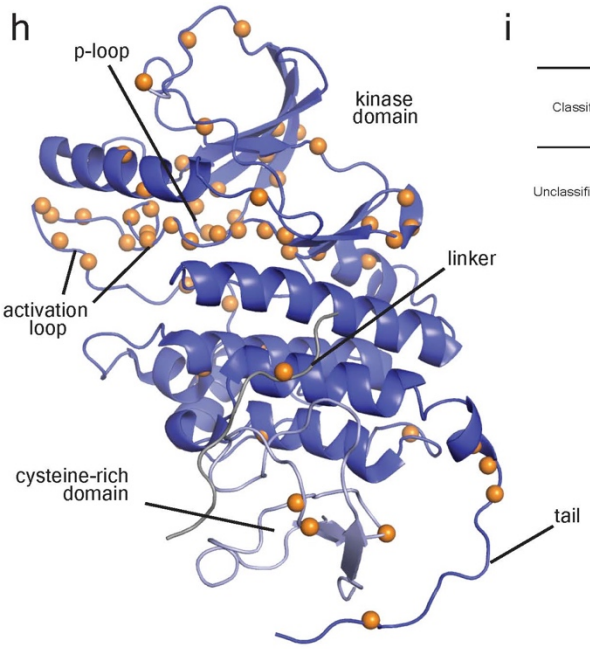

i

	Fold	Number of Positions (% of 80)
Classified	β-Stranded	10 (12.50%)
	Helical	9 (11.25%)
	Bend	17 (21.25%)
	Turn	6 (7.500%)
Unclassified	Resolved in structure but unclassified	21 (26.25%)
	Unresolved in structure	17 (21.25%)

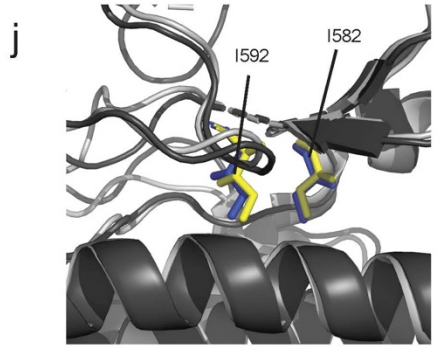

700 **Extended Data Fig. 3 | BRaf variant library construction and abundance. a,** Western blot analysis of RPLP
701 cells co-expressing tdMCP-BRaf variants and CRaf. **b,** Western blot analysis of HEK293T cells stably
702 expressing Flag-tdMCP-BRaf or untagged BRaf. **c,** Domain architecture of BRaf and the number of positions
703 in each domain included in the tdMCP- and untagged BRaf variant libraries. Positions were chosen by
704 compiling all missense and nonsense BRaf variants appearing in the COSMIC database and The Cancer
705 Genome Atlas and choosing positions where there are records of (1) at least 3 total variants and (b) at
706 least 2 unique variants. **d,** Distributions of unique barcode sequences assigned to each variant in the MCP-
707 tagged and untagged BRaf libraries. **e,** Western blots of data shown in Fig. 3d. **f,** Scatterplot showing
708 abundance score correlations between the two independent biological replicates shown in Fig. 3e
709 (Pearson's R^2 = 0.75). **g,** Abundance scores for all variants in the tdMCP-BRaf variant library, grouped by
710 substitution. **h,** Varied positions in the untagged and tdMCP-BRaf variant libraries are shown as orange
711 spheres on autoinhibited BRaf (PDB ID: 6NYB). **i,** DSSP (Define Secondary Structure of Proteins) structural
712 predictions for BRaf library positions resolved in 6NYB. DSSP predictions for structures 7MFE and 5VR3
713 were referenced for positions not resolved in 6NYB. **j,** Alignment of BRaf's ATP-binding pocket in the active
714 (black, PDB 4MNE) and autoinhibited (gray, PDB 6NYB) conformations, with the two positions (I582 and
715 I592) with the lowest average abundance scores shown as sticks.
716

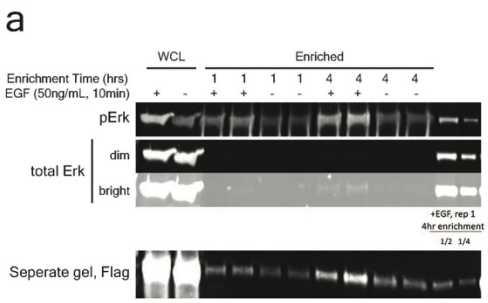

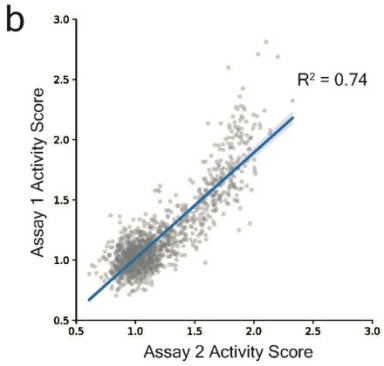

c

	Assay 1		Assay 2	
	Replicate 1	Replicate 2	Replicate 3	Replicate 4
WT	1.00 +/- 0.04	1.00 +/- 0.06	1.00 +/- 0.04	1.00 +/- 0.04
V600E	2.67 +/- 0.65	2.18 +/- 0.30	2.01 +/- 0.17	1.86 +/- 0.20
K601E	2.56 +/- 0.49	2.82+/- 0.49	2.41 +/- 0.16	2.05 +/- 0.17
L597V	1.57 +/- 0.17	1.68 +/- 0.16	1.77 +/- 0.15	1.70 +/- 0.13
G469A	2.10+/- 0.31	2.09 +/- 0.28	2.02 +/- 0.10	1.82 +/- 0.14
N581S	1.55 +/- 0.15	1.58 +/- 0.13	1.93 +/- 0.14	1.49 +/- 0.07
G466E	1.13 +/- 0.08	1.31 +/- 0.11	1.29 +/- 0.06	1.32 +/- 0.06
G596D	1.34 +/- 0.08	1.68 +/- 0.12	1.69 +/- 0.09	1.50 +/- 0.08

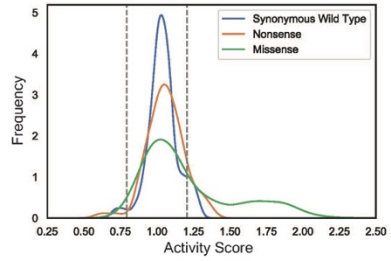

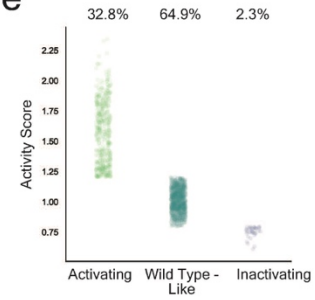

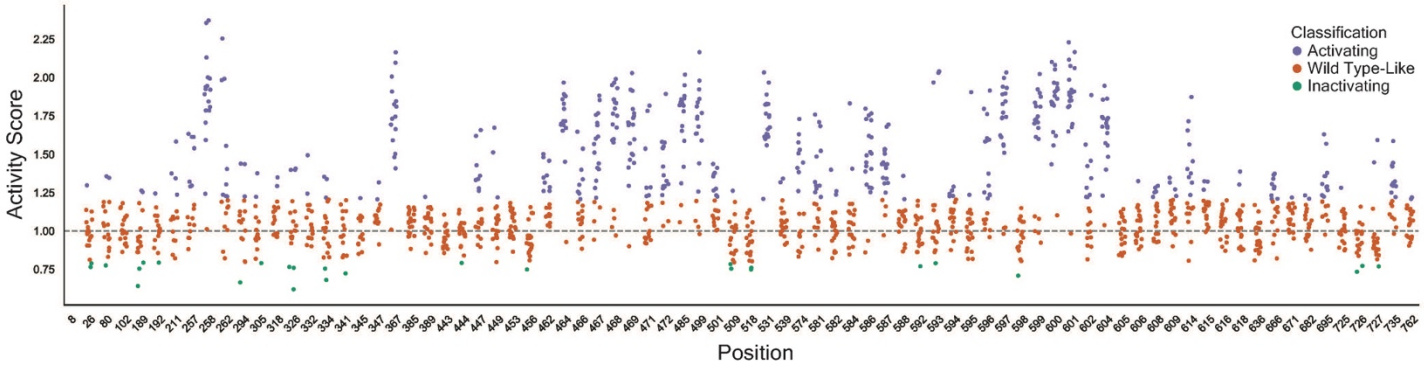

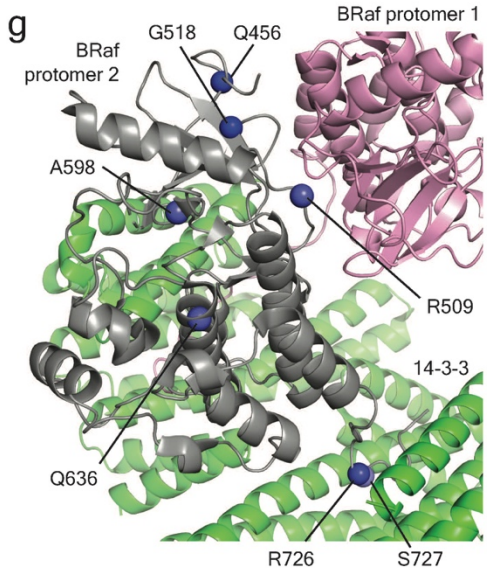

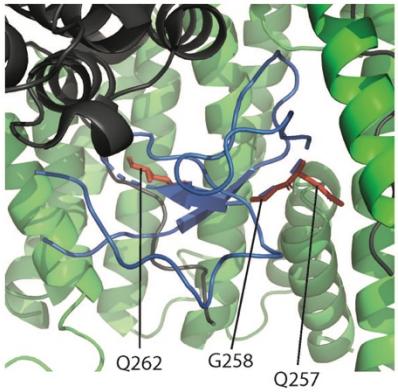

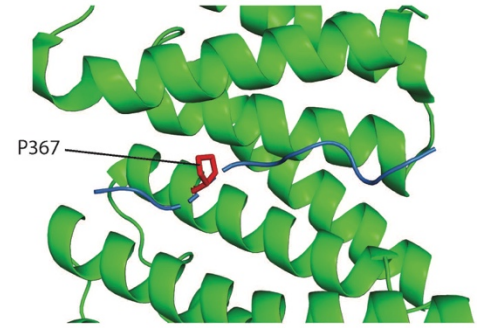

718 **Extended Data Fig. 4 | BRaf variant activity measured with overexpressed CRaf. a,** Western blot analysis
719 of HEK293T cells expressing the pErk reporter and treated with EGF (50 ng/mL, 10 min). Based on
720 quantitative enrichment of pErk, it appears only a small fraction of the pErk reporter is phosphorylated
721 under this regime. **b,** Scatterplot showing activity score correlations (Pearson's R^2 = 0.74) between the
722 averages of replicates 1 and 2 with overexpressed CRaf and the averages of replicates 3 and 4 with
723 overexpressed CRaf. Each replicate involved independent cell culturing, lysis, parallel pErk and Flag
724 immunoprecipitations, and quantification with high-throughput sequencing. Replicates 1 and 2
725 underwent separate transfections with CRaf and the pErk reporter than replicates 3 and 4. **c,** Activity
726 scores with overexpressed CRaf for previously characterized activating BRaf variants. Values shown are
727 the mean +/- SEM of all barcodes representing a BRaf variant. **d,** LABEL-seq activity score distributions for
728 all synonymous WT and nonsynonymous BRaf protein variants with overexpressed CRaf. The gray dashed
729 lines indicate activity score values (>2 standard deviations of the synonymous WT score distribution higher
730 or lower than 1, the WT score) we defined as activating and inactivating. **e,** Activity scores (with
731 overexpressed CRaf) for BRaf variants classified as activating (32.8%), Wild Type-like (64.9%), or
732 inactivating (2.3%). **f,** Activity scores (with overexpressed CRaf) for every BRaf variant at each position. **g,**
733 The 10 positions with the lowest average activity scores shown as blue spheres on an active BRaf complex
734 (PDB ID: 6Q0K). Positions 26, 189, and 443 are not resolved in the structure. **h,** The autoinhibited BRaf
735 complex (PDB ID: 6NYB) with BRaf's CRD shown in blue, non-CRD BRaf positions shown in black, and 14-
736 3-3 shown in green. G258 is positioned within the CRD, which plays a role in autoinhibition, Ras binding,
737 and membrane localization[40]. In autoinhibited BRaf, the phi-psi angles at position G258 are only
738 energetically accessible for glycine, suggesting that substitutions at this position alter the backbone
739 conformation and may disrupt autoinhibitory contacts, thereby leading to activation. **i,** Autoinhibited BRaf
740 (PDB ID: 6NYB) with BRaf P367 shown as red sticks, non-P367 BRaf positions shown in blue and 14-3-3 in
741 green. P367 is positioned in the CRD-kinase domain linker that interacts with 14-3-3 in the autoinhibited
742 BRaf complex. Based on the known binding specificity of 14-3-3 proteins[42], we speculate that P367
743 variants lead to BRaf activation by disrupting autoinhibitory 14-3-3 interactions.
744

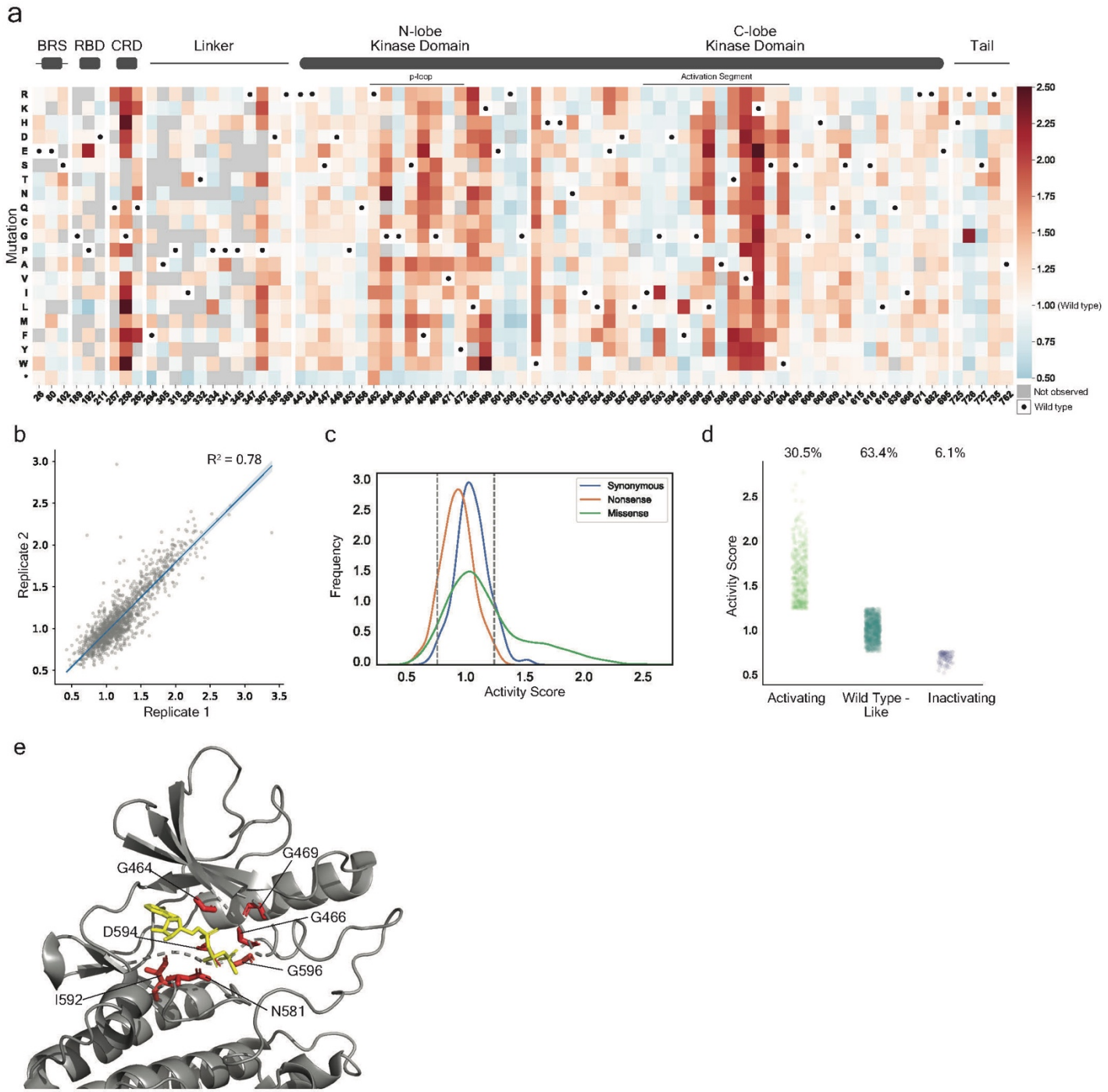
a
BRS
RBD
CRD
Linker
N-lobe
Kinase Domain
C-lobe
Kinase Domain
Tail
p-loop
Activation Segment
Mutation
1.00 (Wild type)
Not observed
Wild type
b
R² = 0.78
Replicate 2
Replicate 1
c
Synonymous
Nonsense
Missense
Frequency
Activity Score
d
30.5%
63.4%
6.1%
Activity Score
Activating
Wild Type - Like
Inactivating
e
G464
G469
G466
D594
G596
I592
N581

746 **Extended Data Fig. 5 | BRaf protein variant activity measured without overexpressed CRaf. a,** Sequence-
747 activity map for BRaf variants in the tdMCP-BRaf library measured without overexpressed CRaf. The
748 activity scores shown are the average of two replicates, each involving independent pErk reporter
749 expression, cell lysis, parallel Flag and pErk immunoprecipitations, and quantification by high-throughput
750 sequencing. Black dots in the map indicate the WT amino acid and gray tiles indicate missing data.
751 Position-averaged abundance scores are shown in the bar graph above the heatmap. **b,** Scatterplot
752 showing activity score (without CRaf) correlations between the two independent replicates shown in **a**
753 (Pearson's R^2 = 0.78). **c,** LABEL-seq activity score (without CRaf) distributions for all synonymous WT and
754 nonsynonymous BRaf protein variants. The gray dashed lines indicate the activity score values (>2
755 standard deviations of the synonymous WT score distribution higher or lower than 1, the WT score)
756 defined as increased and decreased activity. **d,** Activity scores (without CRaf) for BRaf variants classified
757 as activating (30.5%), Wild Type-like (63.4%), or inactivating (6.1%). **e,** Positions highly conserved across
758 the human kinome are represented as red sticks on a structure of BRaf bound to ATP-γ-S (PDB ID: 6NYB).
759

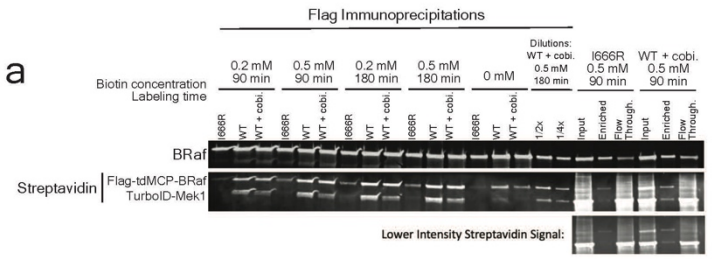
a
Flag Immunoprecipitations
Biotin concentration
Labeling time
0.2 mM 90 min
0.5 mM 90 min
0.2 mM 180 min
0.5 mM 180 min
0 mM
Dilutions: WT + cobi. 0.5 mM 180 min
I666R 0.5 mM 90 min
WT + cobi. 0.5 mM 90 min
BRaf
Streptavidin
Flag-tdMCP-BRaf TurboID-Mek1
Lower Intensity Streptavidin Signal:

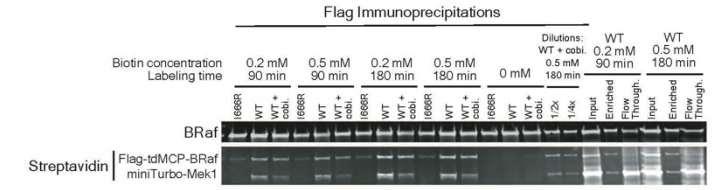
Flag Immunoprecipitations
Biotin concentration
Labeling time
0.2 mM 90 min
0.5 mM 90 min
0.2 mM 180 min
0.5 mM 180 min
0 mM
Dilutions: WT + cobi. 0.5 mM 180 min
WT 0.2 mM 90 min
WT 0.5 mM 180 min
BRaf
Streptavidin
Flag-tdMCP-BRaf miniTurbo-Mek1

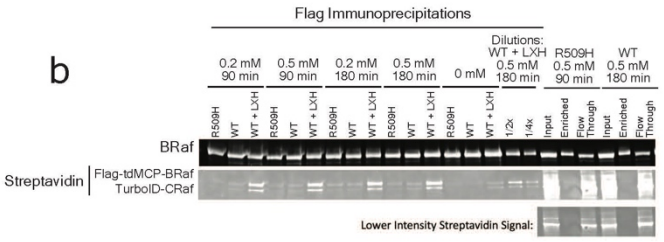
b
Flag Immunoprecipitations
0.2 mM 90 min
0.5 mM 90 min
0.2 mM 180 min
0.5 mM 180 min
0 mM
Dilutions: WT + LXH 0.5 mM 180 min
R509H 0.5 mM 90 min
WT 0.5 mM 180 min
BRaf
Streptavidin
Flag-tdMCP-BRaf TurboID-CRaf
Lower Intensity Streptavidin Signal:

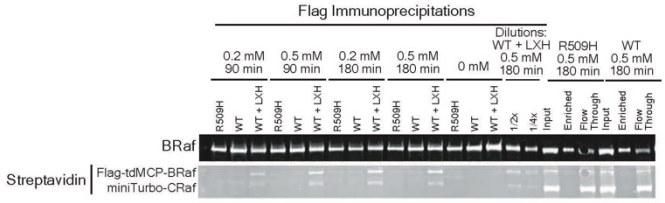
Flag Immunoprecipitations
0.2 mM 90 min
0.5 mM 90 min
0.2 mM 180 min
0.5 mM 180 min
0 mM
Dilutions: WT + LXH 0.5 mM 180 min
R509H 0.5 mM 180 min
WT 0.5 mM 180 min
BRaf
Streptavidin
Flag-tdMCP-BRaf miniTurbo-CRaf

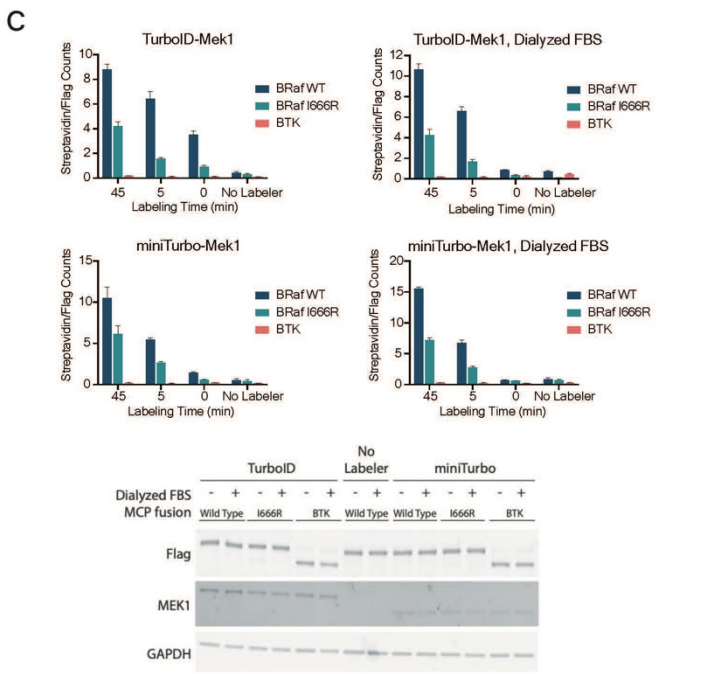
c
TurboID-Mek1
TurboID-Mek1, Dialyzed FBS
miniTurbo-Mek1
miniTurbo-Mek1, Dialyzed FBS
Streptavidin/Flag Counts
Labeling Time (min)
BRaf WT
BRaf I666R
BTK
No Labeler
TurboID
No Labeler
miniTurbo
Dialyzed FBS
MCP fusion
Wild Type
I666R
BTK
Flag
MEK1
GAPDH

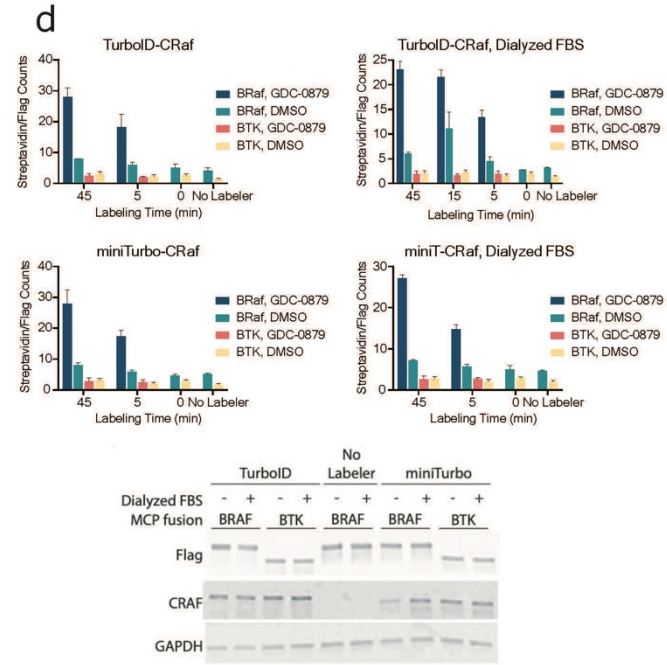
d
TurboID-CRaf
TurboID-CRaf, Dialyzed FBS
miniTurbo-CRaf
miniT-CRaf, Dialyzed FBS
Streptavidin/Flag Counts
Labeling Time (min)
BRaf, GDC-0879
BRaf, DMSO
BTK, GDC-0879
BTK, DMSO
No Labeler
TurboID
No Labeler
miniTurbo
Dialyzed FBS
MCP fusion
BRAF
BTK
Flag
CRAF
GAPDH

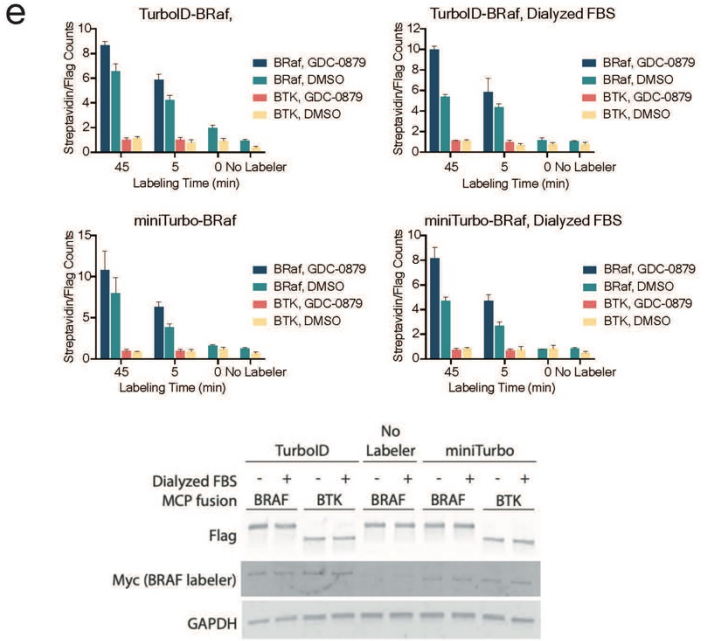
e
TurboID-BRaf,
TurboID-BRaf, Dialyzed FBS
miniTurbo-BRaf
miniTurbo-BRaf, Dialyzed FBS
Streptavidin/Flag Counts
Labeling Time (min)
BRaf, GDC-0879
BRaf, DMSO
BTK, GDC-0879
BTK, DMSO
No Labeler
TurboID
No Labeler
miniTurbo
Dialyzed FBS
MCP fusion
BRAF
BTK
Flag
Myc (BRAF labeler)
GAPDH

761 **Extended Data Fig. 6 | Optimization of proximity labeling conditions. a,** Biotinylation levels of Flag-
762 tdMCP-BRaf variants in HEK293 cells co-expressing TurboID-Mek1 (top) or miniTurbo-Mek1 (bottom),
763 treated with 10 µM cobimetinib or DMSO for 4 h, and labeled with biotin. **b,** Biotinylation levels of Flag-
764 tdMCP-BRaf variants in HEK293 cells co-expressing TurboID-CRaf (top) or miniTurbo-CRaf (bottom),
765 treated with 10 µM LXH254 or DMSO for 2 h, and labeled with biotin. (**c-e**)**,** Biotinylation levels
766 (represented as the ratio of streptavidin and Flag barcode sequence counts) of Flag-tdMCP-BRaf variants
767 and the background control Flag-tdMCP-BTK in HEK293T cells co-expressing TurboID-Mek1 (**c**), TurobID-
768 CRaf (**d**), or TurboID-BRaf (**e**) and MS2-circRNAs. Cells were cultured in regular or dialyzed FBS and treated
769 with biotin for 0, 5, or 45 min. Following biotin treatment, cells were lysed and pooled, parallel
770 streptavidin and Flag enrichments were performed, co-enriched barcodes were sequenced by high-
771 throughput sequencing, and the ratio of streptavidin and Flag counts for each co-enriched MS2-circRNA
772 barcode sequence was calculated (n=3 barcodes/treatment, values shown = mean, error bars represent
773 +/- SEM). Whole-cell lysate samples were reserved for western blots, which are shown below the bar
774 graph (corresponds to the data shown in Fig. 5c, 5e, and 5f as well). TurboID-Mek1 (dialyzed FBS), TurboID-
775 CRaf (dialyzed FBS), and TurboID-BRaf (dialyzed FBS) data are the same as in **Fig. 5c,e,f** respectively.
776

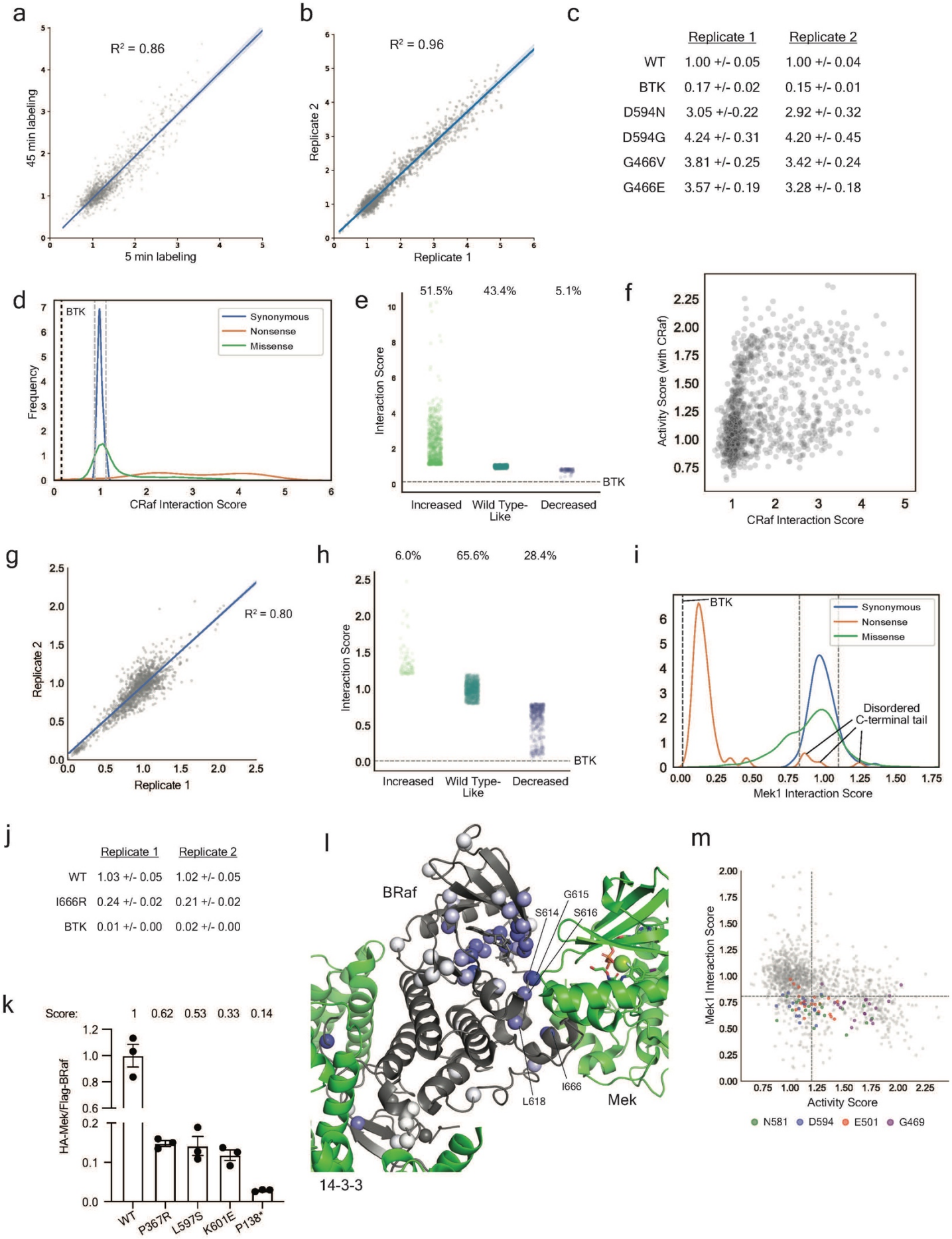

c

	Replicate 1	Replicate 2
WT	1.00 +/- 0.05	1.00 +/- 0.04
BTK	0.17 +/- 0.02	0.15 +/- 0.01
D594N	3.05 +/-0.22	2.92 +/- 0.32
D594G	4.24 +/- 0.31	4.20 +/- 0.45
G466V	3.81 +/- 0.25	3.42 +/- 0.24
G466E	3.57 +/- 0.19	3.28 +/- 0.18

j

	Replicate 1	Replicate 2
WT	1.03 +/- 0.05	1.02 +/- 0.05
I666R	0.24 +/- 0.02	0.21 +/- 0.02
BTK	0.01 +/- 0.00	0.02 +/- 0.00

Extended Data Fig. 7 | Quantifying BRaf variant interactions with CRaf and Mek1. a, Scatterplot showing CRaf interaction score correlations between 5 min and 45 min biotin labeling regimes (Pearson's R^2 = 0.86). Each score is the average of two replicates corresponding to parallel biotin labeling, streptavidin and flag enrichments, and quantification by high-throughput sequencing. **b,** Scatterplot showing CRaf interaction score correlations between the two 5 min biotin labeling replicates shown in Fig. 5h (Pearson's R^2 = 0.96). **c,** CRaf interaction scores shown in Fig. 5h for BRaf variants previously shown to exhibit elevated heterodimerization with CRaf. Values shown are the mean +/- SEM of all barcodes representing a BRaf variant. **d,** LABEL-seq CRaf interaction score distributions for all synonymous WT and nonsynonymous BRaf variants. The gray dashed lines indicate the CRaf interaction score values (>2 standard deviations of the synonymous WT score distribution higher or lower than 1, the WT score) we defined as increased and decreased interaction, respectively. The black dashed line is the BTK score. **e,** CRaf interaction scores for BRaf variants classified as increased CRaf interaction (51.5%), Wild Type-like (43.4%), or decreased CRaf interaction (5.1%). **f,** Scatterplot comparing activity scores (with CRaf) to CRaf interaction scores. **g,** Scatterplot showing Mek1 interaction score correlations between the two independent replicates shown in Fig. 5j (Pearson's R^2 = 0.80). **h,** Mek1 interaction scores for BRaf variants classified as increased Mek1 interaction (6.0%), Wild Type-Like (65.6%), or decreased Mek1 interaction (28.4%). **i,** LABEL-seq Mek1 interaction score distributions. The gray dashed lines indicate the Mek1 interaction score values (>2 standard deviations of the synonymous WT score distribution higher or lower than 1, the WT score) we defined as increased and decreased interaction, respectively. The black dashed line is the BTK score. **j,** Mek1 interaction scores for the decreased interaction control variant I666R and Flag-tdMCP-BTK. Values shown are the mean +/- SEM of all barcodes representing BRaf I666R or BTK.. **k,** Co-immunoprecipitations of HA-Mek1 and Flag-BRaf variants (without tdMCP). LABEL-seq Mek1 interaction scores are shown above the plot (n=3, value shown = mean, error bars = SEM). **l,** The number of variants at each position that were classified as decreased Mek1 interaction in Fig. 5j projected onto a structure of the autoinhibited BRaf complex (PDB ID: 6NYB). White = 0 decreased interaction variants, darkest blue = 19 decreased interaction variants. **m,** LABEL-seq Mek1 interaction and activity (with CRaf) scores. Variants at select positions within the ATP-binding pocket are highlighted. Notably, these BRaf variants possessed a range of activity scores but similarly decreased Mek1 interaction scores, indicating that differences in Mek1 interactions cannot solely be attributed to the formation of pMek, which has a lower affinity for BRaf[49]. Scores to the right of the vertical dashed line are classified as activating and scores below the horizontal dashed line are classified as decreased Mek1 interaction.

a

Activity (with CRaf)

CRaf Interaction

Mek1 Interaction

Abundance

b

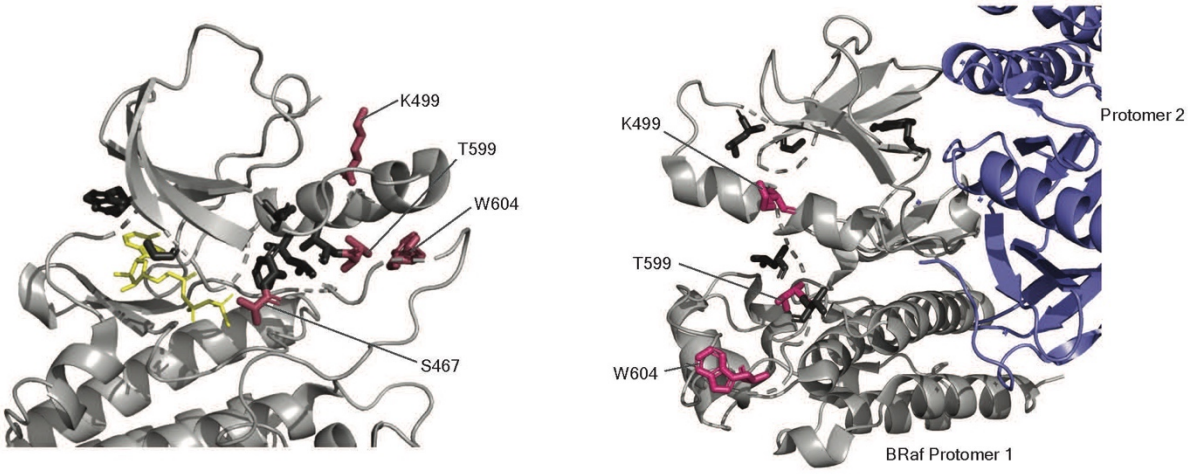

811 **Extended Data Fig. 8 | Pairwise comparisons of protein variant scores. a,** All pairwise comparisons of
812 activity scores (with CRaf), CRaf interaction scores, Mek interaction scores, and abundance scores. The
813 histograms are the relative frequency of each score in the library. **b,** Cluster 1 (black sticks) and cluster 2
814 (maroon sticks) positions shown on autoinhibited BRaf (left, PDB ID: 6NYB) and the active BRaf dimer
815 (right, PDB ID: 4MNE).
816

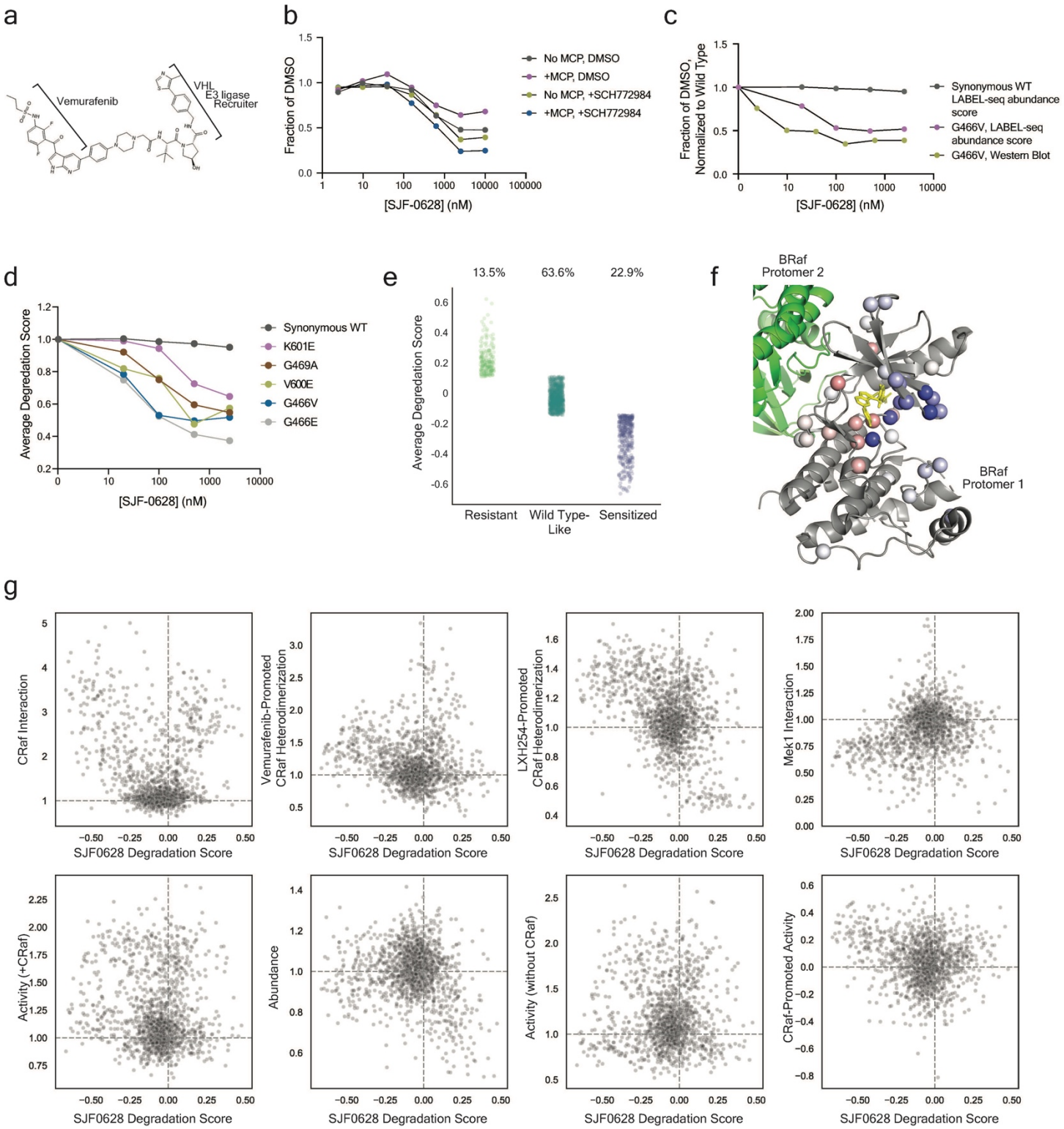
a
Vemurafenib
VHL
E3 ligase
Recruiter
b
Fraction of DMSO
[SJF-0628] (nM)
No MCP, DMSO
+MCP, DMSO
No MCP, +SCH772984
+MCP, +SCH772984
c
Fraction of DMSO, Normalized to Wild Type
[SJF-0628] (nM)
Synonymous WT LABEL-seq abundance score
G466V, LABEL-seq abundance score
G466V, Western Blot
d
Average Degredation Score
[SJF-0628] (nM)
Synonymous WT
K601E
G469A
V600E
G466V
G466E
e
13.5%
63.6%
22.9%
Average Degredation Score
Resistant
Wild Type-Like
Sensitized
f
BRaf Protomer 2
BRaf Protomer 1
g
CRaf Interaction
Vemurafenib-Promoted CRaf Heterodimerization
LXH254-Promoted CRaf Heterodimerization
Mek1 Interaction
Activity (+CRaf)
Abundance
Activity (without CRaf)
CRaf-Promoted Activity
SJF0628 Degradation Score

818 **Extended Data Fig. 9 | SJF0628-mediated degradation of BRaf protein variants. a,** Structure of SJF0628.
819 **b,** SJF0628-induced degradation of BRaf WT expressed with and without a tdMCP fusion in HEK293T cells.
820 **c,** SJF0628-induced degradation of tdMCP-BRaf synonymous WT and G466V variants measured using
821 western blotting and the LABEL-seq abundance assay. **d,** Average LABEL-seq SJF0628 degradation scores
822 for five BRaf variants previously shown to be sensitive to SJF028 (n=2). **e,** Degradation scores for BRaf
823 variants classified as resistant (13.5%), Wild Type-like (63.6%), or sensitized (22.9%). Variants with
824 degradation scores more than two standard deviations of the synonymous distribution above or below
825 WT were classified as resistant or sensitized, respectively. **f,** SJF0628 degradation scores at 2.5 µM SJF0628
826 at each position in the tdMCP-BRaf variant library (represented as spheres) shown on BRaf's kinase
827 domain bound to Vemurafenib (PDB ID: 3OG7). The average degradation score at a position is represented
828 by the shade of red or blue: darkest red = 0.18, darkest blue = - 0.51. **g,** Scatterplots showing relationship
829 between SJF0628 degradation score and other LABEL-seq biochemical measurements. Data shown for
830 missense variants only. Gray dashed lines correspond to the WT score.
831

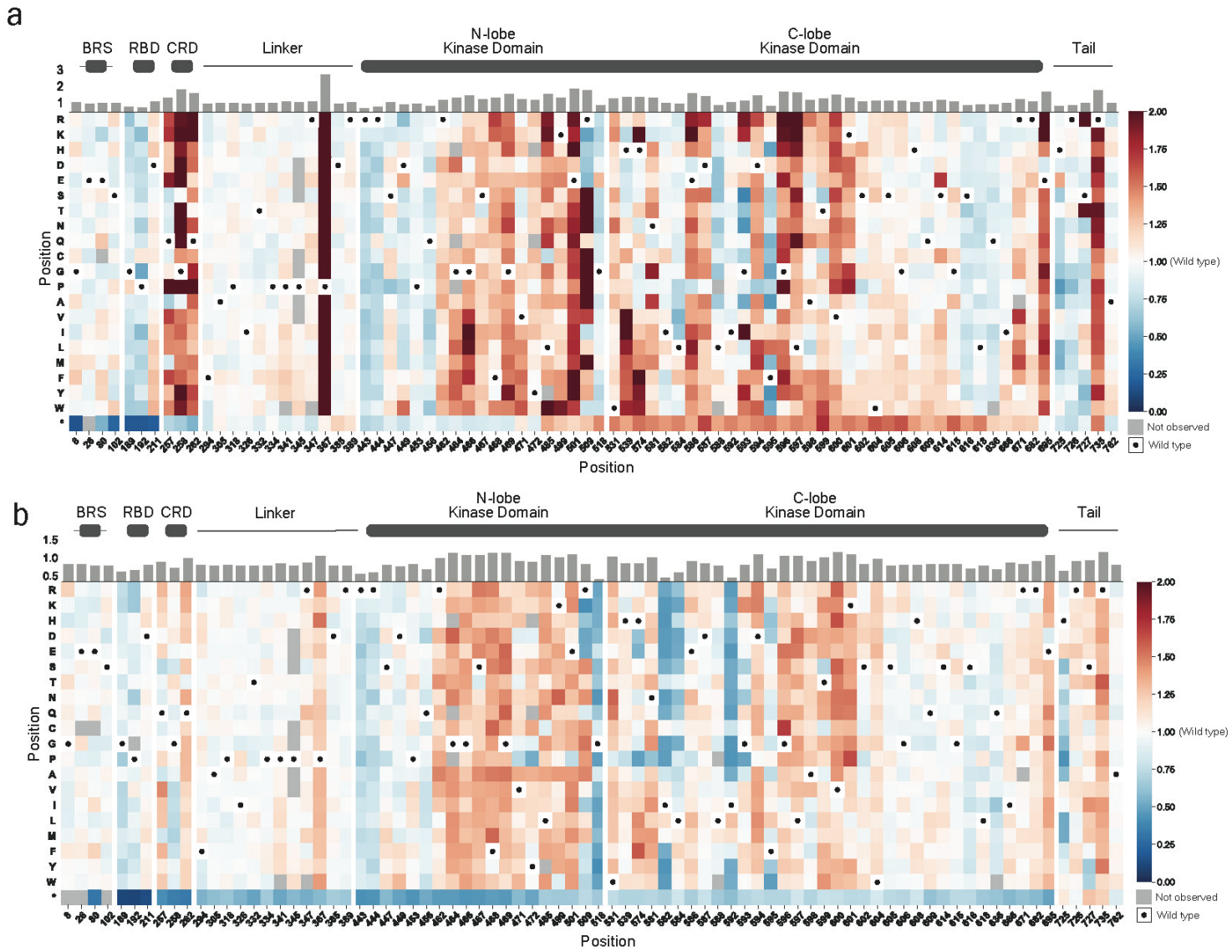

Extended Data Fig. 10 | Small molecule-promoted BRaf:CRaf heterodimerization. a-b, Sequence-CRaf interaction maps for variants in the tdMCP-BRaf library co-expressed with TurboID-CRaf, treated with Vemurafenib (a) or LXH254 (b), and labeled with biotin. The interaction scores shown are the average of two replicates, each involving an independent cell culturing, biotin labeling, parallel streptavidin and Flag enrichments, and quantification with high-throughput sequencing. Black dots in the map indicate the WT amino acid and gray tiles indicate missing data. Position-averaged CRaf interaction scores are shown in the bar graph above the heatmaps.

870 **Methods**
871
872 **Cloning**
873 All plasmids, except those encoding libraries, were constructed using gibson assembly and standard
874 protocols then validated through Sanger or whole-plasmid sequencing.
875
876 **Expression of MS2-circRNA architectures**
877 HEK293T cells were seeded to 80% confluent in 12-well plates and transfected with a mix of 0.7 µg of
878 plasmid encoding MS2-circRNA barcode + 0.1 µg pMAX-GFP (to estimate transfection efficiency) + 2.4 µL
879 PEI. 48 hrs after transfection, media was removed, cells were resuspended directly in TRIzol (Invitrogen,
880 Cat #15596026), and total RNA was extracted according to the manufacturer's instructions. Total RNA
881 concentrations were normalized using a NanoDrop 2000 (Thermo Scientific).
882
883 **Pulldowns with gel-based visualization of MS2-circRNA**
884 To prepare dasatinib-conjugated sepharose, 1.25 mL of NHS-activated sepharose slurry (Cytiva cat
885 #17090601) was washed twice with 50% DMF/50% EtOH then incubated with 64 µL 50mM dasatinib-
886 amine + 240 µL 1M EDC + 1.6 mL 50% DMF/50% EtOH overnight at room temperature rotating end-over-
887 end. After coupling, beads were washed three times with 50% DMF/50% EtOH then capped with
888 ethanolamine by incubating with 544 µL 1M ethanolamine + 240 µL 1M EDC + 1056 µL 50% DMF/50%
889 EtOH overnight at room temperature rotating end-over-end. Capped beads were washed three times with
890 50% DMF/50% EtOH, two times with 0.5M NaCl, then one time with 20% ethanol in water. Washed beads
891 were resuspended in 20% ethanol to make a 50% bead/50% solvent slurry and stored at 4°C.
892
893 For pulldowns, HEK293T's were seeded to 80% confluent in 12-well plates and transfected with a mix of
894 0.75 µg tdMCP-protein fusion plasmid + 0.75 µg MS2-circRNA plasmid + 0.15 µg pMAX-GFP (to estimate
895 transfection efficiency) + 5 µL PEI. 48 hrs after transfection, cells were resuspended in 160 µL lysis buffer
896 (50mM Tris pH=7.6, 150mM NaCl, 10mM NaF, 4mM $MgCl_2$, 5% glycerol, Halt protease inhibitor tablet (1
897 tablet/50mL, Fisher cat# A32965), 2mM PMSF, RiboLock RNase Inhibitor (4 µL/mL, Fisher
898 cat#FEREO0382)) and lysates were cleared at 17,000g for 10 min at 4°C. Prior to enrichment, 40 µL of
899 supernatant was incubated with 15 µM free dasatinib (1% DMSO) or 1% DMSO for 30 min at 4°C. To
900 enrich, 10 µL of dasatinib-conjugated sepharose (pre-washed with lysis buffer) was added to each sample
901 and incubated for 2.5 h at 4°C, rotating end-over-end. Protein-bound beads were washed three times with
902 100 µL of lysis buffer. For western blot analysis, beads were resuspended in 3xSDS. For analysis of RNA
903 enrichment, beads were resuspended in 100 µL TRIzol (Invitrogen cat# 15596026). All samples were
904 stored at -20°C. RNA was extracted and purified using RNA cleanup columns (IBI scientific TRI-Isolate RNA
905 Pure Kit, VWR cat# 76006-526), eluted into 25 µL of water and immediately visualized by ge (see "Gel-
906 based visualization of RNA")
907
908 **Gel-based visualization of MS2-circRNA**
909 To visualize broccoli by gel, total RNA containing MS2-circRNA (1 µg for scaffold test expression, 7 µL for
910 pulldown samples) was mixed 1:1 with 2x TBE-urea sample buffer (Invitrogen, Fisher cat #LC6876), heated
911 to 75°C for 5 min, then briefly cooled on ice. Samples were loaded onto precast 6% TBE (Invitrogen, Fisher

912 cat #EC62655BOX) or 10% TBE-Urea (Invitrogen, Fisher cat #EC68755BOX) gels and run at 270V in TBE
913 buffer to completion. Gels were washed three times for 5 min in milliQ water then stained for 20 min at
914 room temperature in DFHBI buffer (10 µM DFHBI-1T, 40mM HEPES, pH 7.4, 100mM KCl, and 1mM MgCl2),
915 both steps on an orbital shaker. Broccoli was imaged on a Typhoon FLA 9000 using preset settings for
916 Alexa Fluor 488 (495nm excitation and 519nm emission).
917
918 **Generating the RNA-Protein Landing Pad (RPLP)**
919 To stably generate a high-efficiency Bxb1 landing pad containing Pol II- and Pol III-driven promoters, Flp-
920 In™ T-REx™ 293 cells (Fisher cat#R78007) were plated into a 6-well dish and transfected with 1 µg of
921 landing pad plasmid containing an FRT site, 1 µg Flp recombinase expression plasmid (pOG44), 6 µL PEI,
922 and 100 µL serum-free DMEM. 48 hrs after transfection, cells were re-seeded to ~20% confluent. After an
923 additional 24 hrs, media was supplemented with 200 µg/mL hygromycin (Mirus Bio cat#MIR 5930) to
924 initiate selection. Cells were expanded and maintained in 200 µg/mL hygromycin until >95% of cells were
925 GFP positive indicating near-complete selection, and stocks were cryo-preserved until needed.
926
927 **Cloning single variant barcode libraries**
928 To generate a library of barcodes, attB plasmid containing genes for tdMCP-protein fusions and a MS2-
929 circRNA barcode were digested overnight at 37°C to remove existing barcode sequence (2 µg plasmid, 5
930 µL 10x CutSmart buffer, 2 µL BsrGI-HF (NEB cat#R3575S), nuclease-free water to 50uL). The next day,
931 fragments were dephosphorylated by adding 5 µL antarctic phosphatase buffer and 2 µL enzyme (NEB
932 cat#M0289S) and incubating for 1 h at 37°C. Fragments were then separated by gel electrophoresis and
933 the band corresponding to digested vector was extracted using a Zymo kit (Zymo cat#D4002) and eluted
934 into 20 µL nuclease-free water.
935
936 To generate a double-stranded barcode fragment (dsBC), 50pmol of the single stranded barcode oligo
937 (JJS29), 50pmol of the second strand synthesis primer (ssSynth primer, JJS30), 5 µL NEB2.1 10x buffer, and
938 nuclease-free water to a total volume of 48 µL were combined. Oligos were annealed by heating to 94°C
939 for 5 min, ramping 0.1°C/s to 71°C (Tm) and holding for 5 min, then ramping 0.1°C/s to 37°C. ssSynth
940 primer was extended by adding 1 µL 10mM dNTP's (Fisher cat#FERR0192) and 1 µL Klenow polymerase
941 (NEB cat#M0210S) then incubating at 37°C for 1hr. The resulting dsBC was cleaned using a Zymo column
942 (Zymo cat#D4014) and eluted into 12 µL nuclease-free water.
943
944 dsBC was cloned into the digested vector by combining 200ng vector (~0.035pmol, 8uL), 10ng dsBC
945 (~0.175pmol, 2uL) and 10 µL 2x NEBuilder® HiFi DNA Assembly Master Mix (NEB cat#E2621L) and
946 incubating at 50°C for 1hr. A separate vector-only reaction was run in parallel using 200ng vector, 10 µL
947 NEBuilder Master Mix, and nuclease-free water to 20 µL (without barcode) to estimate vector-only
948 background transformants. After incubation, reactions were cleaned (Zymo cat#D4014) and eluted into
949 10 µL nuclease-free water.
950
951 Cleaned reactions were transformed into NEB® 5-alpha Competent *E. coli* (NEB cat#C2987H) following the
952 manufacturer's instructions. Following outgrowth, transformed cells were added to 50 mL LB broth
953 supplemented with 100 µg/mL carbenicillin. The library was bottlenecked to the desired number of

954 barcodes by making serial dilutions of the culture in LB+carb. 200 µL of each dilution was plated on
955 LB+carb plates to enumerate transformants. Liquid cultures were grown at 37°C overnight to saturation
956 and DNA was extracted using QIAGEN® Plasmid Plus Midi Kit (Qiagen cat#12945)
957
958 **Generating stable cell lines**
959 Stable cell lines expressing protein and RNA barcodes were generated in the HEK293 RPLP. Stable lines
960 not expressing circRNA barcodes were generated in the HEK293T lenti landing pad (LLP-iCasp9-Blast[24]).
961 The following protocol applies to both cell lines.
962
963 Cells were maintained in high glucose DMEM (Fisher cat #11-965-118) supplemented with 10% FBS and 2
964 µg/mL doxycycline (DOX, Sigma cat#D9891, 0.01% DMSO final concentration). Genes of interest were
965 cloned into Bxb1 attB-containing plasmids using standard Gibson assembly cloning techniques (NEB cat
966 #E2621L). To stably recombine the attB plasmids under control of the landing pad promoters, cells were
967 plated the day before transfection in 6-well dishes to 40% confluence using DOX-free media. The following
968 day, cells were transfected with a mixture of 1.7 µg attB plasmid + 0.2 µg pCAG-NLS-Bxb1
969 (Addgene#51271) + 0.2 µg pMAX-GFP + 7.8 µL Fugene 6 (for LLP lines, Promega cat#E2691) or Fugene HD
970 (for RPLP lines, Promega cat#E2311) + 100 µL serum-free DMEM (Fisher cat #11-965-118). 48-hours after
971 transfection, cells were expanded to 10cm dishes in media containing 2 µg/mL DOX. 24-48 hrs after DOX
972 induction, media was supplemented with 10nM AP1903 (Fisher cat#50-115-1810) to select for successful
973 recombinants. 12-24 hrs after addition of AP1903, media was exchanged for AP1903-free media (+2
974 µg/mL DOX), the resulting stables were expanded in +DOX media, and stocks frozen until required.
975
976 **Barcode sequence missassociation experiment**
977 Two barcode libraries were cloned as described in the 'Generating single protein variant barcode libraries'
978 section, each containing 20,000-30,000 unique barcode sequences and either 3xFlag- or 2xMyc-tdMCP-
979 BRaf wild type. Plasmid libraries were individually recombined into the RPLP as described in the
980 'Generating stable lines' section.
981
982 The day before enrichment, equal numbers of cells from both libraries were combined and plated into 15
983 cm dishes in +DOX media. On the day of enrichment, cells were trypsinized and all plates pooled. The pool
984 aliquots were then divided into 5 enrichment samples: 2 no-dummy samples ($30x10^6$ cells each), 2
985 +dummy samples ($10x10^6$ cells each), and 1 input sample ($10x10^6$ cells each). Each aliquot was washed
986 once with DPBS, then fully resuspended in 1,650 µL (no dummy samples) or 550 µL (+dummy and input)
987 modRIPA without detergent (i.e. resuspension buffer: 50mM Tris pH=7.6, 150mM NaCl, 10mM NaF, 4mM
988 $MgCl_2$, 5% glycerol, Halt protease inhibitor tablet (1 tablet/50mL, Fisher cat# A32965), 2mM PMSF,
989 RiboLock RNase Inhibitor (4 µL/mL, Fisher cat#FEREO0382)). For +dummy samples, the resuspension
990 buffer also contained 400ng/ µL total RNA previously extracted from HEK293T cells which were transiently
991 transfected with dummy MS2-circRNA (an MS2-circRNA architecture which contains the MS2 hairpin but
992 the reverse transcription priming sites). Immediately after resuspending cells in resuspension buffer, cells
993 were lysed by adding an equal volume of modRIPA containing 0.1% NP40. Addition of buffer with
994 detergent marked the beginning of the incubation time. Lysates were cleared by centrifugation at 17,000g
995 for 10 min at 4°C. Each enrichment sample was split into two aliquots (1.5 mL ea. for no dummy, 0.5 mL

996 ea. for +dummy) and transferred to low-bind eppendorf tubes (Fisher cat#13-698-792). To enrich tdMCP-
997 protein fusions, 150 µL (no dummy) or 50 µL (+dummy) of anti-flag (Sigma cat#M8823) or anti-myc (Fisher
998 cat#PI88842) beads were added to the lysates and rotated end-over-end at 4°C for the indicated time.
999 500 µL samples of bead suspension were collected at each timepoint and washed 3 times with 500 µL
1000 modRIPA (including 0.1% NP40). After washing, all buffer was removed before resuspending beads in 75
1001 µL nuclease-free water and 300 µL TRIzol, then stored at -20. The input sample was resuspended in 1.5
1002 mL TRIzol and stored at -20. RNA was extracted using IBI scientific TRI-Isolate RNA Pure Kit, concentrated
1003 using Zymo RNA Clean & Concentrator (Zymo Research Cat #R1015), eluted into 10 µL nuclease-free
1004 water, and stored at -80°C.
1005
1006 **Variant abundance assay, proof of concept experiment**
1007 HEK293T LLP cells stably expressing 3xFlag-tdMCP-BRaf wild type or G466V were transfected in 24-well
1008 plates, each well receiving 300 ng pcDNA5 2xMyc-tdMCP-SNAP + 200 ng of an equal mix of 4 plasmids,
1009 each containing a unique circRNA barcode + 50 ng pMAX GFP + 50 µL DMEM + 1.65 µL PEI. 6 transfections
1010 per variant encompassing a total of 48 unique barcodes were performed. 24 hrs after transfection cells
1011 were treated with SJF0628 or DMSO for an additional 24 hrs. After drug treatment, cells were lysed in
1012 120 µL modRIPA (0.1% NP40, 50mM Tris pH=7.6, 150mM NaCl, 10mM NaF, 4mM $MgCl_2$, 5% glycerol, Halt
1013 protease inhibitor tablet (1 tablet/50mL, Fisher cat# A32965), 2mM PMSF, RiboLock RNase Inhibitor
1014 (4uL/mL, Fisher cat#FEREO0382)) and lysate cleared by centrifugation at 17,000g for 10 min at 4°C.
1015 Samples were taken for western blot analysis before pooling 40 µL lysate from all 12 wells. Pooled lysate
1016 was subsequently split into 2x200 µL aliquots and protein was enriched by adding 20 µL anti-flag (Sigma
1017 cat#M8823) or anti-myc (Fisher cat#PI88842) beads and rotating end-over-end at 4°C for 1 hr. Beads were
1018 washed 3 times with modRIPA, resuspended in 50 µL nuclease-free water and 200 µL TRIzol, then stored
1019 at -20°C. Enriched RNA was extracted and sequenced as described in the 'Preparation of RNA for Genewiz
1020 Amplicon-EZ sequencing' section.
1021
1022 Sequencing ratios were computed by dividing the sequencing counts in the flag enrichment by counts in
1023 the Myc enrichment then normalizing to the mean flag/myc ratio for wild type cells treated with DMSO.
1024 The mean ratio of all barcodes in a well was reported. Similarly, for western blot ratios the intensity of the
1025 flag signal was divided by the intensity of the Myc signal. Ratios were normalized to the average ratio of
1026 wild type cells treated with DMSO. The three data points correspond to the three transfections.
1027
1028 **Variant activity assay, proof of concept experiment**
1029 HEK293T LLP cells stably expressing untagged BRaf wild type or V600E were transfected in 12-well plates
1030 with 0.5 µg 3xFlag-tdMCP-Erk2 + 0.4 µg of an equal mix of 4 plasmids, each containing a unique circRNA
1031 barcode + 0.1 µg pMAX-GFP + 50 µL DMEM + 3 µL PEI. Transfections of each variant were performed in
1032 triplicate, encompassing a total of 24 unique barcodes. 48 hrs after transfection cells were lysed in 150 µL
1033 modRIPA (0.1% NP40, 50mM Tris pH=7.6, 150mM NaCl, 10mM NaF, 4mM $MgCl_2$, 5% glycerol, Halt
1034 protease inhibitor tablet (1 tablet/50mL, Fisher cat# A32965), 2mM PMSF, RiboLock RNase Inhibitor (4
1035 µL/mL, Fisher cat#FEREO0382), 100 µL each phosphatase inhibitor cocktails 2 and 3 (Sigma Cat #P5726
1036 and P0044)) and lysate cleared by centrifugation at 17,000g for 10 min at 4°C. 30 min after lysis all samples
1037 were pooled. The pooled lysate was divided into two 350 µL aliquots and protein was enriched by adding

1038 35 µL anti-flag (Sigma cat#M8823) or anti-pErk beads (see 'Basal Activity Scan' for instructions on
1039 generating pErk beads), rotating end-over-end at 4°C for 2 hr. Beads were washed 3 times with modRIPA,
1040 resuspended in 50 µL nuclease-free water and 200 µL TRIzol then stored at -20°C. Enriched RNA was
1041 extracted and sequenced as described in the 'Preparation of RNA for Genewiz Amplicon-EZ sequencing'
1042 section.
1043
1044 pErk/Flag ratios were computed by dividing the sequencing counts in the flag enrichment by counts in the
1045 pErk enrichment. The mean ratio of all barcodes in a well was reported.
1046
1047 **Proximity labeling time course**
1048 Prior to the experiment, MS2-circRNAs 1b comprising 48 unique barcode sequences were expressed
1049 individually in HEK293T's. 48 hrs after transfection, cells were collected and total RNA was extracted using
1050 TRIzol (Invitrogen, Cat #15596026) and isopropanol precipitation following the manufacturer's
1051 instructions. The extracted total RNA was diluted to ~1µg/µL in nuclease-free water, aliquoted, and stored
1052 at -80.
1053
1054 HEK293T LLP cells stably expressing tdMCP fusions (BRaf wild type, BRaf I666R, or BTK) were seeded into
1055 plates using DMEM supplemented with regular or dialyzed FBS. Cells were carried through the entire
1056 experiment in the same type of FBS (regular or dialyzed). After seeding, cells were transfected with
1057 TurboID- or miniTurbo- fusions (Mek1, CRaf, or BRaf). Transfection mixes per $1x10^6$ cells included 1.8 µg
1058 pCDNA5 TurboID/miniTurbo plasmid + 0.2 µg pMAX GFP to estimate transfection efficiency + 6 µL
1059 Turbofectin (Origene cat# TF81001)+ 100 µL DMEM. 24 hrs after transfection, transfected cells were re-
1060 seeded to ~80% confluency into 96-well poly-D-lysine coated plates. ~24 hrs after moving to 96-well
1061 plates, cells were treated with DMSO or 10 µM GDC-0879. After 2 h pre-treatment with drug, biotin
1062 treatment was initiated by supplementing media with biotin to a final concentration of 150 µM biotin and
1063 10 µM GDC-0879. Subsequent biotin labelings were initiated to achieve 5, 15, or 45 min labeling. Labeling
1064 was quenched for all samples simultaneously by removing media, washing 3x with warm DPBS, and
1065 immediately adding 40 µL cold modRIPA (50mM Tris pH=7.6, 150mM NaCl, 10mM NaF, 4mM $MgCl_2$, 5%
1066 glycerol, Halt protease inhibitor tablet (1 tablet/50mL, Fisher cat# A32965), 2mM PMSF, RiboLock RNase
1067 Inhibitor (4uL/mL, Fisher cat#FEREO0382), 0.1% NP40) to each well. Cells were incubated at 4°C for 20
1068 min on an orbital shaker to ensure cells were fully lysed. During the 4°C incubation, total RNA stocks
1069 containing MS2-circRNA's were thawed and diluted 1/75 in cold modRIPA. 10 µL of the diluted RNA was
1070 added to each lysate-containing well, with each well receiving a unique barcode sequence. Lysates were
1071 incubated with RNA at 4°C for 2 h on an orbital shaker to equilibrate MS2-circRNA-tdMCP binding. After
1072 incubation, 50 µL cold modRIPA supplemented with 1mg/mL BSA was spiked into each well and 80 µL
1073 from each well were pooled. Lysates were cleared by centrifugation at 17,000g for 10 min at 4°C. 1.9 mL
1074 of supernatant was combined with 95 µL anti-flag beads (sigma) or streptavidin conjugated-agarose
1075 (Fisher cat# PI20361) and rotated end-over-end at 4°C for 1hr. After incubation, the beads were washed
1076 3x1 mL cold modRIPA then resuspended in 75 µL water and 300 µL TRIzol and stored at -20°C. MS2-
1077 circRNA was extracted and sequenced as described in 'Preparation of RNA for Genewiz Amplicon-EZ
1078 sequencing'.
1079

1080 **Preparation of RNA for Genewiz Amplicon-EZ sequencing**
1081 Enriched RNA was extracted from TRIzol using IBI scientific TRI-Isolate RNA Pure Kit, eluted into 25 µL
1082 nuclease-free water and stored at -80°C. SuperScript™ IV Reverse Transcriptase (Invitrogen
1083 Cat#18090010) was used to generate cDNA from circRNA barcodes, following the manufacturer's
1084 instructions for gene-specific priming. Total reaction volume was 5 µL including 1 µL of extracted RNA and
1085 JJS1 as the primer.
1086
1087 To generate amplicons, 5 rounds of PCR were run using Q5® Hot Start High-Fidelity 2X Master Mix (NEB
1088 cat #M0494) following the manufacturer's instructions with a 63°C annealing temperature and 30s
1089 extension. A 25 µL reaction scale was used including 12.5 µL Q5® Master Mix, 1.25 µL each of JJS2 & JJS3
1090 (10 µM stocks), 2.5 µL cDNA reaction, 7.5µL nuclease-free water, and 0.75 µL DMSO. PCR reactions were
1091 cleaned with Sera-Mag Select beads (Cytiva #29343052) using a 2.5:1 ratio of beads:reaction and eluted
1092 using 25 µL nuclease-free water.
1093
1094 A second round of PCR was run on the eluted amplicons using 12.5 µL Q5® Master Mix, 1.25 µL each JJS4
1095 & JJS5 (10 µM stocks), 5 µL eluted amplicon, 5 µL nuclease-free water, 1x SYBR gold (Invitrogen
1096 Cat#S11494), and 2% DMSO. Reaction progress was monitored using a Bio-Rad CFX Connect Real-Time
1097 PCR Detection System and halted in the linear phase of amplification. Reactions were equally pooled
1098 based on their final RFU values and amplicons of the correct size were selected using Sera-Mag Select
1099 beads with a 0.65:1 ratio of beads:reaction. Amplicons were eluted into nuclease free water and
1100 submitted to Genewiz using their Amplicon-EZ service for sequencing.
1101
1102 **Western blotting of individual variants**
1103 **(applies to library score vs quantification by western plots)**
1104 HEK293T LLP cells stably expressing flag-tagged BRaf variants of interest were lysed in cold modRIPA
1105 (50mM Tris pH=7.6, 150mM NaCl, 10mM NaF, 4mM $MgCl_2$, 5% glycerol, Halt protease inhibitor tablet (1
1106 tablet/50mL, Fisher cat# A32965), 2mM PMSF, 0.1% NP40, 1% each phosphatase inhibitor cocktails 2 and
1107 3 (Sigma Cat #P5726 and P0044). Lysates were cleared at 17,000g, 4°C for 10 min and total protein
1108 concentrations were measured then normalized using Pierce™ 660nm Protein Assay Reagent (Fisher
1109 cat#PI22660). Samples were mixed 2:1 with 3xSDS loading buffer (188 mM Tris-Cl (pH 6.8), 3% SDS, 30%
1110 glycerol, 0.01% bromophenol blue, 15% β-mercaptoethanol) and heated to 95°C for 5 min. 3-10 µg total
1111 protein was loaded and run on AnykD™ Criterion™ TGX™ Precast acrylamide protein gels (Biorad
1112 cat#5671125) then transferred to nitrocellulose (Biorad cat#1704159). Nitrocellulose was incubated at
1113 room temp for one hour in 5% dry milk in TBST then treated overnight with primary antibody diluted in
1114 5% dry milk in TBST at 4°C. The next day, nitrocellulose was washed 3 times for 5 min in TBST then
1115 incubated for at least 1 h with secondary antibody (Licor cat#926-68070 or 926-32211) diluted 1:10,000
1116 in 5% dry milk in TBST. Westerns were scanned on a LI-COR Odyssey® and quantified using Image Studio
1117 software.
1118 pErk was probed using CST#4370L, total Erk CST#9107S, BRaf CST#14814S, Flag Sigma #F1804, GAPDH
1119 Santa Cruz Biotechnology #365062, streptavidin fluorophore LI-COR #926-32230, pMek CST cat#9154S,
1120 HA CST#3724, BRaf pS729 Abcam #ab124794, Vinculin CST#13901.
1121

1122 **Mek1 co-immunoprecipitations**
1123 HEK293T LLP cells stably expressing flag-tagged BRaf variants (wild type, P367R, K601E, L485S, P318*)
1124 were transfected in 6-well plates in triplicate with 1.8 µg pcDNA5 HA-Mek1 + 0.2 µg pMAX GFP + 6 µL PEI
1125 + 100 µL DMEM. 48 hrs after transfection, cells were lysed using 200 µL high-glycerol modRIPA (0.1%
1126 NP40, 50mM Tris pH=7.6, 150mM NaCl, 10mM NaF, 4mM $MgCl_2$, 10% glycerol, Halt protease inhibitor
1127 tablet (1 tablet/10mL, Fisher cat# A32955), phosphatase inhibitor cocktails 2 and 3 (100uL/10mL, Sigma
1128 Cat #P5726 and P0044)) and lysates were cleared by centrifugation at 17,000g for 10 min at 4°C. To enrich
1129 Mek-Raf complexes, 150 µL of supernatant was combined with 12 µL anti-flag beads (50% slurry, washed,
1130 (Sigma cat#M8823)) and rotated end-over-end at 4°C for 1 h then quickly washed three times with 100 µL
1131 modRIPA. Enriched complexes were eluted from the bead by resuspending in 30 µL 3xSDS and heating to
1132 95°C for 5 min.
1133
1134 **Cloning tdMCP-BRaf variant library**
1135 A site saturation mutagenesis library of BRaf consisting of variants at 79 chosen residues was purchased
1136 from Twist Bioscience. The double stranded DNA pool contained the entire 3xFlag-tdMCP-BRaf open
1137 reading frame with flanking 5' and 3' vector overlaps. The gene fragment library was cloned into the
1138 linearized attB vector using Gibson assembly.
1139
1140 To generate a linearized vector the following was combined and incubated at 37°C overnight: 2 µg attB
1141 library vector, 1.5 µL AflII (NEB cat#R0520S), 1.5 µL NheI-HF (NEB cat#R3131S), 5 µL CutSmart 10x buffer,
1142 nuclease-free water to 50uL. The next day, 2.5 µL recombinant shrimp alkaline phosphatase (NEB
1143 cat#M0371S) was added and incubated at 37°C for 2 hrs. Digested DNA was run on a 1% agarose gel,
1144 extracted (Zymo cat#D4008), and eluted into 30 µL nuclease-free water.
1145
1146 The gene fragment library was cloned into the linearized vector using a 1:2 molar ratio of vector:insert by
1147 combining the following and incubating at 50°C for 1hr: 80ng linearized vector, 95ng gene fragment
1148 library, 40 µL NEBuilder® HiFi DNA Assembly Master Mix (NEB cat#E2621L), and nuclease-free water to
1149 80uL. To estimate background transformants, a vector-only reaction was run in parallel using 80ng
1150 linearized vector, 40 µL NEBuilder Master Mix, and water to 80 µL (no gene fragment library). After
1151 incubation, reactions were cleaned (Zymo cat#D4014) and eluted into 20 µL nuclease-free water.
1152
1153 Cleaned reactions were transformed into NEB® 5-alpha Competent E. coli (High Efficiency) (NEB
1154 cat#C2987H) per the manufacturer's instructions. Briefly, 4 replicate transformations were performed on
1155 the library, each using 40 µL cells and 4 µL cleaned gibson reaction and single replicate was performed in
1156 parallel to estimate vector-only transformants. Cells were incubated with DNA on ice for 30 min, heat
1157 shocked at 42°C for 30 sec, and put back on ice for 5 min. Subsequently, 760 µL SOC was added to each
1158 replicate and cells were incubated at 37°C for 1 h at 220 rpm. All library replicates were then pooled and
1159 added to 40 mL LB supplemented with 100 µg/mL carbenicillin (Fisher cat#BP2648250). From this culture,
1160 200uL, 20uL, and 2 µL was plated onto carbenicillin-selective agar plates to estimate transformants. 200
1161 µL vector-only was also plated onto agar to estimate background. The 40 mL liquid culture was grown
1162 overnight to saturation at 37°C and 220rpm. The following day DNA was harvested (Qiagen cat#12145).
1163

1164 Variant library was barcoded and bottlenecked to desired number of transformants as described in
1165 'Generating single protein variant barcode libraries'.
1166
1167 **Cloning untagged BRaf variant library**
1168 To clone a BRaf variant library without the 3xFlag-tdMCP fusion, the attB 3xFlag-tdMCP-BRaf variant
1169 library (containing a single barcode) was digested by combining the following and incubating overnight at
1170 37°C: 2 µg plasmid + 5 µL CutSmart buffer (10x) + 2 µL AflII (NEB cat# R0520S) + 2 µL BlpI (NEB cat# R0585S)
1171 + nuclease-free water to 50 µL. The next day, 1 µL recombinant shrimp alkaline phosphatase (NEB
1172 cat#M0371S) was added to the reaction and incubated at 37°C for 1hr. The digest was run on a 1% agarose
1173 gel, the correct fragment extracted (Zymo cat#D4008), then eluted into 30 µL nuclease-free water.
1174
1175 To generate a double stranded bridging fragment the following was combined: 1 µg (36.1pmol) JJS6 +
1176 870ng (36pmol) JJS7 + 5 µL NEBuffer 2 (10x) + nuclease-free water to 48uL. Oligos were annealed by
1177 denaturing at 94°C for 5 min, ramping 0.1°C/s to 65.5°C (Tm), holding at 65.5°C for 5 min, then ramping
1178 0.1°C/s to 37°C and holding. 1 µL dNTP's (10mM each, NEB cat#FERR0192) and 1 µL Klenow polymerase
1179 (NEB cat#M0210S) was added to the annealed oligos. Oligos were extended by incubating at 37°C for 1hr,
1180 inactivating the enzyme at 75°C for 20 min, re-annealing the DNA by ramping 0.1°C/s to 42°C, then holding
1181 at 4°C. DNA was cleaned and concentrated (Zymo cat#D4014), then eluted into 30 µL nuclease-free water.
1182
1183 Digested variant library was re-circularized using gibson assembly at a 1:5 molar ratio of vector:bridge as
1184 recommended by the manufacturer. Briefly, the following was combined and incubated at 50°C for 1hr:
1185 200ng (5 µL) digested vector, 20ng (2 µL) dsBridge, 13 µL nuclease-free water, 20 µL 2x HiFi DNA Assembly
1186 master mix (NEB cat#E2621L). After incubation, reactions were cleaned (Zymo cat#D4014) and eluted into
1187 20 µL nuclease-free water.
1188
1189 Cleaned gibson reactions were transformed into NEB® 5-alpha Competent E. coli (High Efficiency) (NEB
1190 cat#C2987H), transformants enumerated, and DNA harvested as described in 'Cloning MCP-tagged gene
1191 library into attB library vector'.
1192
1193 Variant library was barcoded and bottlenecked to desired number of transformants as described in
1194 'Generating single protein variant barcode libraries'.
1195
1196 **Generating variant library cell lines**
1197 Barcoded libraries were stably recombined into the HEK293 RPLP cell line, maintained in high glucose
1198 DMEM (Fisher cat #11-965-118) supplemented with 10% FBS and 2 µg/mL doxycycline (Sigma cat#D9891).
1199 The day before transfection RPLP cells were plated into two 15cm dishes using DOX-free media (+10%
1200 FBS) to reach ~85% confluent during transfection. On the day of transfection, media was replaced with
1201 dox-free DMEM (+10% FBS) supplemented with 100nM SCH772984. Transfection mixes were prepared by
1202 combining per 15cm dish: 16.5 µg attB-plasmid library + 3 µg pCAG-NLS-Bxb1 + 2 µg pMAX-GFP + 2150 µL
1203 serum-free DMEM + 80 µL FugeneHD (Promega cat# E2311), then incubated at room temperature for 15
1204 min and added dropwise to cells. 48 hrs after transfection cells were expanded and maintained in DMEM
1205 (+10% FBS) supplemented with 2 µg/mL doxycycline and 100nM SCH772984 moving forward. 4 days after

1206 transfection cells were further expanded and a sample analyzed by flow cytometry to quantify
1207 recombination efficiency via the mCherry reporter. 6 days after transfection, selection was initiated by
1208 supplementing media with 10nM AP1903. After 6 hrs, media was replaced with fresh +AP1903 media. 24
1209 hrs after initiating selection, cells were further expanded in media supplemented with 1 µg/mL puromycin
1210 (+2 µg/mL DOX, +100nM SCH772984) until ready to freeze aliquots.
1211
1212 **Generating barcode sequence:protein variant map**
1213 Barcoded variant libraries were digested overnight with SpeI-HF (NEB cat # R3133S) and NheI-HF (NEB
1214 cat# R3131S) then submitted to University of Washington PacBio Sequencing Services for further
1215 processing. Briefly, PacBio libraries were generated with the SMRTbell Library Prep kit (Pacific Biosciences)
1216 and sequenced on a Sequel II SMRT Cell 8M (Pacific Biosciences). Reads were processed using a custom
1217 analysis pipeline available at https://github.com/shendurelab/AssemblyByPacBio to identify and link
1218 genes with associated barcodes. Enrich2 was used to convert DNA variants into protein coding mutations.
1219
1220 **Abundance assay**
1221 The day before transfection MCP-tagged BRaf variant library cells were plated into 4x15cm at ~45%
1222 confluent. The next day, each plate of cells was transfected with 17 µg (pCDNA5) Myc-tdMCP-SNAP + 1.7
1223 µg (pMAX) GFP + 70 µL Fugene HD (Promega cat# E2311) + 935 µL serum-free DMEM. 48 hrs after
1224 transfection, cells were trypsinized and combined into two aliquots (2x15cm plates per aliquot). Each
1225 aliquot of cells was fully resuspend in 2 mL cold resuspension buffer, which is modRIPA without detergent
1226 supplemented with dummy barcode to minimize off-target barcode enrichment (50mM Tris pH=7.6,
1227 150mM NaCl, 10mM NaF, 4mM $MgCl_2$, 5% glycerol, Halt protease inhibitor tablet (1 tablet/50mL, Fisher
1228 cat# A32965), 2mM PMSF, RiboLock RNase Inhibitor (4uL/mL, Fisher cat#FEREO0382), 100ng/µL total RNA
1229 containing dummy barcode). To lyse the resuspended cells, an equal volume of lysis buffer (50mM Tris
1230 pH=7.6, 150mM NaCl, 10mM NaF, 4mM $MgCl_2$, 5% glycerol, Halt protease inhibitor tablet (1 tablet/50mL,
1231 Fisher cat# A32965), 2mM PMSF, RiboLock RNase Inhibitor (4uL/mL, Fisher cat#FEREO0382), 0.2% NP40)
1232 was added. Lysates were cleared by centrifugation at 17,000g, 4°C, 10 min then each sample was split into
1233 1.2 mL and 2.8 mL aliquots and combined with 120 µL anti-flag beads (washed, Sigma cat#M8823) or 140
1234 µL anti-myc beads (washed, CST cat#5698S) respectively. Lysates were rotated end-over-end at 4°C for 3
1235 hrs to capture protein. The beads were subsequently washed 3 times with cold wash buffer (50mM Tris
1236 pH=7.6, 150mM NaCl, 10mM NaF, 4mM $MgCl_2$, 5% glycerol, 0.1% NP40) then resuspended in 75 µL
1237 nuclease-free water and 300 µL TRIzol and stored at -20.
1238
1239 **Activity assay**
1240 Anti-pErk beads were generated by combining the following components the day before enrichment and
1241 rotating end-over-end at 4°C until ready to use: 350 µL protein A beads (CST cat# 73778L) + 350 µL Tris
1242 buffered saline + 70 µL anti-pErk antibody (CST cat# 4370L).
1243 To prepare libraries, untagged BRaf variant library cells were plated into two 15 cm dishes (+2 µg/mL DOX,
1244 +100nM SCH772984) the day before transfection. On the day of transfection, the media was replaced with
1245 fresh media without SCH772984. In activity scans run with overexpressed CRaf, each 15 cm plate was
1246 transfected with 17 µg pcDNA5 CRaf-IRES-pErk reporter + 1.7 µg pMAX GFP + 70 µL Fugene HD (Promega
1247 cat#E2311) + 950 µL serum-free DMEM. In scans run without overexpressed CRaf, cells were transfected

1248 with 2 µg pcDNA5 pErk reporter + 14 µg empty plasmid + 1.6 µg pMAX GFP + 66 µL FugeneHD + 880 µL
1249 serum free DMEM.
1250 48 hrs after transfection, each plate of cells was trypsinized, washed once with DPBS, then fully
1251 resuspended in 1 mL cold resuspension buffer supplemented with 1% each phosphatase inhibitor cocktails
1252 2 and 3 (Sigma Cat #P5726 and P0044). To lyse the resuspended cells, an equal volume of lysis buffer was
1253 added. The lysates were subsequently cleared by centrifugation at 17,000g, 4°C, 10 min then each sample
1254 was split into 1.75 mL and 250 µL aliquots. 150 µL of anti-pErk beads or 25 µL anti-flag beads (Sigma
1255 cat#M8823) were added to the 1.75 mL and 250 µL aliquots respectively. The lysates were incubated with
1256 beads for 4 hrs at 4°C, rotating end-over-end. After enrichment, the beads were washed three times with
1257 1 mL cold wash buffer, resuspended in 75 µL nuclease-free water and 300 µL TRIzol, then stored at -20.
1258
1259 **CRaf interaction assay**
1260 TurboID-CRaf was introduced to the tdMCP-BRaf variant library using lentivirus. To generate virus, one
1261 10cm dish of HEK293T cells were transfected with 6 µg transfer plasmid pLJM1 Myc-TurboID-CRaf, EGFP-
1262 IRES-BlastR + 3 µg pMDLg/pRRE-Gag & Pol + 1.5 µg pRSV-Rev + 1.5 µg VSV-G envelope + 42 µL Fugene 6
1263 (Promega cat#E2691) + 600 µL serum-free DMEM. 48 hrs after transfection the media was collected and
1264 filtered through a 0.4 µm frit. Half of the filtered media was applied to a 15cm dish of the tdMCP-BRaf
1265 variant library. Prior to transduction, the variant library was supplemented with RPLP cells stably
1266 expressing barcoded Flag-tdMCP-BTK at a frequency of 0.1% of the cell population. BTK barcodes were
1267 used as an internal indicator of background labeling and non-specific enrichment. The transduced cell
1268 population was maintained for 3 days in complete media (+2 µg/mL DOX, +100nM SCH772984)
1269 supplemented with regular FBS. On day 3, the cells were transferred to media containing dialyzed FBS
1270 (+DOX, +SCH772984). On day 4 the cells were plated into 2x15cm and 2x10cm dishes, each 50% confluent
1271 in media without SCH772984. Drug treatment, biotin labeling and enrichments were performed on day 5.
1272
1273 On day 5, cells were treated with DMSO (0.1% final concentration), 2 µM LXH254, or 5 µM Vemurafenib.
1274 After 1 h incubation with drug, in-cell proximity labeling was performed by adding biotin to a final
1275 concentration of 200 µM (0.15% DMSO final concentration). The cells were returned to the incubator for
1276 7.5 min at which point the labeling was quenched by trypsinizing the cells, washing once with DPBS, then
1277 proceeding immediately to cell lysis. The cells in the 10cm plates were not treated with biotin and were
1278 reserved for flag enrichment.
1279
1280 To lyse the cells, each cell pellet was first fully resuspended in 1mL (15 cm plates) or 500 µL (10 cm plates)
1281 cold resuspension buffer. To initiate lysis, an equal volume of lysis buffer was added to the resuspended
1282 cells. The resulting lysate was cleared by centrifugation at 17,000g, 4°C, for 10 min. To enrich biotin-
1283 labeled variants, 2 mL of cleared lysate was combined with 100 µL streptavidin conjugated-beads (Fisher
1284 cat# PI20361). 1 mL lysate from unlabeled plates was combined with 100 µL anti-flag beads (Sigma
1285 cat#M8823). Samples were rotated end-over-end at 4°C for 1 h then the beads were washed 3 times with
1286 1 mL cold wash buffer. After removing the buffer, the beads were resuspended in 75 µL water and 300 µL
1287 TRIzol then stored at -20.
1288
1289 **Mek interaction assay**

1290 The day prior to transfection, MCP-tagged BRaf variant library cells were plated into two 15 cm dishes.
1291 On the day of transfection cells were washed once with DPBS and plated with fresh media containing
1292 DMEM supplemented with 10% dialyzed FBS (Sigma-Aldrich cat# F0392) and 2 µg/mL doxycycline +
1293 100nM SCH772984. This variant library was also supplemented with RPLP cells stably expressing barcoded
1294 Flag-tdMCP-BTK at a frequency of 0.1% of the population which was used as an internal metric of
1295 background signal. The resulting mixed-population was transfected with 16 µg pcDNA5 TurboID-Mek1 +
1296 1.6 µg pMAX GFP + 66 µL Fugene HD (Promega cat#E2311) + 880 µL DMEM. 24 hrs after transfection, the
1297 culture was expanded to two 15 cm plates and two 10 cm plates in DMEM (+dialyzed FBS, +DOX, +100nM
1298 SCH772984). 48 hrs after transfection biotin labeling was performed on the 15cm cultures. To label, cells
1299 were incubated at 37°C in media supplemented with 250 µM biotin for 5 min. To halt labeling cells were
1300 trypsinized, washed once with DPBS and immediately lysed.
1301
1302 To lyse, the collected cells were first fully resuspended in 1 mL (15 cm plates) or 440 µL (10cm plates)
1303 resuspension buffer. To lyse the resuspended cells, an equal volume of cold lysis buffer was added. The
1304 resulting lysates were cleared by centrifugation at 17,000g, 4°C, 10 min. 100 µL streptavidin beads
1305 (washed, Fisher cat# PI20361) was added to the 2 mL of supernatant corresponding to each biotin-labeled
1306 replicate. 50 µL anti-flag beads (Sigma cat#M8823) were added to 800 µL of supernatant corresponding
1307 to the unlabeled samples. Lysates were rotated end-over-end at 4°C for 45 min then beads were washed
1308 3x1 mL using cold wash buffer. After washing, beads were resuspended in 75 µL nuclease-free water and
1309 300 µL TRIzol then stored at -20.
1310
1311 **SJF0628 degradation assay**
1312 The reference, 2xMyc-tdMCP-SNAPtag, was introduced to the tdMCP-BRaf variant library using lentivirus.
1313 To generate virus, five 10 cm dishes of HEK293T cells were each transfected with 6 µg transfer plasmid
1314 pLJM1 2xMyc-tdMCP-SNAP, EGFP-IRES-BlastR + 3 µg pMDLg/pRRE-Gag & Pol + 1.5 µg pRSV-Rev + 1.5 µg
1315 VSV-G envelope + 42 µL Fugene 6 (Promega cat#E2691) + 600 µL serum-free DMEM. 48 hrs after
1316 transfection the media from each plate was collected, pooled, and filtered through a 0.4 µm frit. 6% of
1317 the filtered media was applied to each of 9x15cm dishes of the tdMCP-BRaf variant library (+2 µg/mL DOX,
1318 100nM SCH772984). 24 hrs after transduction, media was replaced with fresh media without Erk inhibitor
1319 (+DOX, NO SCH772984). 48 hrs after transduction, cells were expanded to 12x15cm dishes and treated
1320 with SJF0628 (+DOX, NO SCH772984). Final concentrations of SJF0628 were 2.5µM, 500nM, 100nM,
1321 20nM, 4nM, DMSO only and two replicates were performed per drug concentration.
1322
1323 20 hrs after treatment with SJF0628 each plate of cells was lysed. To start, each plate was trypsinized, the
1324 media was removed, and cells were fully resuspended in 1 mL cold resuspension buffer. To lyse the
1325 resuspended cells, an equal volume of lysis buffer was added. Lysates were cleared by centrifugation at
1326 17,000g, 4°C, 10 min then each sample was split into 540 µL and 1260 µL aliquots and combined with 40
1327 µL anti-flag beads (washed, Sigma cat#M8823) or 120 µL anti-myc beads (washed, CST cat#5698S),
1328 respectively. Lysates were rotated end-over-end at 4°C for 3 hrs to capture protein. The beads were
1329 subsequently washed 3 times with 1 mL cold wash buffer then resuspended in 75 µL nuclease-free water
1330 and 300 µL TRIzol and stored at -20.
1331

1332 **Generating library sequencing amplicons**
1333 To prep barcodes for sequencing, RNA was extracted from the enrichment beads using IBI scientific TRI-
1334 Isolate RNA Pure Kit (VWR cat# 76006-526) and eluted into 50 µL nuclease-free water. RNA was further
1335 concentrated using Zymo RNA Clean & Concentrator (Zymo Research Cat #R1015), eluted into 10 µL
1336 nuclease-free water, and stored at -80°C. Following the manufacturer's instructions, concentrated RNA
1337 was reverse transcribed using SuperScript™ IV Reverse Transcriptase (Invitrogen Cat#18090010) and
1338 custom primer JJS1 (this manuscript). Briefly, primer/template mixes corresponding to a single library
1339 enrichment were generated by combining 7 µL concentrated RNA + 0.625 µL JJS1 (2uM) + 0.625 µL dNTP's
1340 (10mM ea.). The primer was annealed by heating mixes to 75°C for 5 min then set on ice. 0.625 µL DTT
1341 (0.1M) + 0.625 µL Ribolock RNase inhibitor (Fisher cat#FEREO0382) + 0.625 µL SSIV enzyme + 2.5 µL SSIV
1342 buffer were added to each reaction. cDNA was generated by heating reaction at 45°C for 30 min, 80°C for
1343 10 min, then holding at 4°C.
1344
1345 cDNA was either stored at -20 or immediately used in PCR round #1 to generate double stranded DNA
1346 and add amplicon adapters. Briefly, each RT reaction was split into two PCR reactions. Each PCR reaction
1347 included 6.25 µL RT reaction + 2.5 µL JJS8 (10uM) + 2.5 µL JJS9-JJS15 (10uM) + 13.75 µL nuclease-free
1348 water + 1.5 µL DMSO + 25 µL Q5® Hot Start High-Fidelity 2X Master Mix (NEB cat #M0494). Cycling
1349 included 98°C for 30s, five cycles of (98°C for 10s > 64°C for 20s > 72°C for 30s), 72°C for 2 min, and 4°C
1350 hold. Replicate reactions were pooled then cleaned with Sera-Mag Select beads (Cytiva #29343052) using
1351 a 2.5:1 ratio of beads:reaction and eluted using 20 µL nuclease-free water. Illumina adapters were added
1352 in a second round of PCR. This reaction included 5-20 µL of cleaned reaction #1 + 2.5 µL JJS16-JJS23 (10uM)
1353 +2.5 µL JJS24 (10uM) + 0.5 µL 10x Sybr gold (Fisher cat#S11494) + 25 µL Q5 MM + 1.0 µL DMSO + nuclease-
1354 free water to 51.5uL. PCR cycling included one round at 98°C for 30s, then cycling at (98°C for 10s > 63°C
1355 for 20s > 72°C for 30s). Reaction progress was monitored on a BioRad CFX Connect and stopped when RFU
1356 reached ~3,000 (10-15 cycles). Amplicons were pooled based on final RFU values, separated by gel
1357 electrophoresis and the band at ~220bp excised using Freeze 'N Squeeze™ DNA Gel Extraction Spin
1358 Columns (Biorad cat#7326166). The DNA was further concentrated using Zymo DNA clean and
1359 concentrate columns (Zymo cat#D4014) and quantified using Qubit™ dsDNA HS Assay Kit (Fisher
1360 cat#Q32851). Amplicons were sequenced on a NextSeq™ 550 or 2000 using custom primers JJS25-28, 16
1361 cycle paired-end reads and 8 cycle dual indexing.
1362
1363 **Sequencing**
1364 Amplicons were sequenced on a NextSeq 500 using a NextSeq 500/550 High Output v2.5 75 cycle kit
1365 (Illumina cat #20024906) or on a NextSeq 2000 using a NextSeq 1000/2000 P2 Reagents 100 cycle kit
1366 (Illumina cat #20046811). Barcodes were read twice by the paired-end sequencing primers JJS25 and
1367 JJS26. Dual indices were sequenced using JJS27 and JJS28. Sequencing reads were converted from BCL to
1368 FASTQ format and de-multiplexed using bcl2fastq. Paired sequencing reads were joined by PANDAseq
1369 (v2.11) using BFSRKM assembly.
1370
1371 **Calculating variant scores and classifications**
1372 Scripts used to filter barcodes and calculate scores are available on the GitHub repository (see URLs
1373 section). Frequency values for each barcode in an experiment (F_b) were generated by calculating the sum

of counts recorded for that barcode in all enrichments and dividing by the sum of counts recorded across all barcodes and enrichments.

$$F_b = \frac{C_{enrichment\ 1} + C_{enrichment\ 2} + C_{enrichment\ 3} + C_{enrichment\ 4}}{\Sigma C_{enrichment\ 1} + \Sigma C_{enrichment\ 2} + \Sigma C_{enrichment\ 3} + \Sigma C_{enrichment\ 4}}$$

For example, in pErk experiments with two replicates there would be four enrichments including two selective anti-pErk immunoprecipitations and two normalizing anti-flag immunoprecipitations. This frequency calculation was performed for each experiment.

These frequency values were used to filter out low-frequency barcodes which we reasoned would contribute undue levels of counting noise. To determine a frequency cutoff for each experiment, we started with the assumption that accurate synonymous wild type variant scores should form a symmetrical distribution centered at the wild type score. Note, in all experiments wild type was overrepresented with approximately 80 barcodes and therefore the wild score was assumed to be highly accurate. In each experiment we evaluated the impact of a range of minimum F_b thresholds on the width and central tendency of the distribution of synonymous wild-type scores by excluding barcodes falling below the specified minimum. The selected threshold F_b values, which were unique to each experiment, minimized the skew of the synonymous distribution while retaining most variants.

For pErk enrichments, an additional filter was applied that removed all barcodes containing the motif 'ATAAA' or 'ATTAA' from our analyses. When compared to other barcodes mapped to the same variant, sequences containing these motifs were disproportionately enriched suggesting they were being directly enriched by the anti-pErk antibody.

To generate variant scores, we first calculated a ratio for each barcode (r_b) that passed the filters above. For activity scans, the ratio ($r_{b,act}$) was the barcode count observed in the selective pErk enrichment (C_{pErk}) normalized to the barcode count observed by enriching all pErk reporter through Flag (C_{Flag}).

$$r_{b,act} = \frac{C_{pErk}}{C_{Flag}}$$

The interaction scan barcode ratio ($r_{b,int}$) was the barcode count observed in the selective streptavidin enrichment (C_{Strept}) normalized to the barcode count observed after enriching all variants through Flag (C_{Flag}).

$$r_{b,int} = \frac{C_{Strept}}{C_{Flag}}$$

The abundance barcode ratio ($r_{b,ab}$) was the barcode count from the variant enrichment (C_{Flag}) divided by the barcode count from the tdMCP standard enrichment (C_{Myc}).

$$r_{b,ab} = \frac{C_{Flag}}{C_{Myc}}$$

In activity, interaction, and abundance assays the variant score (S_{Var}) is the mean r_b across all barcodes mapped to the variant ($\underline{r_{b,Var}}$) normalized to the mean wild type barcode ratio ($\underline{r_{WT}}$).

$$S_{Var} = \frac{\underline{r_{b,Var}}}{\underline{r_{WT}}}$$

Using these definitions, the wild type score is always set at 1. Scores greater than 1 indicate variants with increased activity, interactions, or abundance. Conversely, scores less than 1 indicate variants with decreased activity, interactions, or abundance.

For each scan the distribution of synonymous wild type variant scores was used to classify each variant. First, we calculated a cutoff value defined as two standard deviations from the mean of the synonymous distribution ($2SD_{synon}$). Next, using the wild type score (1) we defined upper and lower threshold values as

$$upper\ threshold\ =\ 1\ +\ 2SD_{synon}$$
$$lower\ threshold\ =\ 1\ -\ 2SD_{synon}$$

Variants with scores greater than the upper threshold value were classified as 'increased abundance', 'increased activity', or 'increased interaction'. Variants with scores lower than the threshold value were classified as 'decreased abundance', 'decreased activity', or 'decreased interaction'. Variants with scores that fell between the threshold values were classified as 'Wild Type-like'.

Hierarchical clustering

To cluster residues by their biochemical properties, we first transformed into zscores our CRaf interaction scores, Mek interaction scores, activity scores measured with CRaf, CRaf-promoted activity scores, and abundance scores. Residues were then clustered using an average distance calculation and giving equal weight to all variants across all scores.

Logistic modeling

The growth factor-independent proliferation predictive model was built using the scikit-learn LogisticRegression package and liblinear solver. Model features were z score-transformed LABEL-seq activity scores, CRaf interaction scores, Mek1 interaction scores, abundance scores, and CRaf-promoted activity.

The model built to predict variant sensitivity to SJF028 degradation was created using the scikit-learn LogisticRegression package with the liblinear solver. While training the model, 20% of the data was reserved for model evaluation. Model features were z score-transformed LABEL-seq activity scores, CRaf-promoted activity, CRaf interaction scores, Mek1 interaction scores, abundance scores, Vemurafenib-promoted heterodimerization scores, and LXH254-promoted heterodimerization scores. Predicted values were LABEL-seq SJF0628 degradation classifications.

Data and code availability

Sequencing data is available in the Sequence Read Archive (SRA) under accession number #########. Scripts written for parsing data and plotting figures are available on Github (http://github.com/MalyLab/########). The code used for PacBio subassembly is also available on Github (https://github.com/shendurelab/AssemblyByPacBio).

Reference list

1. Faure, A.J. et al. Mapping the energetic and allosteric landscapes of protein binding domains. *Nature* **604** , 175-183 (2022).

2. Bandaru, P. et al. Deconstruction of the Ras switching cycle through saturation mutagenesis. *Elife* **6** (2017).

3. Ahler, E. et al. A Combined Approach Reveals a Regulatory Mechanism Coupling Src's Kinase Activity, Localization, and Phosphotransferase-Independent Functions. *Mol Cell* **74** , 393-408 e320 (2019).

4. Chakraborty, S. et al. Profiling of drug resistance in Src kinase at scale uncovers a regulatory network coupling autoinhibition and catalytic domain dynamics. *Cell Chem Biol* **31** , 207-220 e211 (2024).

5. Hayes, T.K. et al. Comprehensive mutational scanning of EGFR reveals TKI sensitivities of extracellular domain mutants. *Nat Commun* **15** , 2742 (2024).

6. Macdonald, C.B. et al. DIMPLE: deep insertion, deletion, and missense mutation libraries for exploring protein variation in evolution, disease, and biology. *Genome Biol* **24** , 36 (2023).

7. Tsuboyama, K. et al. Mega-scale experimental analysis of protein folding stability in biology and design. *Nature* **620** , 434-444 (2023).

8. Kwon, J.J. et al. Structure-function analysis of the SHOC2-MRAS-PP1C holophosphatase complex. *Nature* **609** , 408-415 (2022).

9. Estevam, G.O. et al. Conserved regulatory motifs in the juxtamembrane domain and kinase N-lobe revealed through deep mutational scanning of the MET receptor tyrosine kinase domain. *bioRxiv* (2023).

10. Matreyek, K.A. et al. Multiplex assessment of protein variant abundance by massively parallel sequencing. *Nat Genet* **50** , 874-882 (2018).

11. Laroche, A. et al. Deep mutational engineering of broadly-neutralizing nanobodies accommodating SARS-CoV-1 and 2 antigenic drift. *MAbs* **14** , 2076775 (2022).

12. Esposito, D. et al. MaveDB: an open-source platform to distribute and interpret data from multiplexed assays of variant effect. *Genome Biol* **20** , 223 (2019).

13. Landrum, M.J. et al. ClinVar: public archive of relationships among sequence variation and

1519 human phenotype. *Nucleic Acids Res* **42** , D980-985 (2014).
1520
1521 14. Cancer Genome Atlas Research, N. et al. The Cancer Genome Atlas Pan-Cancer analysis project.
1522 *Nat Genet* **45** , 1113-1120 (2013).
1523
1524 15. Tate, J.G. et al. COSMIC: the Catalogue Of Somatic Mutations In Cancer. *Nucleic Acids Res* **47** ,
1525 D941-D947 (2019).
1526
1527 16. Jeon, H., Tkacik, E. & Eck, M.J. Signaling from RAS to RAF: The Molecules and Their Mechanisms.
1528 *Annu Rev Biochem* (2024).
1529
1530 17. Simanshu, D.K. & Morrison, D.K. A Structure is Worth a Thousand Words: New Insights for RAS
1531 and RAF Regulation. *Cancer Discov* **12** , 899-912 (2022).
1532
1533 18. Wu, J. et al. Self-Assembly of Intracellular Multivalent RNA Complexes Using Dimeric Corn and
1534 Beetroot Aptamers. *J Am Chem Soc* **144** , 5471-5477 (2022).
1535
1536 19. Litke, J.L. & Jaffrey, S.R. Highly efficient expression of circular RNA aptamers in cells using
1537 autocatalytic transcripts. *Nat Biotechnol* **37** , 667-675 (2019).
1538
1539 20. Jeck, W.R. et al. Circular RNAs are abundant, conserved, and associated with ALU repeats. *RNA*
1540 **19** , 141-157 (2013).
1541
1542 21. Peabody, D.S. & Ely, K.R. Control of translational repression by protein-protein interactions.
1543 *Nucleic Acids Res* **20** , 1649-1655 (1992).
1544
1545 22. Wu, B., Chao, J.A. & Singer, R.H. Fluorescence fluctuation spectroscopy enables quantitative
1546 imaging of single mRNAs in living cells. *Biophys J* **102** , 2936-2944 (2012).
1547
1548 23. Lim, F. & Peabody, D.S. Mutations that increase the affinity of a translational repressor for RNA.
1549 *Nucleic Acids Res* **22** , 3748-3752 (1994).
1550
1551 24. Matreyek, K.A., Stephany, J.J., Chiasson, M.A., Hasle, N. & Fowler, D.M. An improved platform
1552 for functional assessment of large protein libraries in mammalian cells. *Nucleic Acids Res* **48** , e1
1553 (2020).
1554
1555 25. Lavoie, H. & Therrien, M. Regulation of RAF protein kinases in ERK signalling. *Nat Rev Mol Cell*
1556 *Biol* **16** , 281-298 (2015).
1557
1558 26. Lavoie, H. et al. Inhibitors that stabilize a closed RAF kinase domain conformation induce
1559 dimerization. *Nat Chem Biol* **9** , 428-436 (2013).
1560

1561 27. Jin, T. et al. RAF inhibitors promote RAS-RAF interaction by allosterically disrupting RAF
1562 autoinhibition. *Nat Commun* **8** , 1211 (2017).
1563
1564 28. Amorosi, C.J. et al. Massively parallel characterization of CYP2C9 variant enzyme activity and
1565 abundance. *Am J Hum Genet* **108** , 1735-1751 (2021).
1566
1567 29. Chiasson, M.A. et al. Multiplexed measurement of variant abundance and activity reveals VKOR
1568 topology, active site and human variant impact. *Elife* **9** (2020).
1569
1570 30. Li, X. & Lehner, B. Biophysical ambiguities prevent accurate genetic prediction. *Nat Commun* **11** ,
1571 4923 (2020).
1572
1573 31. Alabi, S. et al. Mutant-selective degradation by BRAF-targeting PROTACs. *Nat Commun* **12** , 920
1574 (2021).
1575
1576 32. Kondo, Y. et al. Cryo-EM structure of a dimeric B-Raf:14-3-3 complex reveals asymmetry in the
1577 active sites of B-Raf kinases. *Science* **366** , 109-115 (2019).
1578
1579 33. Park, E. et al. Architecture of autoinhibited and active BRAF-MEK1-14-3-3 complexes. *Nature*
1580 **575** , 545-550 (2019).
1581
1582 34. Yao, Z. et al. Tumours with class 3 BRAF mutants are sensitive to the inhibition of activated RAS.
1583 *Nature* **548** , 234-238 (2017).
1584
1585 35. Davies, H. et al. Mutations of the BRAF gene in human cancer. *Nature* **417** , 949-954 (2002).
1586
1587 36. Wan, P.T. et al. Mechanism of activation of the RAF-ERK signaling pathway by oncogenic
1588 mutations of B-RAF. *Cell* **116** , 855-867 (2004).
1589
1590 37. Liau, N.P.D. et al. Negative regulation of RAF kinase activity by ATP is overcome by 14-3-3-
1591 induced dimerization. *Nat Struct Mol Biol* **27** , 134-141 (2020).
1592
1593 38. Park, E. et al. Cryo-EM structure of a RAS/RAF recruitment complex. *Nat Commun* **14** , 4580
1594 (2023).
1595
1596 39. Modi, V. & Dunbrack, R.L., Jr. A Structurally-Validated Multiple Sequence Alignment of 497
1597 Human Protein Kinase Domains. *Sci Rep* **9** , 19790 (2019).
1598
1599 40. Spencer-Smith, R. et al. RASopathy mutations provide functional insight into the BRAF cysteine-
1600 rich domain and reveal the importance of autoinhibition in BRAF regulation. *Mol Cell* **82** , 4262-
1601 4276 e4265 (2022).
1602

1603 41. Roring, M. et al. Distinct requirement for an intact dimer interface in wild-type, V600E and
1604 kinase-dead B-Raf signalling. *EMBO J* **31** , 2629-2647 (2012).
1605
1606 42. Yaffe, M.B. et al. The structural basis for 14-3-3:phosphopeptide binding specificity. *Cell* **91** ,
1607 961-971 (1997).
1608
1609 43. Hu, J. et al. Kinase regulation by hydrophobic spine assembly in cancer. *Mol Cell Biol* **35** , 264-
1610 276 (2015).
1611
1612 44. Koga, T., Suda, K. & Mitsudomi, T. Utility of the Ba/F3 cell system for exploring on-target
1613 mechanisms of resistance to targeted therapies for lung cancer. *Cancer Sci* **113** , 815-827 (2022).
1614
1615 45. Bekes, M., Langley, D.R. & Crews, C.M. PROTAC targeted protein degraders: the past is prologue.
1616 *Nat Rev Drug Discov* **21** , 181-200 (2022).
1617
1618 46. Roskoski, R., Jr. Classification of small molecule protein kinase inhibitors based upon the
1619 structures of their drug-enzyme complexes. *Pharmacol Res* **103** , 26-48 (2016).
1620
1621 47. Yao, Z. et al. BRAF Mutants Evade ERK-Dependent Feedback by Different Mechanisms that
1622 Determine Their Sensitivity to Pharmacologic Inhibition. *Cancer Cell* **28** , 370-383 (2015).
1623
1624 48. Gosavi, P.M. et al. Profiling the Landscape of Drug Resistance Mutations in Neosubstrates to
1625 Molecular Glue Degraders. *ACS Cent Sci* **8** , 417-429 (2022).
1626
1627 49. Gonzalez-Del Pino, G.L. et al. Allosteric MEK inhibitors act on BRAF/MEK complexes to block
1628 MEK activation. *Proc Natl Acad Sci U S A* **118** (2021).
1629